HUNGARIAN UNIVERSITY OF
AGRICULTURE AND LIFE SCIENCES

Solar heat for food industry processes

DOI: 10.54598/005330

PhD Dissertation

by

Rajab Ghabour

Gödöllő
2024

Doctoral school

Denomination: Doctoral School of Mechanical Engineering

Science: Mechanical Engineering

Leader: Prof. Dr. Gábor Kalácska, DSc
Institute of Technology
Hungarian University of Agriculture and Life Sciences,
Szent István Campus, Gödöllő, Hungary

Supervisor: Dr. habil. Péter Korzenszky, PhD
Institute of Technology
Hungarian University of Agriculture and Life Sciences,
Szent István Campus, Gödöllő, Hungary

……...…… ….....……

Affirmation of supervisor Affirmation of head of school

CONTENTS

NOMENCLATURE AND ABBREVIATIONS

Symbols

C	Heat capacity	kJ/kg·℃
G	Global solar radiation	kWh/m^2
H_T / D	Tank height to diameter ratio	m/m
M	Material mass	kg
$\dot{m}$	Flow rate	Kg/h
$\dot{m}$ / A_c	Relative flow rate to collector area	$l/h/m^2$
Q	PCM quantity	g
Ra	Solar radiation	W/m^2
R^2	Coefficient of determination	%
S	PCM samples	Pieces
Std. Error	Standard error	%
τ	Time	hours
T	Temperature	℃
T_{amb}	Ambient temperature	℃
$T_{avg\text{-}tank}$	Average tank temperature	℃
T_{mo}	Pasteurization time	min
T_p	Pasteurization temperature	℃
$T_{Sec\ In}$	Input temperature of the secondary side	℃
$T_{Sec\ Out}$	Output temperature of the secondary side	℃
T_{pc}	Phase change temperature	℃
$T_{Pr\ In}$	Input temperature of the primary side	℃
$T_{Pr\ Out}$	Output temperature of the primary side	℃
V	Storage tank capacity	m^3
Δh	Enthalpy difference	kJ/kg
ΔQ	Storage energy	kJ
ΔT	Temperature change	℃

Greek symbols

β	Inclination angle (slope)	º
β_0	Unknows population intercept	
β_i	Effect on Y_i of a change in X_i holding other X constant	
u_i	Error term (omitted factors)	
X_i	Independent variables (regressors)	
Y_i	Model equation	

Abbreviations

3D	Three-dimension
AFPC	Advanced flat plate collector
AR	Anti-reflective
CFU	Colony-forming unit
CIP	Cleaning in place
CO_2-eq	Carbon dioxide equivalent
COP	Coefficient of performance
CPC	Compound parabolic collector
CSP	Concentrated solar power
CST	Concentrated solar thermal
DF	Diamond foam
DHW	Domestic hot water
EPS	Expanded polystyrene
ESTIF	European solar thermal industry federation
ETC	Evacuated tube collector
EU	European union
FPC	Flat-plate collector
GHG	Greenhouse gas
HTST	High-temperature short time
IMRe	Intelligent measurement system
IoT	Internet of things
LFO	Light fuel oil
LHS	Latent heat storage
LHTES	Latent heat thermal energy storage
LPG	Liquid petroleum gas
MH	Microwave heat treatment
MLTD	Mean logarithmic temperature difference
PCM	Phase change material
pH	Potential of hydrogen
PV	Photovoltaic
PVT	Hybrid (Photosvoltaic & thermal collector)
RSM	Response surface method
SHIP	Solar heat for industrial process
SHS	Sensible heat storage
SHTES	Sensible heat thermal energy storage
TES	Thermal energy storage
TH	Thermostat heat treatment
TMY	Typical meteorological year
UHT	Ultra-high temperature
V4	Visegrád group
WH	Without heat treatment

1. INTRODUCTION, OBJECTIVES

This chapter describes the background and objectives of the current research.

1.1. Introduction

Human civilisation's fast development and technological revolution in the last decades brought an essential environmental consequence. These all drove the researchers to find a better sustainable solution and optimise the current ones. While fossil fuel is currently the primary energy source causing massive carbon dioxide emissions, environment-friendly solutions, like renewable energy systems, have started to appear with long life spans, high reliability and efficiency (Gallego et al., 2013). The utilisation of renewable energies is not just because of the conventional fuel carbon dioxide emissions and being environment friendly, but also because of the continually increased energy demand and the fluctuated oil price, especially after the Russian invasion of Ukraine. Nowadays, renewable technologies are suitable to supply stable, independent energy for isolated areas.

Furthermore, since space heating and all industrial processes need hot water, solar thermal energy can also reduce greenhouse gases (GHG) (Kylili et al., 2018). The solar thermal system does not need much water compared to geothermal or biofuel systems (Yildirim & Genc, 2015). It needs a space like the unutilized rooftop or some square meters on the ground. Low maintenance means a solar thermal system can give enough energy once installed.

For instance, Hungary's desire to support the new renewable energy projects increased because it showed an excellent economic investment with a payback period of fewer than ten years (Alktranee & Bencs, 2020). Even under difficult economic situations, solar heating and cooling proved their place as a driver, according to the data published by ESTIF (European solar thermal industry federation) (Noro et al., 2014).

A substantial amount of heat energy demand can be obtained from solar thermal systems for industrial and agri-food processes, where 77% of the energy needed in Agri-processing is for heating processes (60% of the heat needed must be below 250 ℃) (Barba et al., 2019). Up to 400 ℃ steam or hot water can be supplied in developed economies, giving a chance to cover about half of the energy demand. Also, the variation in industry sectors from food, textile, brick (Pietruschka et al., 2016), and agriculture processes match the variation in the solar thermal energy types like hot water or hot air, which are suitable for drying, washing, dyeing, boiling, pasteurization and sterilization (S. Kalogirou, 2006). Solar thermal technologies have three main types: solar air collectors, solar water collectors, and solar concentrators. For up to 125 - 250 ℃, traditional solar collectors, like flat plate collectors (FPC) or evacuated tube collectors (ETC) (Cocco et al., 2016), can afford not less than 60% solar fraction, mainly in residential applications. However, due to the mid-range temperature, it can also be used in industry.

In the food and beverages sector, 3.3 and 2.2 EJ, with thousands of new vacancies annually (Rivett-Carnac & Scholtz, 2018), are needed for low and medium-range temperatures, respectively. Nevertheless, only 1% of solar thermal technologies are used in industrial processes (Ivancic et al., 2014). The agri-Food sector is also famous for many problems: high carbon emissions, packaging waste, and food waste with massive consumption of water and land, so sustainability is needed urgently in this sector. Any slight improvement in machines, storage, and energy consumption can lead to massive savings (Tolnay et al., 2020).

One method of enhancing the thermal system´s performance is integrating the PCM in the storage tank as the latent heat storage material. The chemical bonds of the material break when it changes its phase; alternatively, it can be used as a storage material (Medrano et al., 2009) to increase the solar system energy capacity for thermal collectors. A significant advantage of the integrated PCMs in solar systems is that they are easy to mount and have no component complexity (Alktranee & Bencs, 2020). It also increases storage density at a small temperature change.

On the other hand, the boiler is an enclosed vessel that transfers the energy from fuel combustion or electricity into hot water or steam. Then, this hot water or pressurized steam transfers the heat to a particular heat process. Usually, the required hot water or steam varies throughout the day, which may be implied on the daily or monthly load. Therefore, several configurations connect the boiler to the solar heating system to ensure the temperature of the final output. The boiler can be connected in series or parallel to improve the overall process's efficiency and reduce running costs. Several computational tools are developed to numerically evaluate the solar system's long-term performance, such as TRNSYS, MATLAB and T*Sol.

This research will lead to a better understanding and optimising of the solar heat for industrial process systems and provide an overall view of the influencing factors from the first and second degrees and the two factors' interactions. This novel cross-over research area will allow the collection of a unique and new prospective dataset. Based on the results, recommendations will be formulated for industrial applications from micro and macro levels. These new findings will be helpful for industrial plants and decision-makers willing to integrate and utilise solar thermal energy not just for final heat processing usage but also for preheating purposes.

1.2. Objectives

MeteoSyn and T*Sol software will extract the meteorological data and operate the simulation process. For the programming process, R-script software is used to identify the essential factors illustrated by Pareto Plots and the two-factor interactions and done by non or linear modelling using the response surface method (RSM). Then, those data are validated and compared with the real-time measurements. Finally, the optimums parameters are identified using Lagrange optimum conditions. The experiments and measurements will consider the most influential factors: collector area, volume flow rate, glycol ratio, tank height to diameter ratio, relative tank capacity, PCM quantity, PCM specimens, and temperature. The general objective of this study is to investigate the technical challenges of integrating food industries with a solar heat system, considering the general assessment of different solar collector types and thermal energy storage enhancement using phase change materials for some parts.

The detailed research objectives can be described as the following:

a) What is the influence of integrating PCM materials such as Soy wax (52 ℃ and 62 ℃ melting temperature) as encapsulated specimens into the solar thermal tank for low-temperature thermal processes?
b) Comparison of the performance of the two Soy waxes and determining the optimum operating values using Lagrange optimum conditions.
c) Comparison of the in-series and in-parallel boiler configuration performance in the solar heat for industrial process.
d) Evaluation of the performance of the tankless solar thermal system under Hungarian weather conditions as a preheating system for industrial processes using low temperatures.
e) What are the optimum flow rates for the primary and secondary circuits for generating the highest energy (kWh) or temperature (℃) of the secondary circuit?

2. LITERATURE REVIEW

This chapter provided a thorough overview of solar heat for industrial processes (SHIP), including the mechanism illustration and the clustering of the aimed temperature in different industrial sectors. The chapter will present the potential integration, focusing mainly on the food and beverage sectors and illustrating the low-to-medium temperature profiles. Furthermore, the most recent efforts to integrate renewable energies with the industrial process are presented. In addition, identifying the gaps and challenges encountered in the literature is the reason for initiating this research.

2.1. Solar heating for industry process (SHIP) system

The food and paper industries have the highest heat demand, and chemical and textiles also have considerable needs. Furthermore, the utilization of the solar thermal system in industrial applications has rapidly grown from 42 MW in 2010 worldwide with an estimated 60000 m^2 (Lauterbach et al., 2012) to 93 MW in 2014 with more than 136000 m^2. Most of these projects have less than 1000 m^2, and 70% use ETC and FPC.

The deployment is not just increasing, but the geographical market, where the last reports showed approximately 20 projects installed in Germany, Greece, Italy, Spain and the USA just in 2017. Moreover, surprisingly, India had the lead, with 61% of its solar thermal systems capacity used for industrial processes. Furthermore, the middle east and the Arabian Peninsula have a high potential for market growth, especially for oil refineries (Kempener & Saygin, 2014).

In most industrial products' manufacturing processes, the heat process is essential with a wide range of temperature needs and sectors in different countries. The heating process can be obtained by fuel, steam, electricity, or many sources. A considerable amount of energy is always needed regardless of the chosen method to produce the heat. Two main types of heating processes are direct and indirect. The direct method is the generated heat at the process place, like microwave or induction. At the same time, the indirect method is when the heat must be transferred to the process place, usually through liquid heating. Another category is the temperature range (Neumann, 2018); low temperature is usually used for rinsing, washing, food, space heating and domestic hot water, while the mid-range temperature is needed for drying and evaporating. Moreover, high temperature is needed for heavy industries like ceramics and metals.

2.1.1. Solar thermal systems for low heat demand <150 ℃

Up to 120 ℃ temperature can be achieved by traditional flat-plate solar collectors (FPC) or (ETC). Whereas FPC mainly uses copper tubes where the fluid flows through. The collectors are carried by insulated, suitable absorber and weather condition-resistant boxes supported by insulation material on the backside to prevent heat losses. It must be noted that the FPC can easily reach 100 ℃ and, with developed insulation material, can reach 150 ℃ (Beikircher et al., 2014) and for multi-glazing layers, can reach 110 ℃ (Föste et al., 2014). While ETC has a row of glass tubes, each is considered a heat pipe where the heated liquid flows surrounded by another tube with a vacuum to prevent losses significantly. So ETC can produce temperatures up to 120 ℃, and due to the reduced losses, this type of collector is suitable more for cold climate countries and can reach 150 ℃ if an ultra-vacuum is used or other gas is injected (S. Kalogirou, 2006). Unglazed collectors can be cost-effective solutions like swimming pool heating for low-temperature applications. Alternatively, a slight temperature increase can be helpful in sewage treatment (Kempener, 2015).

2.1.2. Solar concentrators for medium heat demand (150 – 400 ℃)

Up to 200 ℃ FPC with high vacuum technology is available for the medium heat demand. However, solar concentrators are mainly used for this range of demand. The simplest case is to put compound parabolic concentrators (CPCs) behind the ETC, which reflects all the missed direct radiation and the diffusive radiation back to the evacuated tubes (S. Kalogirou, 2003). Due to this combination, the concentration factor can reach up to 4:1.

2.2. Preheating systems

The cold water is preheated in the solar collectors and fed directly to the industrial process. while if the temperature is still not sufficient, the boiler will heat up to the required temperature, as in Fig. 2.1.

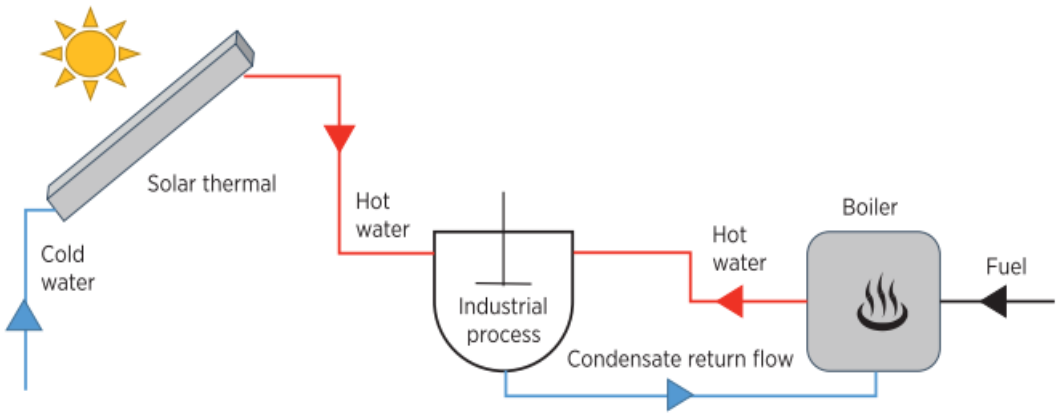

Fig. 2.1. Principle for solar thermal systems for direct heating to process equipment (Epp and Oropeza, 2017)

2.3. Heating systems

The cold water is heated to industrial process required temperature and supplied to the boiler then the temperature is evaluated. If the temperature is sufficient then it can proceed to the industrial process, otherwise the fossile boiler can intervene to heat up till the required temperature, as in Fig. 2.2.

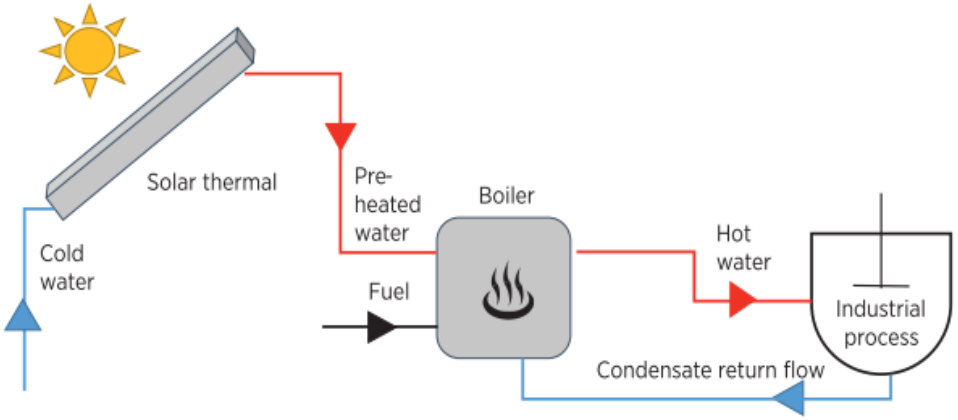

Fig. 2.2. Principle for feeding solar thermal heat for pre-heating of supply water for the steam boiler (Epp and Oropeza, 2017)

2.4. Feasibility assessment and integration of solar heat for industrial process

The main barriers to the market development are the feasibility assessment and the predesign of a suitable solar process heat system. The solar system must overcome economic and technical difficulties to ensure a place in the heat sector of the industry (Schramm & Adam, 2014). Despite having enormous potential to utilize solar heat systems in industry or commercial applications where a huge demand is below 150 °C (Matsuda, 2014), we must be sure that both daily and annual demand have constant energy requirements. Each industry must have the tools, guidelines, and appropriate integration points to facilitate integration (T. N. Anderson & Duke, 2007; Kempener, 2015). As a result, less than one per cent is the share of the global installation of solar heat systems (Ivancic et al., 2014), and the feasibility assessment and the planning are very expensive. A heat recovery system integrated with solar energy can make up to 0.9 MW of thermal energy extra for a dairy plant (Walmsley et al., 2014).

There are three main factors to be considered if a solar system is integrated into the food industry:

- **The temperature**: the temperature coming from the solar source must be 10 °C degrees above the process temperature.
- **Load profile**: where the continuous and long operation period is preferred. Considering that some companies do not work on weekends or night shifts, the buffer tank must be ready with sufficient capacity to harvest the solar energy from those two days and keep it till the working day. For such cases, the solar heat can compensate for the energy losses in the standby system at weekends.
- **Effort for integration**: This is a significant factor in integrating the solar system with an existing process system where the barriers are unfamiliar and constitute an essential bottleneck (Kempener, 2015). For example, hot water for cleaning can result in an extra heat exchanger with some extra fittings. A heat bath system can result in a more complicated system with extra costs and the development of the controlling system (Schmitt, 2016; Schramm & Adam, 2014).

There are many challenges facing solar thermal systems, like more than three years expected pay-back period, relatively low-price fossil fuel, and integration into complex industries. At the same time, lower risks and costs can exist when integrating the solar system during the construction phase (Kempener, 2015).

Heat demand for a fluid stream of for reservoir is needed in most industrial processes, where mainly hot water or steam is provided by a boiler, which uses fossil fuel, coal, or electricity generated by different sources. This gives a chance to replace it with a solar heating system with no less than 20% of the solar fraction annually (Bakyalakshmi Nisha & Madhumitha, 2010). Other case studies show 37% (Antoniadis & Martinopoulos, 2019), wherein India's three over five big plants have 100% solar fraction with 54.86% country average solar fraction (ABPS, 2011). It is leading to solar energy for heating water from 30 °C to 85 °C, saving 200 - 250 litres of oil daily (Desai et al., 2013). In some cases, like breweries or dairies, companies generally have one limiting factor: the roof space (Müller et al., 2014). For a large dairy plant with a low-temperature thermal demand of 3,440 MWh annually, a 5,400 m^2 collector area is needed from a technically feasible perspective (Müller et al., 2014).

2.5. Performance and costs of solar heat for industrial process

It is hard to estimate the costs of industrial solar heat systems, which depends significantly on the needed temperature level, continuity of the demand, solar radiation, and the size of the plant. To understand that, we can compare the EU and India for traditional ETC or FPC solar system costs

where the costs in Europe are between 250 – 1,000 EUR/kW, while in India and Turkey, they vary between 200 – 300 EUR/kW (Turkey 237 EUR/kW) (Kempener, 2015). A significant enhancement happened in the costs in Germany, for example, wherein in 1998, half of the solar system price dropped from 1062 EUR/kW to 523 EUR/kW compared to 2010, where 50 – 70% of the expenses go to the capital, and the rest for integration and installation costs (Rawlins & Ashcroft, 2013). Generally, 50% of the installation cost goes for pipes, 20% for the storage tank, 11% for the heat exchanger, and 5% for the system control. The main cost of the solar system comes from solar collectors at 54% and a storage tank and a heat exchanger at 24% (Karagiorgas & Botzios-Valaskakis, 2000). Local companies help a lot to reduce the prices for mainly small projects like residential applications, but large-scale applications like the FPC heat plant require subsidies. For example, as in Fig. 2.3, in Chile, a turnkey project was for a Danish international company named SunMark.

Fig. 2.3. Application of parabolic trough collector in a dairy processing plant in Mexico (Kasibhatla, 2015).

The costs now for industrial projects are related to the number of suppliers and companies that can do such a complicated project. Even though the global experience shows that the prices are so expensive, a local experience like the Indian market dramatically reduces the costs, as in Table 2.1 and creates local business opportunities (Kempener, 2015).

For the non-subsidized light fuel oil (LFO), only FPC can give a viable solution with significant life cycle savings.

Table 2.1. Cost estimation of different solar collectors (Kalogirou, 2006)

Collector type	**Collector price (€/m^2)**
FPC	110 - 190
AFPC	120 - 220
CPC	180 - 310
ETC	250 - 430
The prices include the mounting and piping work.	

A comparison between residential and industrial-size solar thermal systems leads to the following primary differences:

- There is a significant difference between the heat demand in residential and industrial sectors wherein the industry the demand is times larger than residentials cases.
- Heat demand in the industry is often continuous, resulting in extra control (Schramm & Adam, 2014).
- The temperature level in the industry is high; therefore, advanced technologies are needed to reach the requested level.

Even solar thermal systems have been studied since 1970 (Fuller, 2011), but few projects have been implemented due to high capital costs and lower costs from coal and gas (Kempener, 2015).

2.6. Dairy industry

As the world's most popular drink, milk is essential in many peoples' lives (Yildirim & Genc, 2015). This chapter discusses the milking industry processes and their impact on the environmental

2.6.1. The environmental footprint of the milking industry

The propagation of GHG emissions in the food industry is one of the characterizations of the dairy plant. With a tremendous change in the consumption of milk in the world between 1961 – 2009, from 314 to 583 million tonnes increased by 86% more, where the new technologies had a part in increasing the yield of the cow from 1.8 to 2.3 tonnes per cow it was increased by 31%. where the life cycle assessment is a method to determine the environmental impact to the air, water, and soil (Daneshi et al., 2014; Milani et al., 2011). The dairy industry alone contributes to the world's GHG of 2.7%, as in Fig. 2.4, agriculture activities contribute to about 22% of the total GHG (McMichael et al., 2007), and 78% of the GHG emissions are attributed to industrial processes and fossil fuel usage (Neumann, 2018). It added to 4.0% if the meat is considered a coproduct of the dairy process. Making it one of the highest contributions to the world's GHG production as agriculture at 13.5%, heat and electricity generation at 24.6%, land-use change at 18.2%, and transportation at 13.5%. The significance of the dairy product when it is compared to similar nutritional containment of proteins and fat like the peanut; for example, the GHG of one kg of cheese is 5.9 kg CO_2-eq/kg and 0.17 kg CO_2-eq/kg for peanut butter (Singh et al., 2020), which means 35 times more illustrating the magnitude of its impact (Milani et al., 2011).

In livestock production, the most significant GHGs are Methane and nitrous oxide, where these two gaseous contribute more to the emissions from this sector than carbon dioxide. The current

statistics show that it is increasing rapidly, especially in middle or low-income countries (McMichael et al., 2007), at least for the next four decades. Therefore, in agriculture and mainly the livestock industry, it is essential to control the increase of GHGs and to be a high priority. It is known that reducing the emissions of the livestock industry with the available technologies and reasonable costs in the global market can reduce non-carbon dioxide emissions by less than 20% (Schramm & Adam, 2014). This leads to the fact that it must be more adjusted and controlled, and renewable energies can occur here.

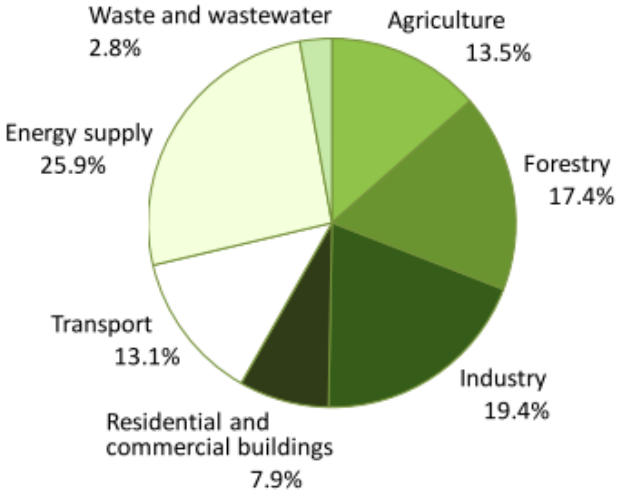

Fig. 2.4. GHG emissions contribution by sectors (Flysjö, 2012).

With renewable energy, GHG emissions will be reduced from 2016 to 2025 in Jordan by 16 million tons of CO_2-eq (Jaber & Khraiwish, 2019), where solar energy has a share of 45% of the total accumulated reduction.

2.6.2. Milk safety

The storing and cooling of food technologies have been changed and developed continuously because uncooked food or beverages can have bacteria, which can be duplicated every 20 minutes, causing severe health diseases (Korzenszky & Adebayo, 2018). Milk production has a high portion of the food industry, around 25%, and drinking one cup of milk daily can contribute significantly to nutrition. Since it is the only drink newborns consume, it has to have all the necessary nutrients for growth and development, such as Amino acids, minerals, energy, and vitamins.

The pasteurising process was developed and discovered by Louis Pasteur, who recognized that the microorganisms that cause diseases and airborne organisms spoil food (Korzenszky et al., 2017).

The standard efficiency of germs destruction is 99 – 100%, where the positionally survived germs cannot reach such a dangerous level during the shelf-time to cause disease. The EU standards show the treated temperature of 71.7 ℃ for 15 seconds. One test commonly used to check the milk after the treatment is the inactivity test of the peroxidase enzyme (Lauterbach et al., 2012).

2.6.3. Milk manufacturing, packaging, and consumption

Most of the milking process is a thermal process. Moreover, this happens at least once from the raw material until the consumable product. One of the main everlasting problems in the dairy plant is the fouling of the heat exchangers, which need high energy to be cleaned with the other

equipment of the plant due to the curdling, which causes fouling and nutrient loss (Enebe & Samuel, 2019). So, any improvements in the design, the cleaning process, and consumed energy will significantly reduce the energy and environmental impact, as new statistics show oil depletion within 20 - 30 years (Bakyalakshmi Nisha & Madhumitha, 2010). The cleaning process takes up to 0.5% of the total plant product value (Milani et al., 2011). Three main milk pasteurizing types:

- Low temperature pasteurizing at 63 ℃ for 30 min
- High temperature pasteurizing at 72 ℃ for 15 sec
- Flash temperature pasteurizing at 75 ℃ for a brief time (Müller et al., 2014)

The energy demand in the dairy plant is divided into two groups (Sandey et al., 2015):

Low-temperature demand <80 ℃

- Bottle washing 60 ℃
- Pasteurization 70 ℃
- Cleaning in place (CIP) 70 – 80 ℃
- Yoghurt maturation 40 – 40 ℃

High-temperature demand >100 ℃

- Bottle sterilization
- UHT treatment at ultra-hot temperature for milk sterilization
- Multiple stage evaporation

The pasteurizing methods are shown in Table 2.2:

Table 2.2. Milk pasteurizing types

Heat treatment procedure	**Temperature (°C)**	**Holding time (s)**	**Application area**
Gentle/long-lasting/slow pasteurization	62 - 65	1200 - 1800	Certain cheeses
Thermalization	65 - 71	15 - 40	Hard cheeses
Fast pasteurization	72 - 76	15 - 40	Consumer milk, mature rennet cheeses, acid-coagulated cottage cheese
High-temperature (HTST) pasteurization	80 - 98	5 - 180	Acid-coagulated products: cottage cheese, cream cheese, flavoured and acidified milk, butter
Instant pasteurization	85 - 95	1 - 5	Milk, cream, sour products, desserts
Ultra-pasteurization (UHT)	136 - 150	2 - 8	flavoured dairy products, creams: whipping cream
Sterilization	110 - 121	1200 - 2400	Condensed milk, coffee cream

2.6.4. Microwave milk pasteurizing

The heat treatment of human-consumed drinks is the only possibility to extend the shelf time and make the product consumable. The electromagnetic field of the microwave has vast applications in food processing, like drying, cooking, and pasteurizing (Chandrasekaran et al., 2013). However, it is not homogeneous, creating an uneven product temperature. Due to the developed technologies and sensors, it was possible to detect the differences between the microwave method, as in Fig. 2.5, and the traditional one. The protein and bacterial content were measured.

Furthermore, the results showed no significant differences between the microwave heat treatment and the convection technology. The properties and quality of the milk vary widely. They can be affected by the workers' actions because the food quality is significantly determined by the raw material, which is due to the animal's nutrition. The heat treatment of the milk has some advantages, like reducing the germs ratio to the acceptable limit, and disadvantages, like protein's and vitamins' denaturation and the properties of the milk (Sierra & Vidal-Valverde, 2000). The nutrition level is higher than the microwave method, which is faster, resulting in higher quality.

Fig. 2.5. Microwave milk pasteurization (Korzenszky et al., 2013).

The result showed significant differences between the untreated samples WH (without heat treatment) and the treated ones TH (thermostat heat treatment) and MH (microwave heat treatment), but almost no differences between TH and MH. The initial amount of the bacteria was 126,500 ± 6,500 CFU/cm^3, and after the treatment, it decreased by 76.4% on average without affecting the protein and fat content (Korzenszky et al., 2013). Another solution is the electrical field (Al-Hilphy, 2013) with up to 40 °C and increased electrical conductivity. The electrical field milk pasteurizing had lower viscosity and good chemical and pH results, with 55 V/cm electrical conductivity causing bacteria elimination and no fouling.

2.7. Providing pasteurizing process energy demand from renewable energies

Making a heat treatment of cow's milk has two main aspects: the food's safety and the energy demand. From a food perspective, the appropriate treatment of the milk is the core element of the process. However, from a manufacturing perspective, safety and energy demand are also important. Utilizing solar energy in this field causes a problem since this energy is not always available, while raw milk material is almost always available. As a result, solar energy thermal and PV can be a suitable green solution (Yadav et al., 2016) that provides a considerable portion of the demand for the assumed isolated Pasteur system. Considering that solar collectors have no risk of food safety, the closed cycle liquid of the collector (propylene-glycol) is not dangerous and

non-toxic. The two liquids can be intersected if there is a defect in the heat exchanger. Propylene glycol can be coloured or dyed to recognize the problem whenever it happens quickly.

Regarding goat milk (Korzenszky, Meixner, and Sembery 2018), there is an advantage that the lactation period of the goat is from March to October. This makes solar energy, solar collectors as hot water sources and solar cells as the electric source a suitable solution since the two periods overlap. In Kenya, cheap FPC low-cost pasteurizer was locally created, as in Fig. 2.6, giving people in arid areas a chance to pasteurize 40 litres of milk daily with less than 10 CFU/ml harmful coliform (Wayua et al., 2013) and the payback period was only 4.3 years.

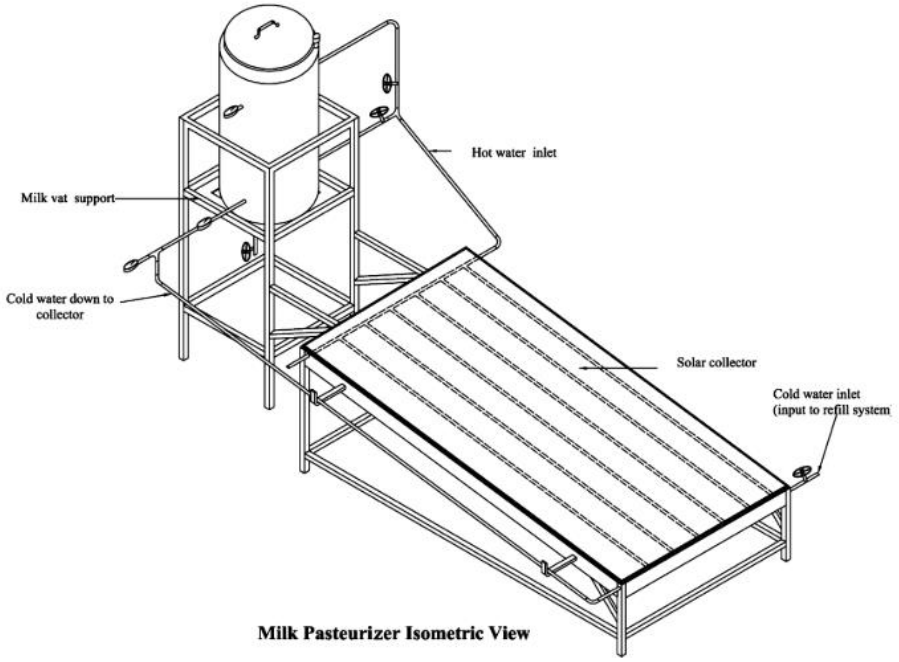

Fig. 2.6. Solar milk pasteurizer prototype (Wayua et al., 2013)

Solar thermal energy has high potential in small-scale dairy plants for many operations like sanitary use and hot water for clean in place (CIP), boiler water preheating, and milk heating and pasteurizing. For CIP in dairy, all equipment must be cleaned and sanitized regularly. In the EU, 70% is needed with temperatures between 65 – 75 ℃ for the dairy industry (T. N. Anderson & Duke, 2007). It is imperative in milking, where bacteria can grow fast and cause illnesses or product spoilage, so all used equipment must be washed with hot water, disinfectants, and detergents. Initially, warm water (<55 ℃) is better for raising the proteins because if hot water is used, it can coagulate and will be harder to clean. Assuming one litre of water must be warmed from 16 ℃ to 55 ℃, the energy needed is 0.045 kWh/litre. A single glass FPC with 3.5 m^2 in such an excellent solar condition area can get up to 200 litres daily from 16 – 55 ℃ (Jitjaroen et al., 2011). For Hungary, where 1 kWh costs around 0.116 € and for similar energy needs, an electric heater would consume around 10 kWh/day, which means 423.4 € per year. With such a solar collector, the payback period would be less than 3 – 5 years, giving long-term cost savings. In freezing conditions, the water-glycol mixture is a suitable fluid with a closed-cycle loop. In this case, a heat exchanger must be added, significantly impacting the payback period and the costs by around 50%. For heating and pre-heating pasteurized milk, a solar thermal system can cover the loads partially or totally, even though there are many types of pasteurizing. However, the high-temperature short-time (HTST) method is the most common. The temperature needed is 72 ℃ for 15 seconds, and assuming the milk is stored at 4 ℃, then 0.0785 kWh/litre is needed for this process. For a similar assumed FPC with good solar conditions (M. Anderson, 2017), 50 litres/day

of milk can be produced. It is important to state that the mathematical relationship between pasteurization time T_{mo} and pasteurization temperature T_p for 99.6% of the pasteurizing process is given by the following equation 2.1 (Mølgaard et al., 2001):

$$T_p = 5.10^{14}\ e^{-0.4353.T_{mo}} \quad (2.1)$$

The number of sunny hours a good indicator from energetic and agriculture prospect for how many hours are available for use in a specific location. For example in Hungary 2,146 hours a year compared to regions such as the Mediterranean European countries with 3,000 hours per year. At the same time, Austria now has more than one million square meters of solar collectors with a 2030 vision focused mainly on the food and beverages, chemical and leather industries, making Austria dominant in those sectors (Farjana et al., 2018). At the same time, 27% of the energy consumption in Germany stands for the industry, as in Fig. 2.7, with 74% share of this demand going for thermal energy and the dairy sector uses thermal energy, 80% of it is for temperature demand between 60 – 80 ℃ (T. N. Anderson & Duke, 2007). These applications give promising application potential for solar thermal technologies; as in Fig. 2.8, it is known that the thermal requirements of pasteurization devices are low temperatures, which encourages the study of the possibility of hybridization with solar energy.

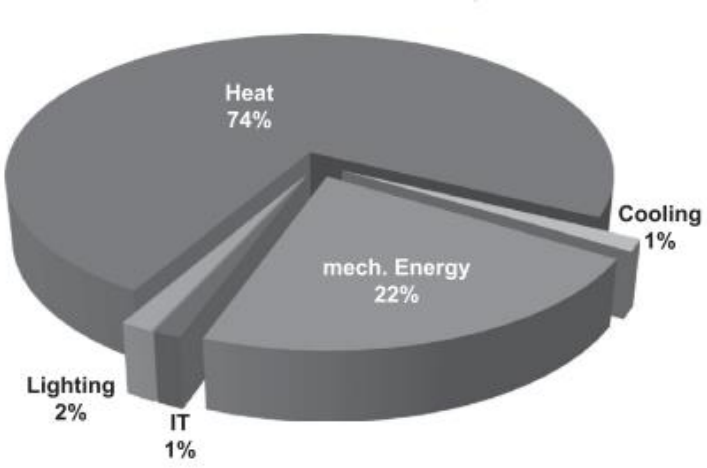

Fig. 2.7. Final energy consumption in industry, Germany 2007 (Lauterbach et al., 2012).

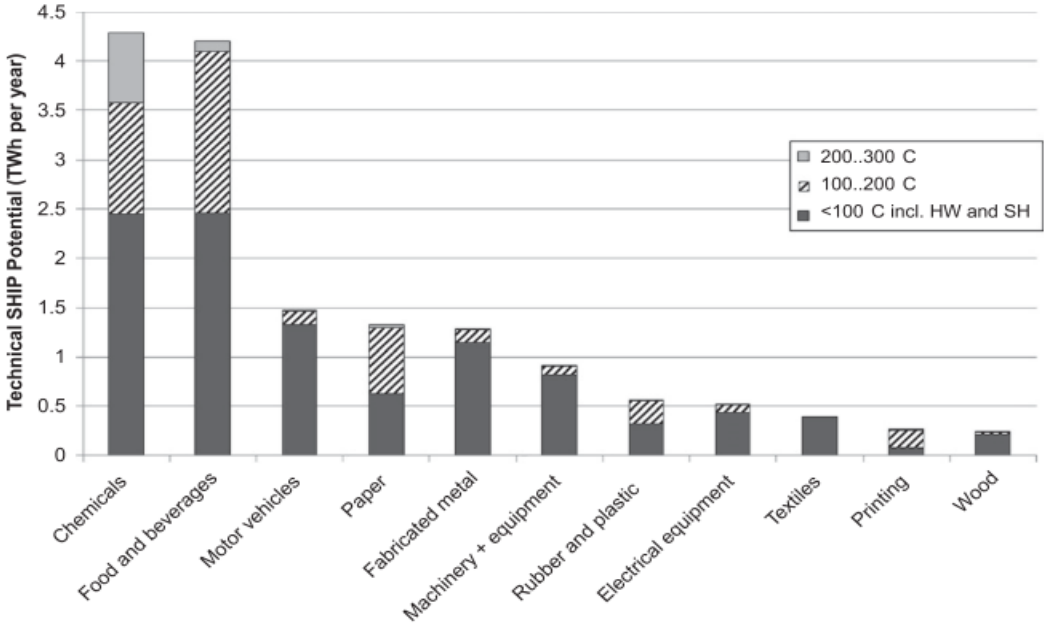

Fig. 2.8. Nine selected sectors' technical potential with temperatures range, Germany (Lauterbach et al., 2012).

A study in Egypt of designing a pasteurization system with FPC during September, October, and November 2009 showed the daily average maximum solar pasteurized milk was 73.9 litres at 63 ℃ temperature, while the lowest was 37.3 litres at 72 ℃ temperature. They were motivated to implement such a system even in winter climate conditions (Fathey Mohamed Atia et al., 2011).

2.7.1. Milk pasteurizing using a heat pump.

With an improved heat pump and heat recovery, carbon emissions in dairy plants can be reduced by up to 33% (Wallerand et al., 2017). The cost drop and availability of renewable energy sources and the developed design of the heat pumps, which has a coefficient of thermal performance between 1.5 - 3.0 (T. N. Anderson & Duke, 2007), led to an exponential utilization of this source in the united states of America growing from 82,000 to 547,694 units just between 1971 - 1979. This cooling and heating solution suits residential, commercial, and industrial facilities.

The heat pump uses the liquid-to-liquid principle to obtain the temperature needed for the pasteurizing (at 63 ℃) and then cools it to 32 ℃, which is the inoculation temperature. As a result of this work, the energy consumption for the heat pump was 4 to 5 times less than the classical systems, as in Fig. 2.9, is more significant than continuously, and we can get more energy from the heat pump than any other primary energy source (Başaran et al., 2021).

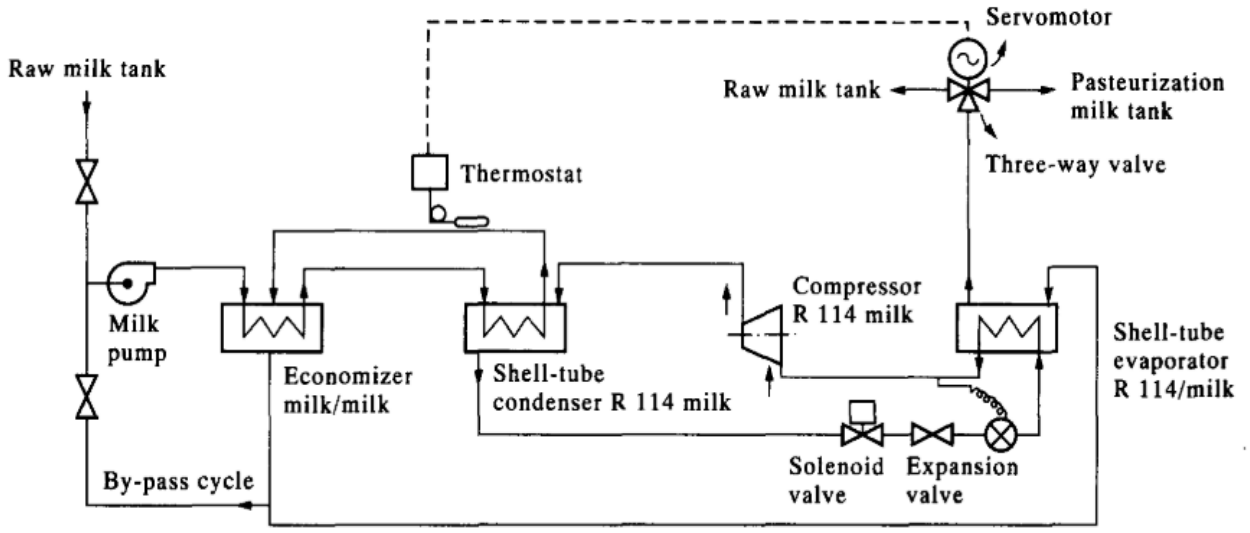

Fig. 2.9. Heat pump integrated with pasteurizer (T. N. Anderson & Duke, 2007).

Energy consumption significantly influences food technology's economy, where no process or procedure does not needs electricity—turning this electricity into heat, usually like pasteurization or sterilization. In addition, the energy needed for cleaning or space heating is sought to recover heat if possible (Walmsley et al., 2015) or utilize renewable energies—for example, the heat recovery of the treated hot milk in the pasteurizing process. After being applied widely in residential apartments, heat pumps can also be used in the food industry. In the soda water, a stage is needed to cool the water from 15 to 10 ℃. A commercial-size heat pump has an electrical capacity of 1.5 - 2.1 kW, resulting in a heat output of 7.5 - 10.1 kW, and this capacity is enough to heat a food industry plant or to generate around 200 litres of water at 60 ℃. Since the evaporating capacity of this pump is 5.8 - 7.8 kW, with 5 ℃ to decrease, the result will be 1000 – 1350 litres per hour can be cooled, which is the amount needed for a small soda water plant (Korzenszky & Géczi, 2016). The geographical position of Hungary makes the soil suitable for geothermal heat pumps, which provide cooling in summer and heating in winter and 4.6 times less energy consumption than traditional sources. As a disadvantage of this system, the heat pump requires an external energy source, making it possible to have a PV solar-assisted supporting system (TÓTH et al., 2017).

2.7.2. Solar air heating

The global installed capacity of solar and wind in 2017 was about 41.4% of 903.1 GW (Lian et al., 2019), and to extend the shelf time, prevent the spoilage of a product, improve food quality, and ease food transportation, air heating systems are used for this purpose (ABPS, 2011). Even though this technology has been used for long time, still new technologies are being improved, as in Fig. 2.10, to develop the convection design and heat storage tank. Where drying is needed in some industries, fossil fuels, coal, or gas are used as an energy source, and this process alone accounted for 50% of the energy demand and expenses. Solar drying collectors can take a role in this area as a cheap solution and give a high, consistent temperature flow rate (Eswara & Ramakrishnarao, 2013). However, it also has some requirements, like capital investment, a backup system, and continuous maintenance.

Fig. 2.10. Direct solar drying for food drying, India (Eswara & Ramakrishnarao, 2013)

The solar dryer has two main classifications firstly according to the flow direction, Direct and indirect, and according to energy, active and passive. Direct flow technology is used mainly for around 30 – 50 kg /batch household level. At the same time, indirect technology is more expensive but with better quality results. Active technology uses a fan to make the air circulation, which reduces the drying time by one-third and space needed six times less, while passive technology uses natural convection or wind energy (Kempener, 2015).

2.7.3. Solar energy pasteurizing

The manufacturing industries are forced now to consider alternative energy solutions due to global warming. Renewable energy is good, but instability and unpredictability are unavoidable energy behaviour. In the food industry, the demand is time-dependent and fluctuates per season, which causes serious problems (Liew et al., 2014). The 100 kW PV system helps to reduce electrical consumption by 39% (Mo, 2016).

New Zealand has high levels of solar radiation and is considered the largest dairy producer globally, with 14 billion litres annually. However, a tremendous amount of energy is needed to treat this vast amount. Solar energy in this sector did not get enough attention even though New Zealand has 30% more solar radiation than Germany. Luckily, in the historical records, solar radiation has its highest density when milk production is the highest in Fig. 2.11. Using the F-chart analysis to simulate the large area solar collector system and determine its suitability and stability for dairy production (T. N. Anderson & Duke, 2007). Four types of solar collectors were examined: FPT, ETC, ETC with CPC, and building integrated solar collectors. It was found that FPT and enhanced ETC with CPC could contribute to heating. Therefore, solar energy is an attractive solution for the future of dairy industry.

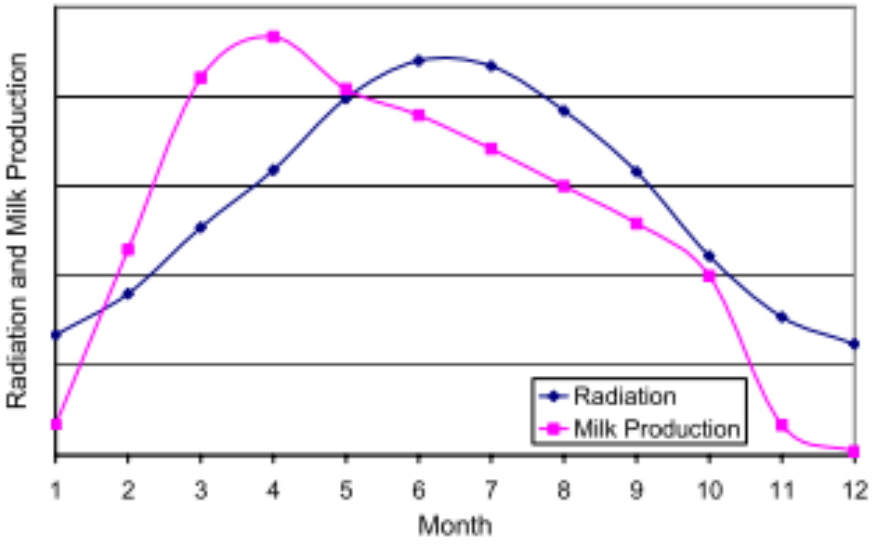

Fig. 2.11. Qualitative relationship between milk production and solar radiation in New Zealand (Anderson and Duke, 2007).

As for the typical dairy plant (T. N. Anderson & Duke, 2007) with 10, 25, and 100 m^3 storage volumes of 50, 75, and 100 litre/$m^{2,}$ respectively, the solar system was modelled for heating temperature from 40 ℃ to 80 ℃. A large-scale dairy factory consumes 120 – 150 m^3 per day for cleaning operations at 80 ℃. The reasearch result shows that a 2000 m^2 collector area with a 100 m^3 solar thermal tank can offer 100 m^3 hot water at 80 ℃ on a daily basis.

2.7.4. Solar thermal energy uptake barriers and market potential

Electricity prices have increased more than four times in the last few decades, giving space for renewable energies since alternatives like LPG, heavy oil, and diesel are also high prices (Rivett-Carnac & Scholtz, 2018). Moreover, half of the global demand stands for heating and cooling (Kasibhatla, 2015), and two-thirds of the industrial energy consumption globally stands for heat processes, with the expectation of one-third rising in consumption by 2040 (Neumann, 2018). Half this heat demand is less than 400 ℃ and 30% below 100 ℃ (SO-PRO Project 2011), making solar energy a perfect solution (Kempener & Saygin, 2014). In contrast, 40 and 41% of the energy used nowadays is from gas and oil in different applications like food, beverages, transportation, textile, and paper. Also, utilizing solar heat technology in the industrial sector has many advantages (Kempener, 2015):

- It eliminates the risk of increased oil, coal, and gas prices.
- No fuel cost.
- It reduces CO_2 emissions.

It must be taken into consideration that:

- Achieving economic scale is affected by the ability of the manufacturers to face the non-sustained demand for solar thermal energy.
- Many parts of the collector can be made locally.
- Industrial-scale solar thermal projects need to fill the gap in the needed skills to optimize the design.

- The costs achieved in Europe are about 400 €/m^2, considering enormous variability of site specifications, high capital costs, and no similar subsidy programs (Kempener, 2015).
- The backup system can result in extra costs.
- Every case is unique in the industry, making the reliability of solar thermal installations low due to the complications of each industry.
- Industrial-scale systems designed especially for the project need certified components to follow the standards.
- Awareness (Kempener, 2015), workers' education, and the government finance industry about such industries are needed.
- Competition from other renewable energies is applied since they can replace heat processes and electricity.
- Low economic growth and uncertainty restrict the industry's desire to invest in new technologies.
- Not enough tools, guidelines and designs (Kempener, 2015).

Even though large scales FPC and ETC have been utilized since the 1980s, significant challenges and problems have been shown, like pipes leaking, dust corrosion, tracking system malfunction, and dust leaking into the collector (Cottrel & Menichetti, 2011).

India, with more than 50% of the world's buffaloes and 20% of the world's cattle (ABPS, 2011), with 300 - 330 sunny days per year, is the largest milk producer of around 13% of the world's production (134 million tons in 2014) with the growth of around 3.6 to 5% annually (Singh et al., 2020). So that, milk and dairy products (cream, ghee, and yoghurt) have a significant contribution to the Indian economy. Since one-third of the energy needed in this sector goes to water heating, and the fuel prices increase, increasing the milk product prices, the industry tends to use new technologies to reduce costs. They lead some companies to make wrong decisions by using lousy quality, polluting the environment, and using dirty fuels. Companies must search for a cleaner, more sustainable solution like concentrated solar thermal (CST) technology. The great advantage is that the steam vapours can be used for all the processes, such as pasteurizing, sterilizing, and washing. While in the traditional process, boiler tanks usually use petroleum fuels for steam generation. Because the temperature needed in the dairy plant is usually less than 80 ℃ (Sandey et al., 2015), a solar collector can produce such demand for almost half of the year. Alternatively, in case of a short harvesting period, the hot water produced can be used for pre-heating before entering the boiler.

Most heat demand that stands as the low temperature is found in food industries, beverages, paper and textiles. In contrast, the medium range is found in the chemical and plastic industries. At least 50% of the energy demand in these industries is in the temperature range below 250, as in Table 2.3 (S. Kalogirou, 2003).

Table 2.3. Temperature range demand for the food and beverage industry

Industrial sector	Unit operation	Temperature range (°C)
Food	Drying	30 - 90
	Washing	60 - 90
	Pasteurizing	60 - 80
	Boiling	95 - 105
	Sterilizing	110 - 120
	Heat treatment	40 - 60
Beverages	Washing	60 - 80
	Sterilizing	60 - 90
	Pasteurizing	60 - 70

2.8. Solar collector types

2.8.1. Flat-plate collector (FPC)

It is the most common collector used nowadays because it is cheap and offers a temperature between 30 – 80 °C, as in Fig. 2.12. Usually, with stationary motion and little maintenance, the absorber absorbs the direct and diffusive radiation after passing the transparent cover and reaching the absorber plate. Thus, the solar radiation becomes thermal energy transferred by a medium thermal fluid in tubes or ducts. In order to avoid frost damage, mainly in countries where the temperature falls below 0°C in winter, the water/glycol mixture is the best medium.

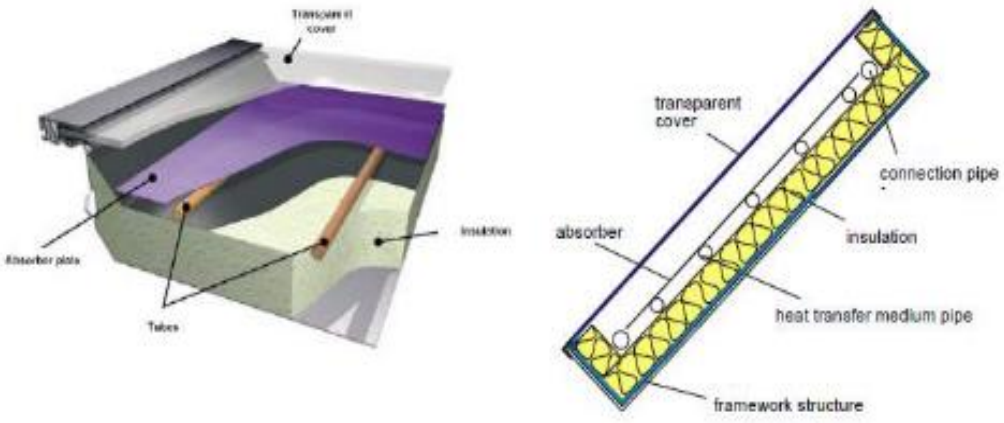

Fig. 2.12. Flat-plat solar collector (Cottrel and Menichetti, 2011).

2.8.2. Advanced flat-plate collector (AFPC)

With high heat losses and improvement needed to cope with high operating temperature ranges, the FPC is being improved and developed to operate at temperature ranges up to 80 – 150 ℃ (Beikircher et al., 2014) by improving the following (Suman et al., 2015):

- Using multiple anti-reflective (AR) glasses instead of a single glass.
- Filling the sealed collector with inert gas.
- Creating negative pressure in the collector (vacuum).
- Using nanofluids.
- Selective coatings.

Those solutions lead to less thermal energy loss and higher optical efficiency, as in Fig. 2.13.

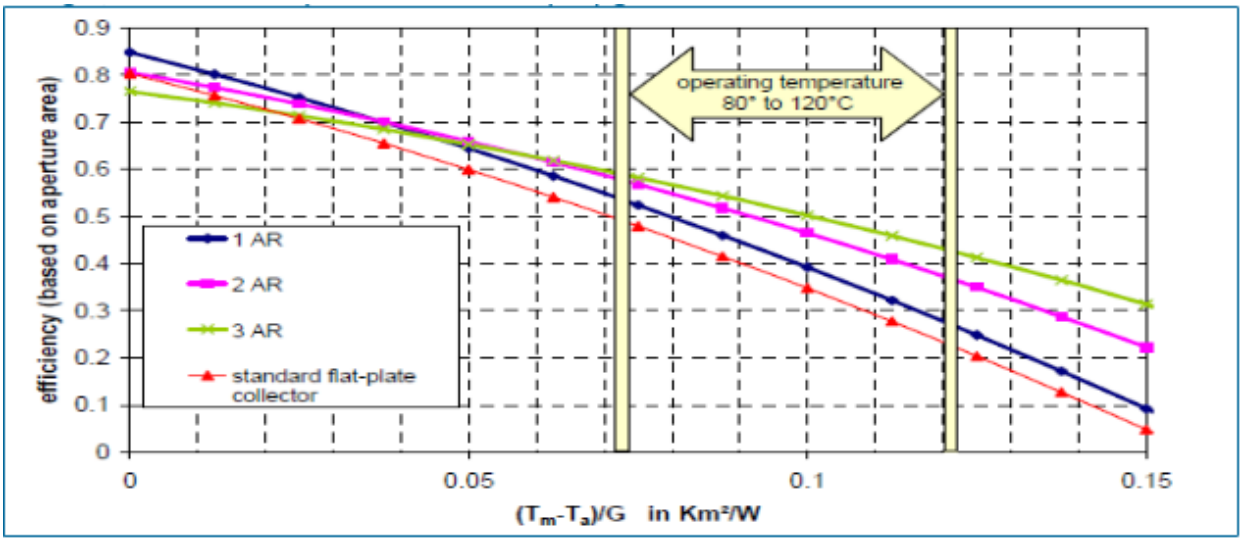

Fig. 2.13. Efficiency comparison between standard FPC and AR glass

(Cottrel & Menichetti, 2011)

2.8.3. Evacuated tube collector (ETC)

C is standard in the market and achieves higher temperatures than FPC, from 50 – 130 ℃ (Sabiha et al., 2015). It is characterized by stationary motion and collecting direct and diffusive radiation. It is made of vacuumed glass tubes where the absence of air reduces conduction and thermal convection losses.

The main characteristics are:

- Each collector consists of a row of parallel glass tubes.
- Inside each tube, the pressure is $<10^{-2}$ Pa.
- The shape of the glass is a tube always to stand the negative pressure.

The evacuated tubes in Fig. 2.14 have a barium indicator where the silver colour turns white in case of air presence, which means the tube is in bad condition (Cottrel & Menichetti, 2011).

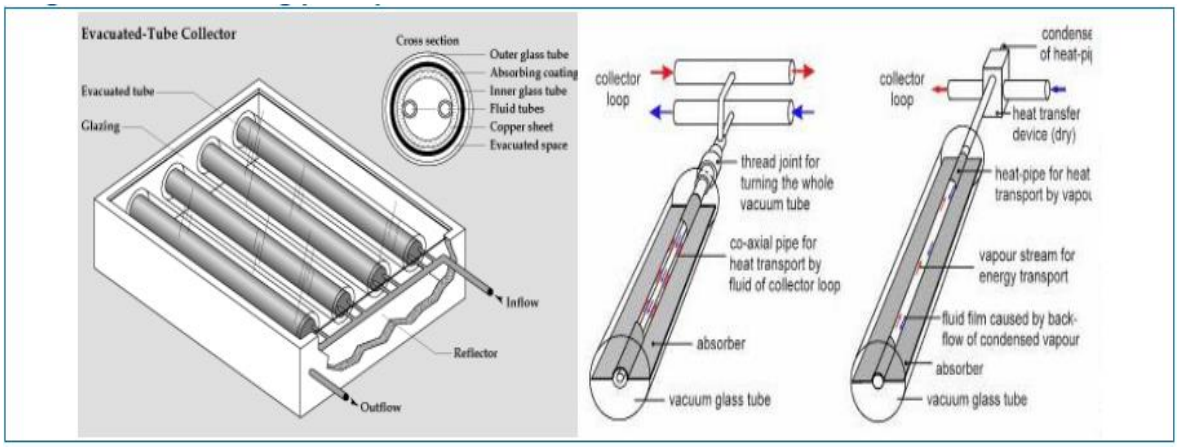

Fig. 2.14. The evacuated tube collectors technology (ETC) (Cottrel & Menichetti, 2011)

2.9. Phase change materials (PCM)

To allow the heat or cold to be used later, thermal energy storage (TES) is used (Kasibhatla, 2015):

- Seasonal solar energy storage.
- Waste heat recovery in the industry.
- Efficiency is improving in district heating, cogeneration plants, heat pumps, and solar thermal collectors.

According to a chemical and physical process, two methods are available (Crespo et al., 2019), as in Fig. 2.15.

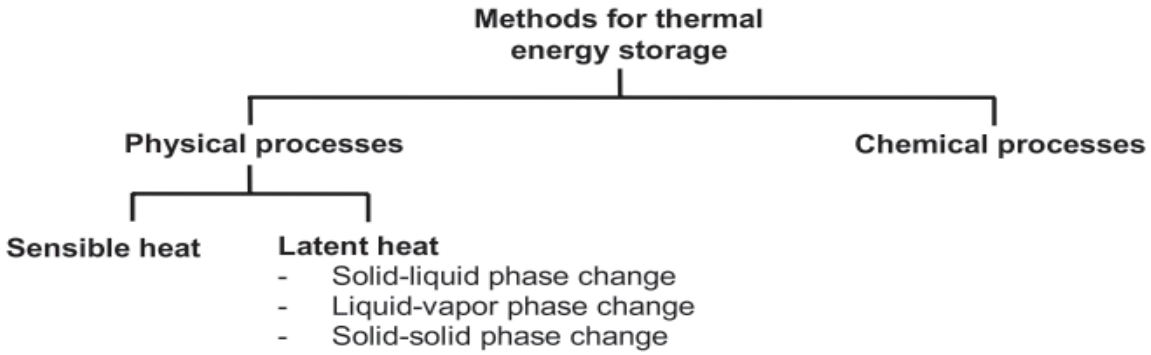

Fig. 2.15. Physical and chemical processes.

Luckily, more than 100 PCMs can be used in this range (Crespo et al., 2019), where inorganic eutectic composites have a high potential to be used due to their fusion heat energy. The last estimation for the European Union is that 15% of the total energy demand is for industrial purposes. Over 50% of the total demand is for industries where the temperature needed is below 250 °C (Jitjaroen et al., 2011). According to this study, solar fraction for medium temperatures can reach 66% for food, 58% for chemical industries, and 30% for textile industries (S. Kalogirou, 2003).

2.9.1. Physical, economic, and technical requirements of PCMs

The appropriate melting temperature and the high melting capacity are the precise requirements for choosing a PCM. However, more requirements are needed when the process reaches a commercial and industrial level, as in Fig. 2.16.

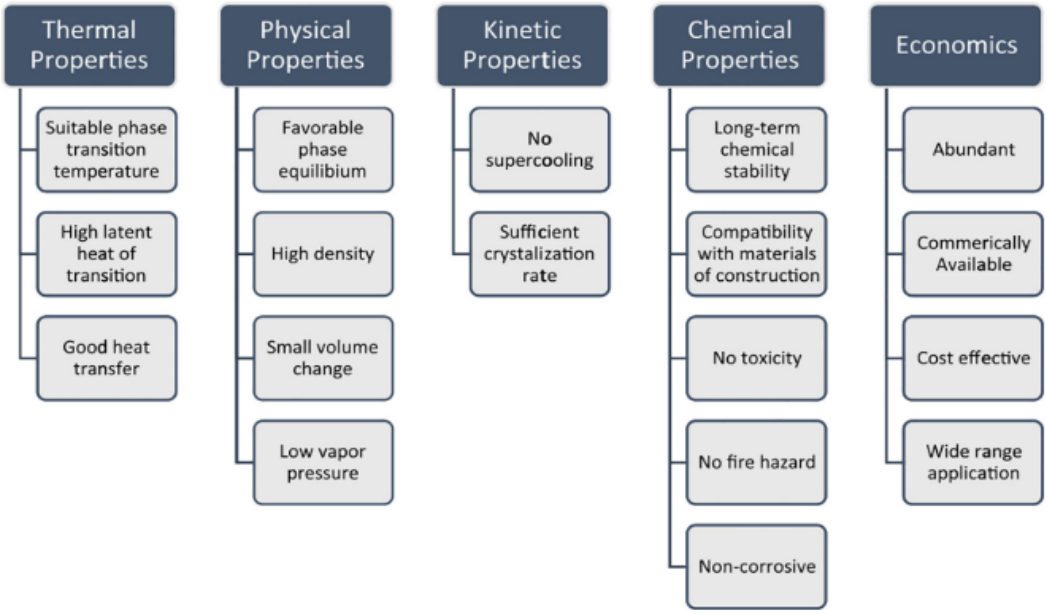

Fig. 2.16. Characteristic properties of LHTES (M. M. A. Khan et al., 2017)

The physical requirements are considered the most critical properties to choosing PCM, and it is as the following:

- Appropriate phase change temperature T_{pc} as in Fig. 2.17.
- A significant phase change in enthalpy Δh is needed to achieve high storage density.
- Cycling stability to ensure the thermal behaviour of the PCM for a long time: This varies from one in the case of PCM fire protection to a couple of thousands in the case of TES.
- Little subcooling, where the PCM temperature falls below the melting temperature until the material starts to solidify again and starts heating.
- High thermal conductivity

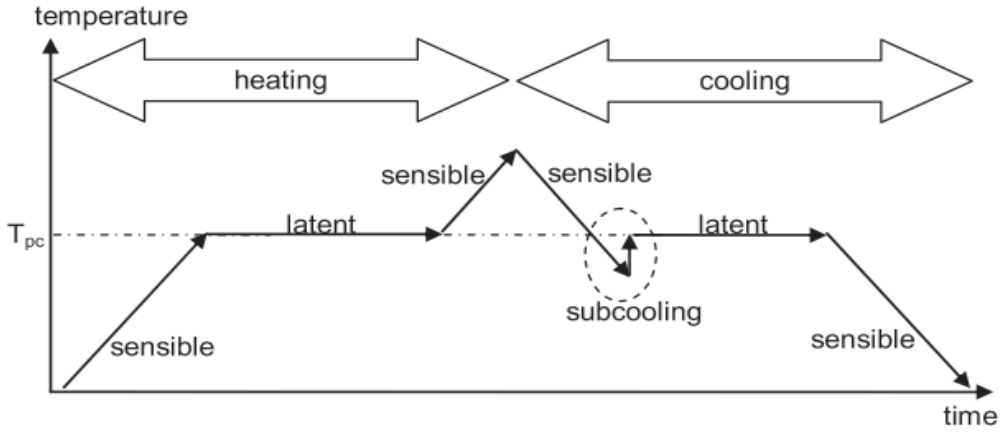

Fig. 2.17. Temperature versus time of PCM (Harald Mehling; Luisa F. Cabeza, 2008)

The chemical requirements are:

- Low vapour pressure to increase the safety factors.
- Small volume change.
- PCM compatibility with other materials, mainly the vessels.
- Safety constraints.

The financial requirements are:

- Low price.
- Recyclable for environmental reasons.

The PCMs cannot usually fulfil all these requirements, but the first material section usually covers physical properties, like PCM melting temperature, enthalpy, stability, and subcooling. However, the thermal conductivity of PCMs is usually, and the inorganic PCMs have subcooling. Furthermore, an investigation for compatibility is needed (Harald Mehling; Luisa F. Cabeza, 2008). So, different strategies have been developed to make better properties of PCMs.

2.9.2. Nano-enhanced PCM characteristics

Nanotechnology enhances the properties of the PCM (Leong et al., 2019) as it improves the following:

- Suitable temperature range
- High thermal conductivity
- High latent heat energy
- Small phase transition change volume
- Low cost
- Safe
- Stable
- High thermal diffusivity

2.9.3. PCM classification

Due to the low thermal conductivity and the high-volume increase/decrease due to the phase change of PCM, beeswax can be used due to its availability and high latent heat (Putra et al., 2019). Table 2.4 shows the differences between paraffine and non-paraffine waxes.

Table 2.4. difference between paraffines and non-paraffines (Khan, Saidur, and Al-Sulaiman, 2017)

	Advantages	**Disadvantages**
Paraffines	Safe Reliable Predictable Less expensive Non-corrosive Low vapour pressure	Low thermal conductivity High volume change when the phase change Non-compatible with a plastic container Slightly inflammable
Non-paraffines	Thermal stability Chemical durability Non-corrosive Non-toxic Available Narrow temperature range	Highly inflammable Low fusion heat Low thermal conductivity Toxic Unstable at high temperatures

In solar thermal applications, specific categories of PCM are organic, inorganic, and composites (organic-organic, organic-inorganic, and inorganic-inorganic). Even though organic is the most common PCMs (paraffine and non-paraffine), inorganic are also used due to their low cost and low volume phase change. Currently, the most studied PCMs are the composites to go over the shortcoming behaviour of organic and inorganic PCMs. Organic PCMs have many advantages: High latent heat fusion, an extensive range of phase change temperatures, and Stable and recyclable. However, the low thermal conductivity restrains the storage/release process up to 5000 times. To go over the low thermal conductivity and phase change volume issues, inorganic PCMs were invented with the great benefit of low cost and high latent heat fusion energy. However, it still has some disadvantages, like corrosion and supercooling, which leads to the extra equipment required to ensure the service life process of the PCM (Qiu et al., 2019). The most common inorganic types are metallic, and slat hydrates with a high melting temperature and thermal conductivity.

2.10. Thermal energy storage (TES)

Energy is usually stored and retrieved as sensible heat, latent heat, or thermo-chemical reaction, all through a change in the internal power of the medium. Firstly, sensible heat storage (SHS) stores by raising the medium's temperature. At the same time, latent heat storage (LHS) utilises the absorbed/released heat when the storage medium changes its phase from solid to liquid, liquid to gas, or vice-versa. The PCM is a latent storage material that absorbs heat almost constantly. This process remains until the whole PCM is transferred into the liquid phase. While the surrounding temperature falls, the PCM starts to solidify, which releases the stored latent heat. The usual range of the melting temperature is wide (from -5 ℃ up to 190 ℃). Within the human comfort zone (20 – 30 ℃), some PCMs are very useful, allowing 5 to 14 times more heat density than conventional storage mediums like water or rocks (Kanimozhi & Bapu, 2012; Zalba et al., 2003).

In China, 28% of the total energy demands account for buildings heating, and integrated PCM within solar TES can result in up to 83.6% solar fraction with 31.7% system efficiency (Ling et al., 2016). There are many integrating possibilities for industrial hot water storage tanks because there are different types of tanks, like constant or variable volume. Alternatively, it can be integrated into the charge and discharge phase of the buffer tank. So, based on the configuration and the tank type, solar heat can maintain the storage temperature or preheat the water or steam. Preheating systems have an open loop, as in Fig. 2.18 integration, where the heated water from the solar system goes to a conventional process heater before being used in the industrial process to ensure the needed temperature. Unlike the open loop, the closed loop in Fig. 2.19, the system contributes directly to the industrial heat process.

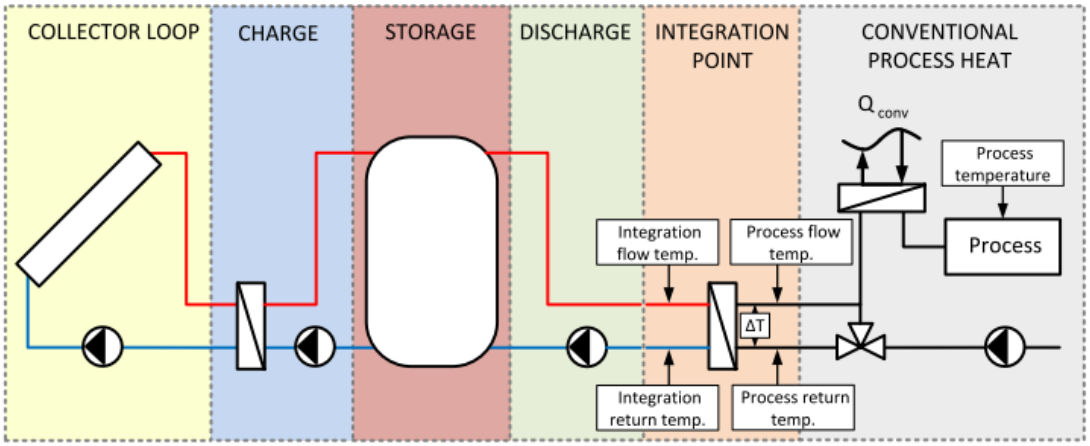

Fig. 2.18. Open-loop SHIP integration subsections for preheating systems (Muster et al., 2015).

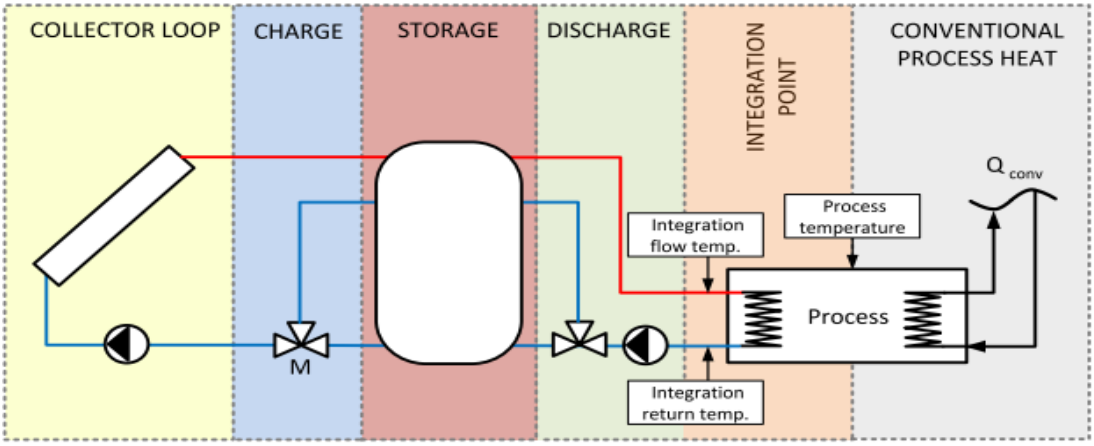

Fig. 2.19. Closed-loop SHIP integration subsections for preheating systems (Muster et al., 2015).

A critical factor is the integration return temperature, which returns after the integration point. This temperature can be constant or varying depending on the system, but at low temperatures, we can have higher system efficiency (Muster et al., 2015).

A moderate amount of thermal solar energy can be stored in phase change material during the daytime and released at night for hot water services or to prevent freezing, antifreeze mixture is used in cold regions when the temperature is less than 5 °C (Chantawong, 2019). In addition, PVT collectors can increase their output power and electrical efficiency by enhancing thermal convection using the PCM sheet (Choubineh et al., 2019). Alternatively, prevent solar collectors from frosting under low temperatures (Zhou et al., 2019).

To fully utilize the solar system heat storage tank as one of the main components of this system and to maintain the extra energy harvested from the sun till the next day or for space heating or demand at night (M. M. A. Khan et al., 2017). Phase change materials suit this requirement due to its thermal behaviour (Wang, Zhang, Dou, et al., 2019). However, due to the low thermal conductivity of the PCM, a diamond foam (DF) with three-dimension (3D) is proposed. The results showed a faster thermal response and an excellent enhancement for the thermal conductivity due to the high thermal conductivity interconnected to the diamond networks. In addition to a fast charge latent heat energy rate of 124.7 kJ/kg and improved shape stability, it is suitable for TES and porous support PCM (Huang et al., 2019; Zhang et al., 2019).

The usage is the central core to choosing between latent heat thermal energy storage (LHTES) and sensible heat thermal energy storage (SHTES), each with advantages and disadvantages. With a more dynamic range and a faster and more straightforward charge/discharge process, SHTES are good but with low thermal storage capacity. At the same time, LHTES has a higher storage capacity with a slower charge/discharge process, while new approaches to have a nervous system of LHTES and SHTES, where both characteristics of the two systems can be achieved. LHTES configured with fins and lauric acid PCM can enhance the storage tank's performance (Deng et al., 2019). It is found that LHTES is more stable than SHTES under variations of solar irradiation.

In contrast, LHTES acts more sensible when low temperature, low irradiation and short-time heat storage conditions (Bie et al., 2019). With different positions of the PCMs capsules and different flow rates (1,3,5,7 and 9 l/min) leads to not just stability in the output characteristics but also in the thermal stratification efficiency and mainly when the PCM balls are smaller in diameter and closer to the inlet (Wang et al., 2020; Wang, Zhang, Huang, et al., 2019). Also, using nano-PCMs for LHTES can achieve optimum thermal performance for an acceptable price for domestic and commercial applications (Z. Khan et al., 2019), knowing that in industrial applications, the solar thermal system can harvest higher yields (Lauterbach et al., 2014). Conventional PCMs have long charge/discharge times due to their low thermal conductivity, but micro/nano PCMs give noticeable thermal conductivity results and boost the charge/discharge process (Leong et al., 2019; Qiu et al., 2019). For example, sodium acetate trihydrate can be a solution with 10 weight per cent can shorten the time by 78.5% of the charge/discharge process (Liu et al., 2019). A lauric acid/SiO_2 Nanocapsulescan reach 165.6 kJ/kg as latent heat energy (Yuan et al., 2019).

Concentrated solar power systems (CSP), as suitable dispatchable renewable energy generation contributed by TES, are a perfect solution (Barba et al., 2019). The molten salt in the TES is the most used technology in commercial CSP. However, researchers seek cheaper and more thermal efficient solutions, and the PCM has the potential to be taken apart due to its low costs and thermal properties (Almsater et al., 2019; Qiu et al., 2019; Sheng et al., 2019). The four buckets of PCM chosen due to the appropriate melting temperature and the material’s latent energy showed similar results to the traditional indirect two-tank molten salt concept, where the annual power production and the net production are well matched (Prieto & Cabeza, 2019).

2.10.1. Sensible heat storage (SHS)

It is the most common type, where the transferred heat to the storage coverts in temperature change of the storage medium as in Fig. 2.20.

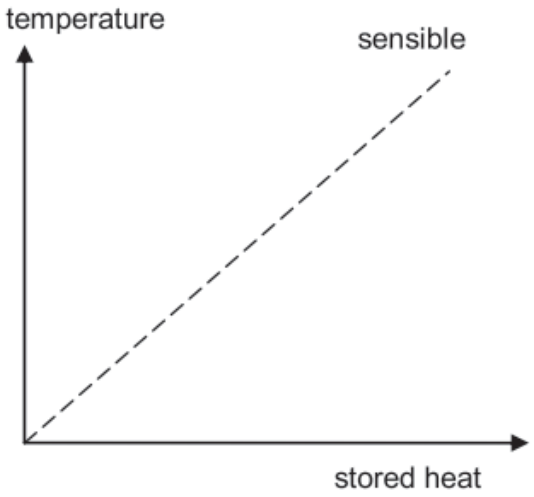

Fig. 2.20. Sensible thermal energy storage behaviour (Jouhara et al., 2020).

To calculate the energy stored in the storage ΔQ, the temperature change ΔT and the heat capacity C are needed:

$$\Delta Q = C \cdot \Delta T = m \cdot c \cdot \Delta T \quad (2.2)$$

Where:

ΔQ the stored energy in the storage (kJ)
m the mass of the material (kg)
c the heat capacity (kJ/kg ℃)
ΔT is the temperature difference (℃)

The main specifications of SHTES are (Buzás et al., 2005):

- High thermal capacity
- High melting point
- High thermal conductivity
- Stability
- Low cost

2.10.2. Latent heat storage (LHS)

If the latent heat is stored, PCM has been used. With several advantages and disadvantages, if a suitable material is chosen, PCM can store a high heat storage density and no toxicity (Ling et al. 2016), making LHTES a good choice for building energy storage. The usual phase change volume is around 10%. After and before the melting process, the process is sensible. Since the temperature is constant, the solid and liquid enthalpy difference calculates the heat stored. It is called the heat of fusion. Fig. 2.21 shows the correlation between temperature and time in LHTES.

$$\Delta Q = \Delta H = m \cdot \Delta h \quad (2.3)$$

Where:

ΔQ the stored energy in the storage (kJ)
m the mass of the material (kg)
Δh the enthalpy difference (kJ/kg)

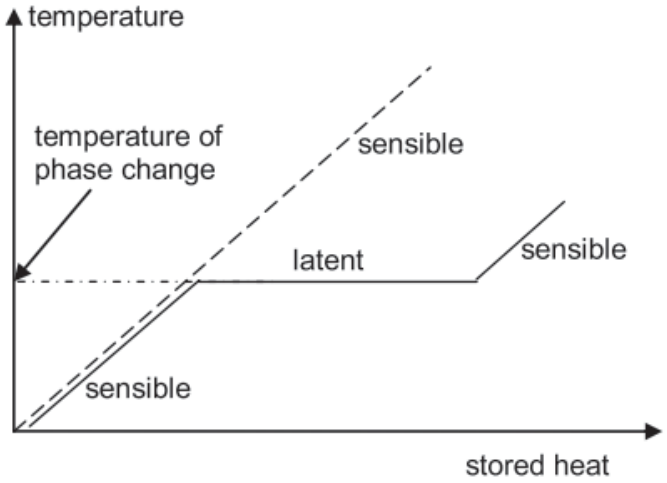

Fig. 2.21. The features of LHTES materials are that it has high energy density and flexible temperature range (Cabeza & Oró, 2016).

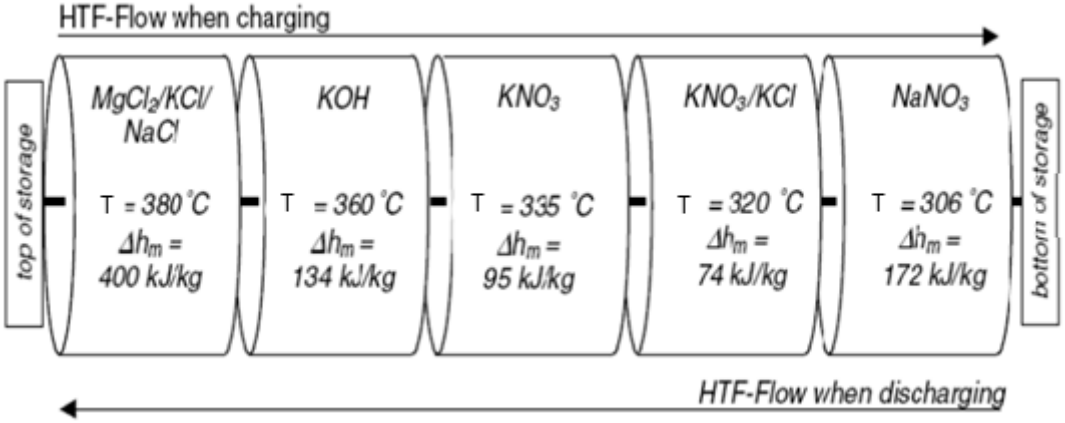

Fig. 2.22. Up to 350 ℃ schematic of cascade LHTES (Muthukumar, 2005).

A domestic space heating PCM can store 3 - 4 times more energy per volume than a sensible heat can, which makes a significant advantage. A sensible heat energy storage tank for domestic hot water integrated with PCM with direct and indirect heat exchange is simulated for single-family houses (Najafian et al., 2015). The valuable result regarding the solar fraction is the energy contribution from the sun to the dispersed needed residential load. As a result, 40% of the tank's volume can be reduced if 50% volume fraction PCMs are integrated. It is essential to choose the PCM due to its melting temperature, which prevents significant temperature fluctuation in the system (Abdelsalam et al., 2020).

2.11. Solar thermal energy usage in other industries

The textile industry in Germany has experienced solar thermal energy in the " Soltex " project through a parabolic trough solar collector with a nominal capacity of 70 kW, which has been running since September 2013 without any serious problems. This project has a COP of 10.1 and an energy fraction of 81%, saving 2.8 MWh (Frey et al., 2015).

In developing countries, contaminated water or drinks still have a significant role in death and diseases, even in the developing world (Abraham et al., 2015; Zahira et al., 2009). Even though

the contaminated water can be treated at different temperature levels by many solutions, solar pasteurising is promising and affordable. Only 2 m^2 solar collectors can achieve around 80 litres of water per day in clear sky conditions. (Carielo et al., 2017). Moreover, the highest achievement happens between 60 – 100 l/m^2 for a constant TES. A developed solar system with a solar tank and appropriate control strategy (Schramm & Adam, 2014) showed increased solar yield by up to 25% for heat process plants, even in low radiation conditions.

A one thousand square meters solar thermal system for a dyeing plant in Tunisia was analyzed with static energy and water consumption and a heat recovery system. Natural gas is used and costs 0.12 €/m^3. The used temperature of 60 ℃ gives the solar thermal FPC field high potential (Frein et al., 2014). Also, SHIP is considerable by using ETC for canned tuna fish in Spain, as in Fig. 2.23 (Quijera et al., 2014).

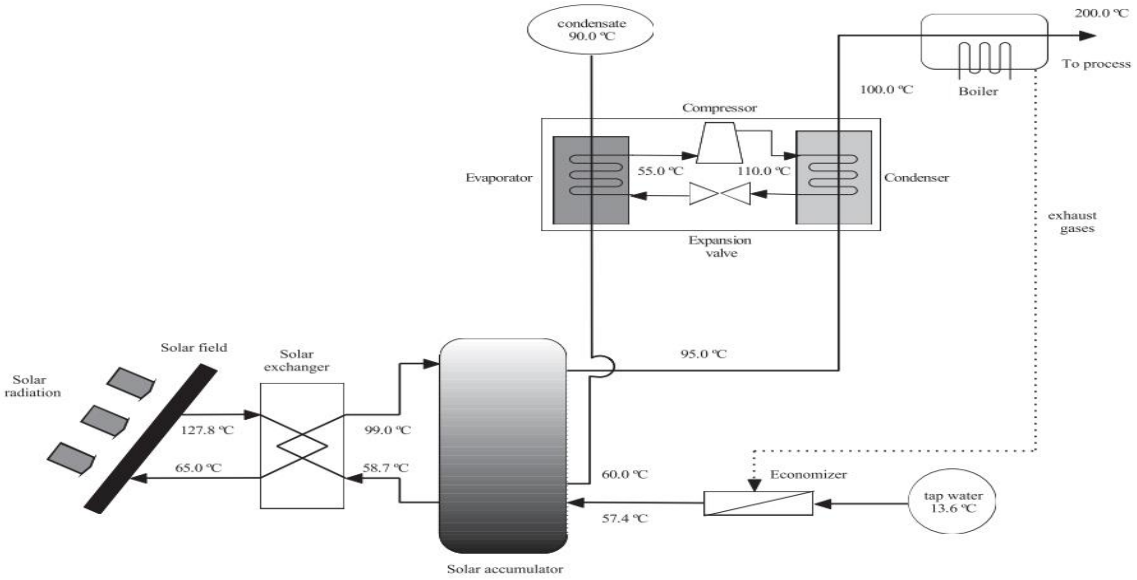

Fig. 2.23. Schematic diagram of the canned fish solar thermal system (Quijera et al., 2014).

(Carielo da Silva et al., 2016; Carielo et al., 2017) Have proposed a solution for decontaminating the water, as in Fig. 2.24, in the semiarid regions, such as Brazil's northeast part. The lack of physical and chemical water quality and water shortage are challenging. In this area, where solar radiation is high, using a solar system in water treatment is possible. In this research, an automatic microbiological decontamination system was used. Many characteristics like turbidity, pH ratio, and others control the system. As a result, the system made treated water based on temperature and time intervals of 3600, 2700, 1800, 900 and 15 s at 55, 60, 65, 75 and 85 ˚C, respectively. Suppose the heat recovery system heats the water before entering the solar collector. In that case, it will be of great importance to increase productivity by approximately 50%, which will allow the system to start working at lower solar irradiation at 8.3 MJ/m^2. Furthermore, using the heat exchanger is essential since it gives extra productivity of about 10% more and a significant reduction in the cutting level of solar irradiation at about 6.6 MJ/m^2. This solution leads to a stable temperature at 85˚C for 15s, showing the absence of the total coliforms and Escherichia coli and a 98.7% average reduction of heterotrophic bacteria at different water samples.

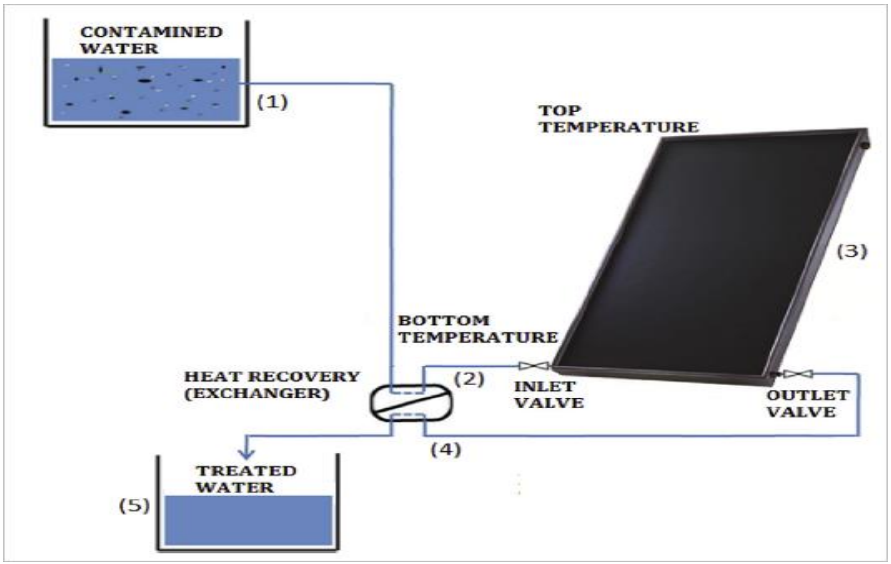

Fig. 2.24. Schematic diagram of the system with the heat exchanger and electrical control of the inlet water to the solar collectors (Carielo et al., 2017)

2.12. Solar process heat systems modelling

Until now, in an industry where profit means everything, on the first hand, the solar thermal system still costs more than a conventional boiler using fossil fuel or gas. So, this is how the decision is made. On the other hand, the main reason is still the lack of knowledge about this energy and its possibility in the industry. Significant time, budget, and financial means are currently needed for industrial companies in order to be able to present the profitability of a solar thermal system. It would be easier to provide accessible, simple, and accurate estimations and feasibility studies if the software can handle it (Asgharian & Baniasadi, 2019). If so, the restraint will be lowered, and the potential of having such systems in the industry will be higher. This tool can give fast, location-dependent estimation of a solar thermal system's gain based on hourly radiation data.

Many tools have been developed to calculate the energy outcome of a solar thermal system, like TRNSYS (S. Kalogirou, 2003; S. A. Kalogirou, 2001), Polysun, and T*Sol. Those tools are usually closed-source, complicated, and, in many aspects, are not editable. Despite a limited number of systems' templates, T*Sol gives accurate model results, where we can edit or create our system. T*Sol and Polysun software has a simple interface compared to TRNSYS, where experience is needed to handle the simulation. Over these three tools, Polysun gives the most significant advantages of the editable system, pre-designed models, editable source code, accuracy, and free charge.

This approach was started by (Frasquet, 2016), as in Fig. 2.25, to make an open-source online page for solar heat in industrial processes (SHIP). However, it has uneditable meteorological data, making thresholds to specify the location data. Although SolGain has limited location data, it allows adding the weather data in TMY format (Ilchmann et al., 2015).

Fig. 2.25. SolGain input and output system boundary (Frasquet, 2016).

Low- to medium-temperature solar collectors can be employed in the food industry, where a wide range of processes uses a temperature between 60 – 80 °C. In southern Europe, 15% of the energy demand is for industrial heat processes. With four types of collectors, the annual energy gain in Cyprus is between 610 – 910 kWh/m^2, and the resulting cost from the solar heat system is between 0.028 - 0.05 €/kWh, depending on the collector type. Low to medium solar stationary collectors have recently developed well, resulting in a good relationship between cost and performance. The system consists of a solar thermal system array, a circulating pump, and a storage tank, as in Fig. 2.26. All the control systems are needed, and a thermal safety valve activates when the storage tank temperature exceeds the pre-set value. The simulation uses the mean monthly ground temperature for the mains water.

Moreover, when the storage temperature exceeds the needed temperature, it will be mixed with the mains water to reach the required temperature. If there is no suitable temperature in the storage tank, an auxiliary heater will be used before the output. A typical meteorological year (TMY) for Nicosia is used, with daily average solar radiation of about 5.4 kWh/m^2 on the horizontal plane; Cyprus has high solar potential where the sunshine hours vary from 5.5 in winter to 12.5 in summer. Resulting in 2.3 kWh/m^2 daily global solar radiation in December and January, and 7.2 kWh/m^2 daily global solar radiation in July.

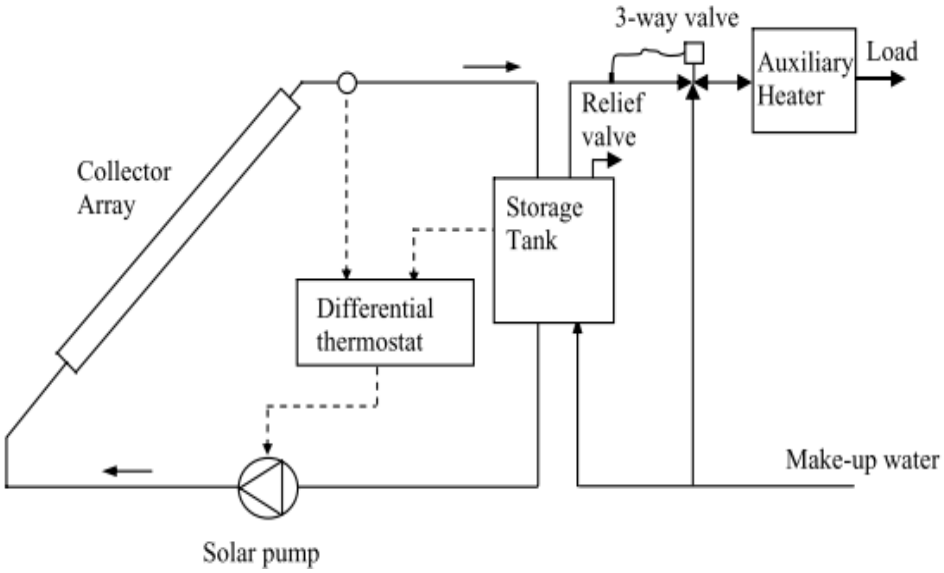

Fig. 2.26. Emerging existing heat supply with solar system (S. Kalogirou, 2006).

The study specifies a temperature between 60 – 180 °C as a load with a flow rate of 2000 Kg/h with one shift per day from 8.00 AM - 4.00 PM and the following assumptions: The gross area of the collectors is 400 m^2 and inclined as the local latitude 5º, while CPC is inclined 35º. The length

of the pipes is 30 m long, so the heat losses are included. The storage tank capacity is 25 $m^{3,}$ and the collector circulation rate is 6 kg/s. The results showed no relation between the system performance and the load. Moreover, as in Fig. 2.27, all systems perform well for low-temperature demand water and have a more than 85% solar fraction. Furthermore, the ETC shows the best energy contribution with the highest solar fraction, and the worst is the FPC, which gives the final decision to the essential factor, which is the economic factor.

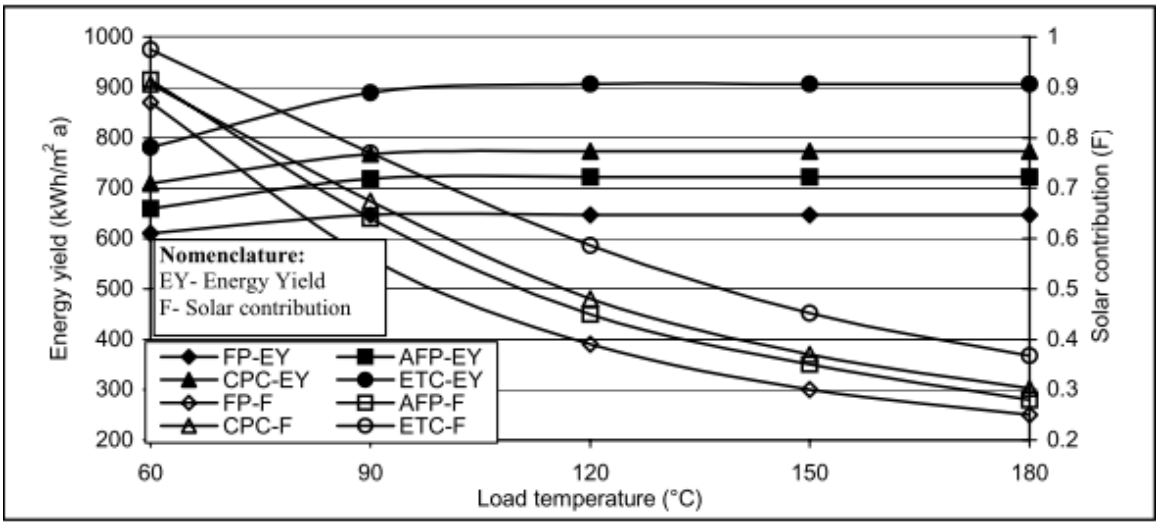

Fig. 2.27. Annual energy yield and solar fraction for different systems (S. Kalogirou, 2006). FPC- flat-plate collector, CPC- compound parabolic collector, ETC- evacuated tube collector, AFP- advanced plate collector.

2.13. Hungarian energy status

All over the Europe Union (EU), solar water heater systems are given financial incentives to encourage the usage of renewable energy, except for Finland, Greece, and Denmark. In Hungary, which is part of the "Visegrád group - V4 group," solar capacity has increased tenfold in the past three years (2017 - 2020) due to the favourable investment environment and the lower cost of solar technology (Lados et al., 2020). Hungary also has ten solar power plants with more than 10 MWp and five solar power plants under 10 MWp spread all over the country (Kumar et al., 2021). Moreover, 40% of the energy consumed goes for heating and cooling (Hungarian Ministry of National Development, 2012). Since energy security is a worldwide concern, all nations have framed energy policies in contrast with sustainable growth.

Similarly, the EU framed two targets (by 2030 and 2050) to reduce greenhouse emissions by at least 55% compared to 1990 (Khanam et al., 2017). Reducing carbon emissions is a significant challenge in all EU and especially V4 countries due to the dependency on conventional energy sources. The EU aims to increase the renewable energy share to 32% by 2030, while Hungary plans for 21% by 2030, and the current status reports that the renewable energy share will be 12% in 2019 (Dyduch & Skorek, 2020). According to the available records, solar, biomass, biogas, hydro, and wind are the most significant resources in Hungary, as in Fig. 2.28. Biomass was the primary renewable energy source for energy production, and it was reduced drastically in less than ten years from 67% to 48%.

On the other hand, bio-based sources have increased slightly, and wind and hydropower have maintained their share. In contrast, solar energy has the most extensive share growth in the last decade, from almost 0% to 16% (coefficient of determination $R^2 = 0.9902$). If the trendline and

conditions remain the same, it can reach more than 30%. Consider that the new technological advancements can positively affect the long-term aims.

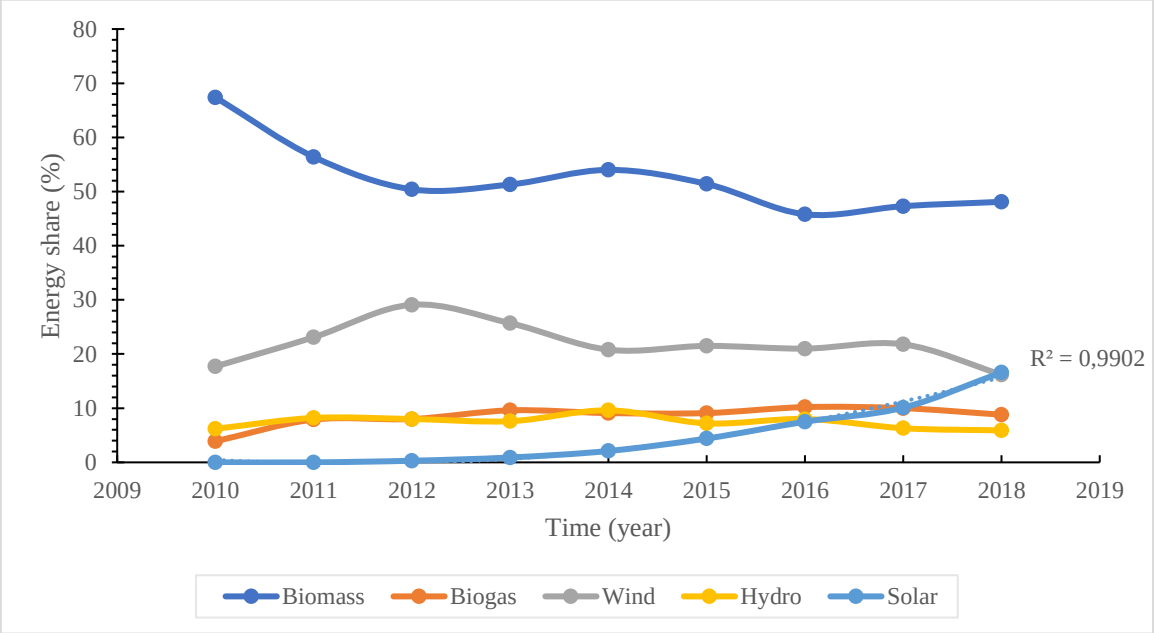

Fig. 2.28. Review of various renewable energy sources in Hungary between (2010 - 2018)

Several solar parks with small to high-power capacities were installed throughout Hungary in the last decade. According to the Hungarian solar Association, the growth parameters have doubled in the last few years. Comparing it with the neighbourhood countries is essential to unfold the potential capacity. For example, Germany has the highest number of solar panels in Europe, though Hungary has 50% more solar radiation than Germany throughout the year. Moreover, in Vienna, Austria, the annual solar radiation is less or equals Budapest, Hungary. Nevertheless, Austria is the world-leading country in solar water heating systems regarding the thermal energy produced (kWh) per 1,000 capita (Jahangiri et al., 2021). Two clusters with more significant and lesser than 10 MWp solar park capacities were studied to determine more accurate results. The graph confirms that the expected growth of solar parks is more significant than 10 MWp if further developments are achieved in this technology.

The regional map analysis helps visualize the region's current falling and irradiance scenario. The recorded global irradiance data is a powerful tool for accurately predicting solar potential (Urbán et al., 2022). According to the regional maps, Hungary receives the highest region V4 in annual irradiation of 1200 - 1400 kWh/m^2. So, the annual energy generation prediction was the highest, with a range of 900 - 1050 kWh/m^2. While the optimally inclined collectors can harvest 1300 - 1600 kWh/m^2 energy per year, and the annual energy production is 975 - 1200 kWh/m^2, as in Fig. 2.29.

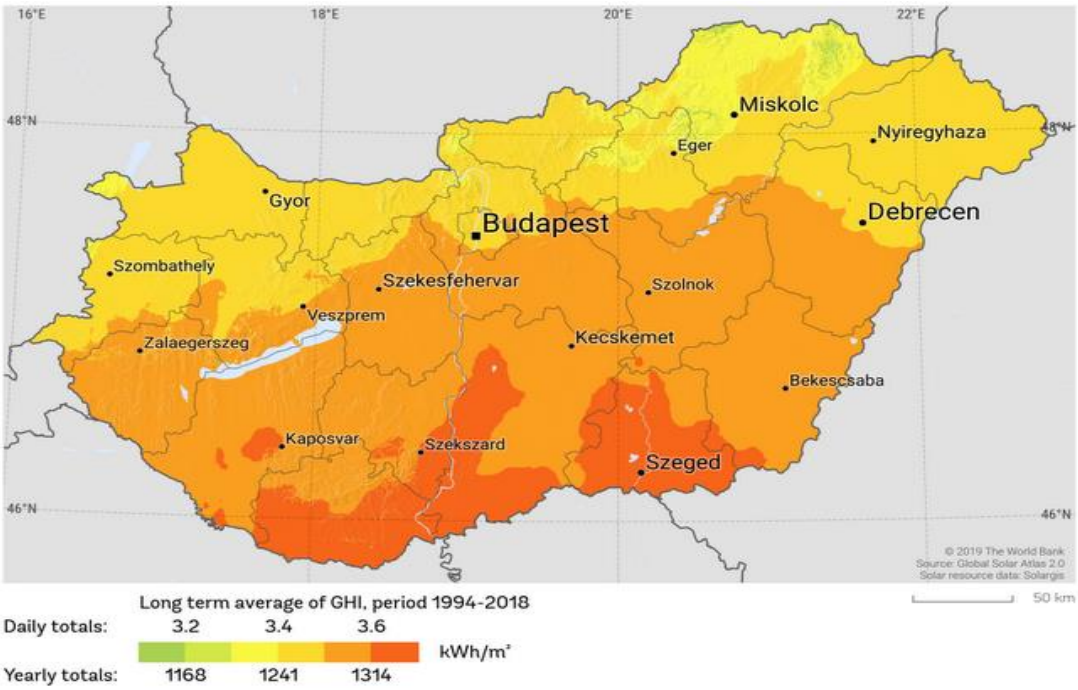

Fig 2.29. Long term average global solar radiation on a horizontal surface in Hungary

2.14. Summary of literature review

The main goal of this literature is to bring to bear that solar thermal systems are used widely everywhere in the globe to substitute fossil fuels and to mitigate environmental impacts. However, advanced solar thermal collectors, like AFPC ETC, achieve up to 150 ℃. However, the usage of those technologies in the industry remains under one per cent because of low awareness, integration difficulties, lack of pre-designed projects, and complex modelling.

The food and beverage industry is essential and available everywhere. Luckily, the temperature range used is usually less than 100 ℃. It is giving the chance of solar thermal systems to provide this demand. Integrating such systems requires a deep study of the plant to determine the appropriate points for integration. However, the literature shows two main designs: one for preheating, where the solar thermal system works as a support system and another for directing heating systems, where the solar thermal system is integrated directly into the industrial heat process. Anyhow, for any new plant, the integration points must be justified in the scheme of the plant.

According to the literature, the direct heating method of pasteurizing and sterilisation has been done experimentally. However, the annual performance and the solar fraction are not identified due to modelling difficulties. Until now, the modelling programs are unavailable or very expensive. Expertise is needed due to the usual difficulties in using the program interface and the extra thermal energy harvested, which can be stored in solar thermal tanks integrated with latent or sensible PCMs. Many pieces of literature show a wide range of saving possibilities with latent or sensible methods integrated, usually with PCMs.

Several used modelling tools in the literature were assessed. The most common ones are TRNSYS, T*sol, and Polysun. Where different specific features, programming abilities, and accessibility. However, the most appropriate is T*sol, which specialises in only thermal system modelling and has three different solar thermal systems for heat processes with high programming accessibility. Moreover, a comparison discussion between the results of the same project shall be done.

This study investigates the extent of the abovementioned problems of solar thermal integration in industrial thermal processes. The study will consider different food and beverage plant demands and schemes, different solar thermal collectors, and different TES tanks integrated or non-integrated with PCMs by using and comparing analytical and modelling program results by optimizing the best solar thermal system with new or retrofitted plants.

3. MATERIALS AND METHODS

This chapter presents the materials, equipment, procedures, and processes employed in the current research. It also includes the experimental measurements' scientific methods and the test systems' description to accomplish the set research aims.

3.1. PCM integration into TES

The laboratory conducted mathematical and experimental modelling of a Soy wax PCM integrated into the solar tank using the response surface method. A capsulated PCM Soy wax 52 ℃ and 62 ℃ in a 5 litre insulated water tank was conducted. The response surface approach with non-linear correlation was used for the charging phase to determine the appropriate number of samples and the quantity of PCM at two temperature levels. The method will illustrate the first-degree effect of the Temperature, sample numbers, and wax quantity. Furthermore, each two-factor interaction contour plot is depicted.

As in Fig. 3.1, the experiment components are a water tank, heater, sensors, datalogger (ALMEMO 2890-9), and wax. The system comprises a well-insulated water tank with 5 cm of expanded polystyrene (EPS). This oil-based insulation material acts as a perfect insulator in foam. This foam is a non-degradable, environmentally friendly material that maintains its qualities throughout time.

Furthermore, the tank has 42 x 13 x 16 cm dimensions and can hold up to 8.7 litres of water. As shown in . Fig. 3.1, it was only filled with 5 litres during the measurement, and the remaining amount was for the specimen tray. The tray comprises 7 x 3 specimens, each of which may hold 50 ml of the allocated material.

The heater is turned to a required temperature range between (20 – 100) ℃. Once the specimen tray is fixed inside the tank and filled with the assigned material, the by-pass line helps to mix the water throughout the heating process better, resulting in temperature uniformity in the tank. Meanwhile, the data logger (Almemo 2890-9) with nine input channels, as shown in Fig. 3.2, stores the information from the sensors. A data logger is a device that measures and displays signal voltages plotted with time or another signal voltage. Until the user stops the data recorder, it measures in a continuous stream mode. Every time new samples are taken during the measurement, they are transferred straight to the computer, where they are processed, displayed, and, if desired, stored on disk. The presence of a change in an input signal is immediately apparent.

Two temperature sensors, NiCr-Ni type k (-40 →1000 ℃), are located on the right and left sides of the tank, as well as one ambient temperature sensor used as a reference temperature to determine when the container cools down to near ambient temperature (the laboratory temperature). In addition, another sensor inside was placed into the PCM capsule, and two heat flux sensors in the internal and external parts of the insulation. The experiment continues until the internal temperature of the tank approaches the ambient temperature by a difference of 1 ℃. Equation 3.1 shows how the heat balance difference is calculated:

$$T_{avg\_tank} - T_{amb} \leq +1\ ℃ \tag{3.1}$$

where,

T_{avg_tank} – average tank temperature (^oC);

T_{amb} – ambient temperature (^oC);

The experiment aims to determine the system's thermal inertia time (τ (h)), i.e. the time it takes for the tank to cool down to ambient temperature.

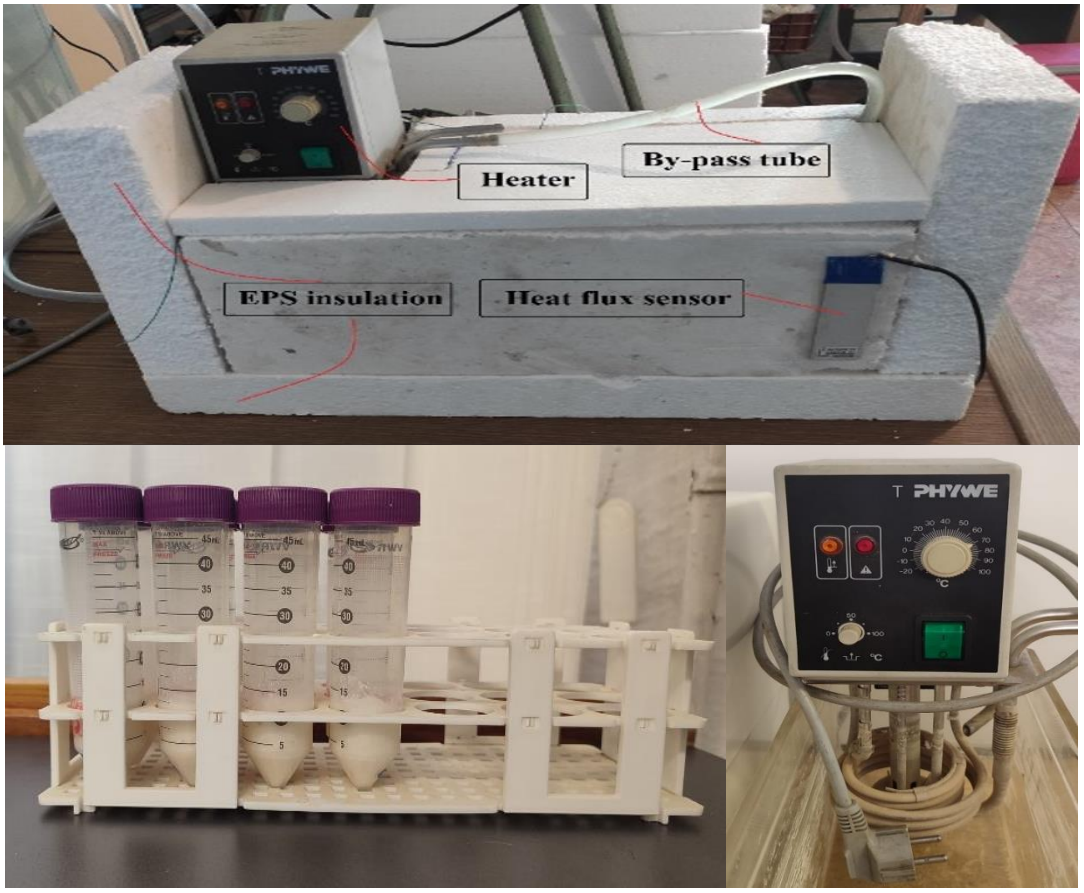

Fig. 3.1. The insulated thermal tank with PCM tray and heater

Fig. 3.2. ALMEMO 2890-9 type data logger

The model was built using the R programming language, with coded values ranging from [-1, +1] for each variable, and the variables being "S" for Sample numbers, with the code (-1) for four samples and (+1) for eight samples. The quantity of PCM in each sample is denoted by the letter "Q," where (-1) code equals 5 g and (+1) code equals 10 g. Finally, the temperature is represented by the letter "T," with code ((-1) denoting 45 °C and code (+1) denoting 75 °C for Soy wax 62 °C and (-1) denoting 30 °C and (+1) denoting 40 °C for Soy wax 52 °C). As seen in Fig. 3.3, this results in a cube pattern, with each corner representing a set of these three variables, resulting in a single experiment. The number of experiments is determined using the form 2^k, where k is the number of variables, therefore $2^{3,}$ resulting in eight measurements, as in Table 3.1. To detect the

second-degree non-linear coefficients, additional measurement was undertaken inside or outside the border of the cube to illustrate the non-linear effects.

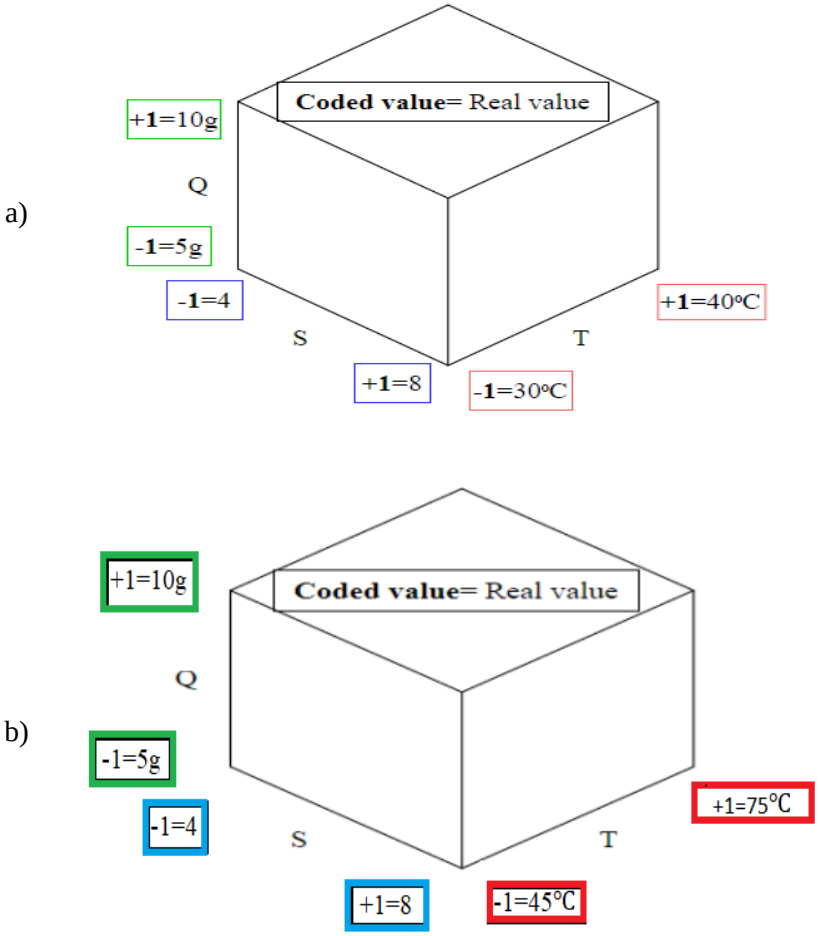

Fig. 3.3. Cube model with modelled parameters Q, S and T values for two different Soy waxes. a) 52 °C Wax; b) 62 °C Wax

Equation 3.2 represents the relationship transferring between coded values and real values:

$$Coded\ value = \frac{Real\ value - Center\ point}{\frac{1}{2}(range)} \quad (3.2)$$

Table 3.1. Number of settings and model values of experimental parameters

Number of experimental setups	**1**	**2**	**3**	**4**	**5**	**6**	**7**	**8**
S - Samples	-1	+1	-1	+1	-1	+1	-1	+1
Q - Quantity (g)	-1	-1	+1	+1	-1	-1	+1	+1
T - Temperature (℃)	-1	-1	-1	-1	+1	+1	+1	+1

The least-squares method was developed by Carl Friedrich Gauss in 1795 and offered the overarching justification for the best-fit line placement among the data points. Iterations are used to solve the non-linear model in our experiment. The coded equation 3.3 represents the created model:

$$Y_i = \beta_0 + \beta_1 X_{1i} + \beta_2 X_{2i} + u_i,\ i = 1..., n \quad (3.3)$$

Where:

X_1 and X_2 - the two independent variables (regressors);

(Y_i, X_{1i}, X_{2i}) - denote the i^{th} observation on Y, X_1, and X_2;

β_0 - unknown population intercept;

β_1 - effect on Y of a change in X_1, holding X_2 constant;

β_2 - effect on Y of a change in X_2, holding X_1 constant;

u_i - "error term" (omitted factors).

3.2. Model development and simulation of tankless SHIP

A dynamic analysis tool is needed to accurately describe the system's response to the rapid environmental change in weather conditions to study the SHIP system's performance (Kádár, 2014; Kalbasi et al., 2021). T*sol software is a professional simulation program for designing solar thermal systems, including domestic hot water (DHW), swimming pool heating, district heating, and heat process systems. It calculates and simulates the thermal process in these systems by providing the components and tools of the solar systems and all relevant data (Jahangiri et al., 2018). This software enables the engineers to design the system optimally at a low cost and time. The calculations are based on the energy balance flows and provide predictions according to the hourly meteorological data (Pahlavana et al., 2018).

This section develops the comprehensive models of the tankless SHIP system by collecting the meteorological data for an entire year and comparing it with the average data records between 1995 and 2012 with a deeper focus on the summertime results.

3.2.1. SHIP concept

The SHIP comprises a solar collector integrated with an external heat exchanger in a closed loop. In this external loop, a water and propylene glycol mixture run in the piping system to convey the absorbed energy from the solar collector (FPC with active 1.92 m2 area, 33º inclination) to the heat process using a heat exchanger (Alfalaval 960 W HX). The concept assumes that the flow goes out of the solar collector at a specific temperature (denoted by $T_{Pr\ In}$), which is the same input temperature of the primary side of the heat exchanger since the piping system is well-insulated. Moreover, the output temperature from the heat exchanger in the primary loop (denoted by $T_{Pr\ Out}$) is the same temperature that flows in the collector for the same reason. On the secondary side of the heat exchanger, there is an open loop that warms up the network water (denoted by $T_{Sec\ In}$) by exchanging the heat with the fluid on the primary side so it can be ready for the heat process at the required temperature (denoted by $T_{Sec\ Out}$). The schematic concept of the system is shown in Fig. 3.4. The concept assumes no possibility of mixing between the fluid on the primary and the secondary side to avoid mixing the antifreeze liquid with the process heat, which can be risky for human health, mainly in food processing like pasteurizing.

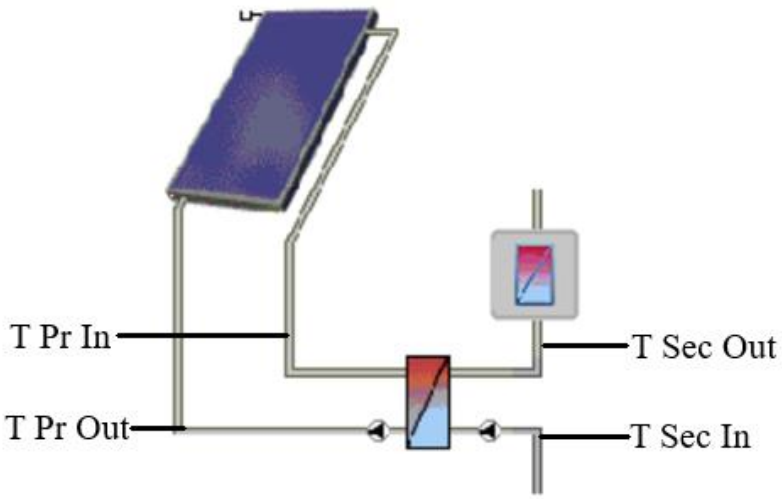

Fig. 3.4. A tankless solar system with heat exchanger and FPC collector schematic where:

T - temperature, Pr - primary side, Sec - secondary side, In - input and Out - output

*3.2.2. Modelling in T*sol*

The simulation is carried out using the outputs of the six actual experiments to reach the optimum operating configuration from two aspects: the highest output temperature and the highest energy gain. These different configurations of the food process industry aim to assess and optimize the working parameters according to the Hungarian meteorological conditions. So, it is crucial to consider The following assumptions and inputs:

- The weather data is used for the geographical location of Budapest (KMI weather station), Hungary.
- The solar fraction can reach up to cover the whole required energy during certain weather conditions. However, central Europe's annual feasible solar fraction is 40 – 60%. Therefore, an auxiliary heating system is considered in natural systems to cover the rest of the demand and ensure a continuous supply of the process heat.
- The efficiency of the solar thermal collector is dependent on the ambient temperature. Therefore, an average ambient temperature of 25 °C is relevant for the modelling analysis.
- The examined case study of the food process requires several temperatures for processing and cleaning.
- The temperature of the network water is taken from the data records.

3.2.3. Experiment configurations

The components used in the T*sol model configuration are (1) single FPC. (2) external heat exchanger transfers the absorbed energy from the primary loop to the secondary one. (3) heat exchanger as described in Fig.3.5. The water flows in the pipes using an active circulation pump in a closed loop in the primary loop. The flow rate of the primary loop is 60 litres per hour. The fluid is a mixture of glycol and water with an 18% volumetric percentage to avoid freezing and bursting during low temperatures.

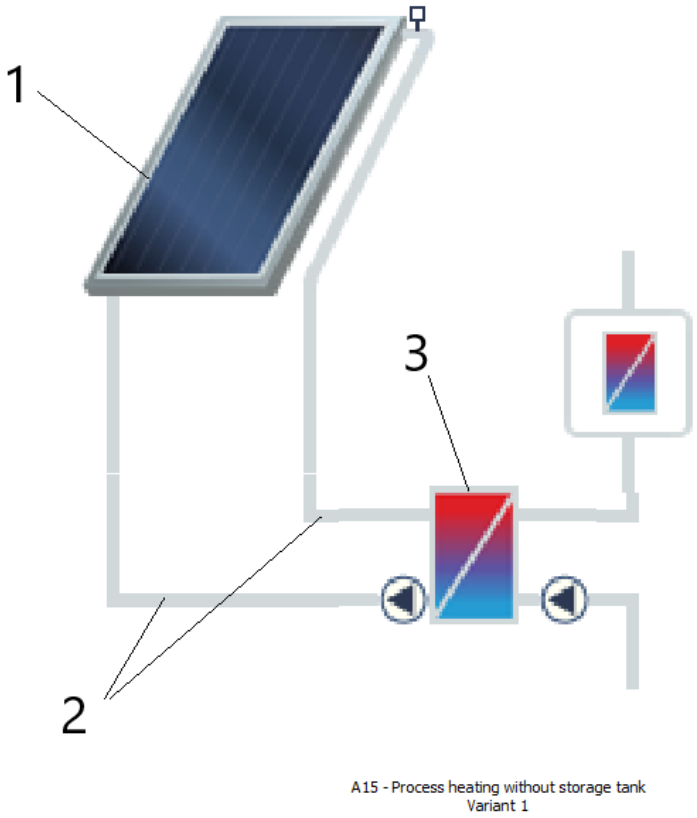

Fig 3.5 T*sol model configuration where:

1) Solar collector, 2) piping system, 3) heat exchanger

The intended experimental setup consists of several primary data logging and instrumentation components as in Fig. 3.6: (1) IMRe, (2) data logger (ALMEMO® 2890-9) in a universal input data logger that connects nine sensors through multiple channels, (3) pyranometer, (4) mechanical flow meter, (5) temperature sensor (K-type). (6) Open Energy Monitor is a monitoring, modelling, and assessment tool to monitor live data and records. (7) TECH controller to adjust the working schedule of the process heat. The measurement ranges and the accuracy of each instrument are shown in Table 3.2.

1) 

2) 

3) 

4) 

5) 

6) 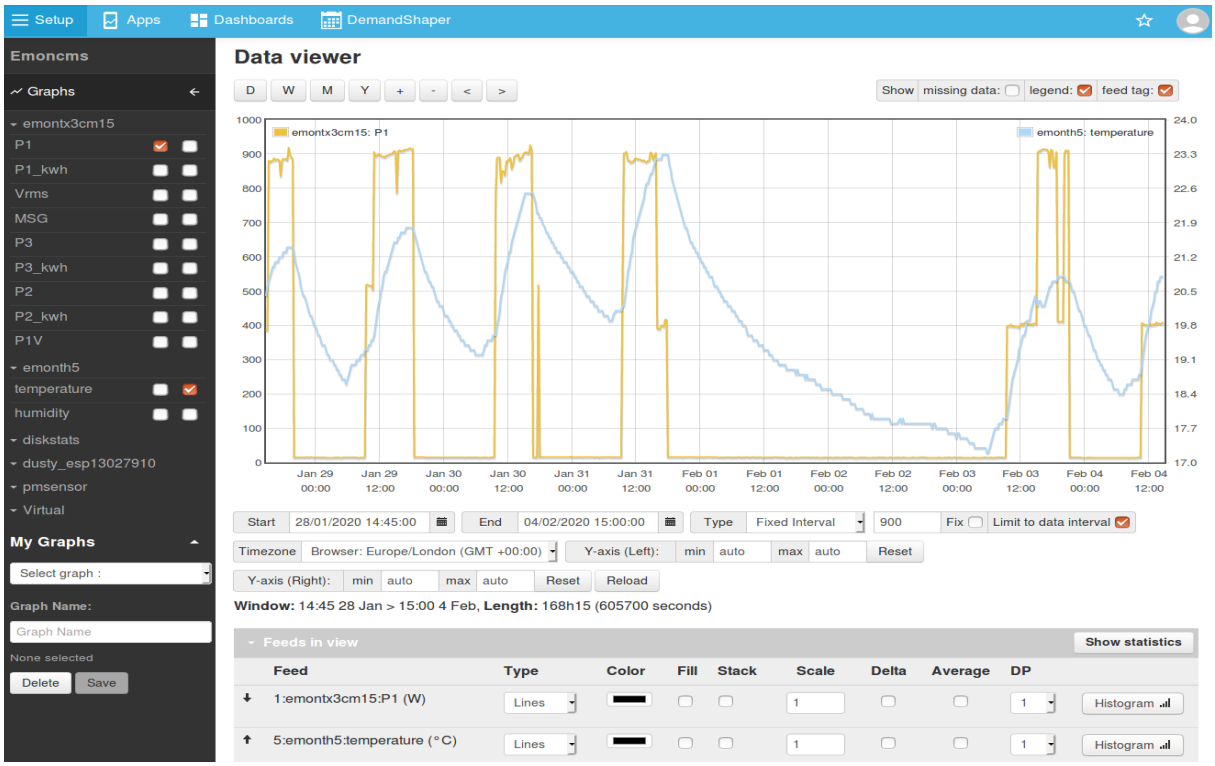

Fig. 3.6. IMRe controlling system

1) IMRe 2) Data logger 3) Pyranometer 4) flow meter 5) Temperature sensor

6) Energy monitoring software

The experiment set up has been installed in the Hungarian University of Agriculture and Life Sciences renewable energy laboratory, Gödöllő, Hungary. Experiments were carried out 24 hours a day during August and September 2021, when the weather was relatively stable, with rain interruptions for a few days during the whole period. All the data have been recorded persistently by the data logger every minute.

The actual experiment (mainly the solar collector) was mounted on a metallic structure and directed at an angle of 33º facing the south to harvest the maximum radiations throughout the day. Knowing that this angle is the optimum angle for Budapest during the summer climate was recommended by the solar electricity handbook 2019.

Table 3.2. Measurement tools and measuring range

Instrument	Type	Measuring range	Accuracy
Data logger	ALMEMO® 2890-9	over 70 measuring ranges	-
Pyranometer	THEODOR FRIEDRICHS 6003.000 BG	0 - 1300 (W/m^2)	< 10%
Mechanical flow meter	Zenner DE-07-MI001-PTB010 (R80HR40V) with impulse output	0.05 (l) to 10,000 (m^3)	cold water ± 5% hot water ± 3%
Thermocouple (K-Type)	Programmable Resolution 1-Wire Digital ThermometerDS18B20	-55 to +125 (°C)	0.5 (±°C)
IoT device	IMRe	Relative to each sensor	

The IMRe system is an internet of things (IoT) device that collects the energy usage data of a specific case and uploads the sensor data directly to the internet (József et al., 2018). A single user can collect data using one or more devices, which provides higher scalability and flexibility if required. The collected data can be viewed and evaluated using an internet browser. The monitoring system has two main parts: the local group, which contains IMRe hardware and sensors. The second group is the cloud, where a server runs Emoncms framework processes for all raw signals and then converts them into their corresponding physical values (Hermanucz & Benécs, 2019). It should be mentioned that it is possible to build and generate additional calculated values in the server. All these data are stored in the cloud database and can be easily visualized to the end-user.

3.3. Boiler configurations within the SHIP system

An indirectly forced circulations solar thermal system for heat process applications with external heat exchanger integration and antifreeze fluid in the primary flow loop is modelled in this study. The secondary loop is the process heat section where the boiler is connected to the process in parallel or series. The parallel connection can be used by attaching the boiler's input and output directly into the buffer tank, as in Fig. 3.7 (a), while a series connection is by installing the boiler directly into the piping system between the process heat and the buffer tank as in Fig. 3.7 (b).

When the primary loop receives solar irradiation, it transports it from the solar collectors to the primary side of the external heat exchanger (hot side). Since the study is in a relatively cold climate, where the ambient temperature falls below zero degrees during wintertime, the fluid in the primary loop is a glycol solution in water. The simulations measure both systems' performance under different volumetric glycol ratios to avoid freezing in the primary loop. To allow the absorbed energy to be transferred to the buffer tank, the external heat exchanger does not only this but also separates the glycol in the primary loop from being mixed with the duty water in the buffer tank in the secondary loop. Before the heat process, the temperature sensor checks the output hot water temperature to see if it matches the needed temperature. If not, the auxiliary heater (a gas, pallet, oil-fired boiler or even a heat pump) runs to heat up the output water to the desired level. This auxiliary demand occurs mainly on overcast days where solar irradiation is insufficient. On

the contrary, when the produced water exceeds the desired temperature, a 3-way valve adds more cold water to adjust the output temperature.

According to the recent literature reviews, two simulations' sets are conducted to optimise the solar system's performance. The first one is to optimise the system performance (considering the solar fraction as the critical factor) for the given characteristics of a solar collector. At the same time, the second type optimises the solar collectors' efficiency. Nevertheless, most of the studies are done using MATLAB or TRNSYS software.

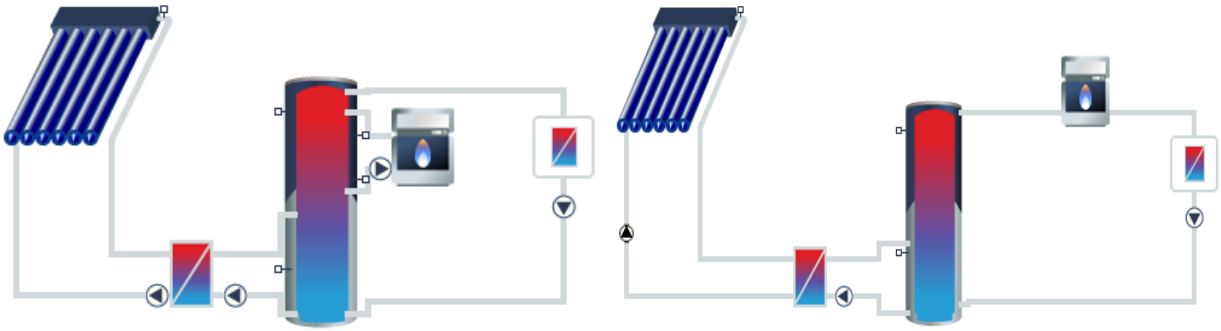

(a) (b)

Fig. 3.7. Solar thermal system for heat process (a) parallel boiler connection (b) series connection

The working profile of a pasteurising plant generally continues during the whole year with short breaks, for example, during Sundays with half working days, Christmas, and summer holidays. As in Fig. 3.8, the heat process starts every day from 6 AM till 4 PM, starting with the cleaning process at 100% capacity and 90 ℃ or steam compared to 20% capacity and around 73 ℃ for the pasteurising heat process. At a higher temperature, it is preferable to clean all the possible residuals in all system components, such as pipes or heat exchangers, which may cause serious health issues due to the existing pathogens in all dairy products. Indeed, not all pasteurising plants have the same working profiles since they may have different processes, such as cheesing or packaging. However, this study concerns the primary process of all pasteurising plants.

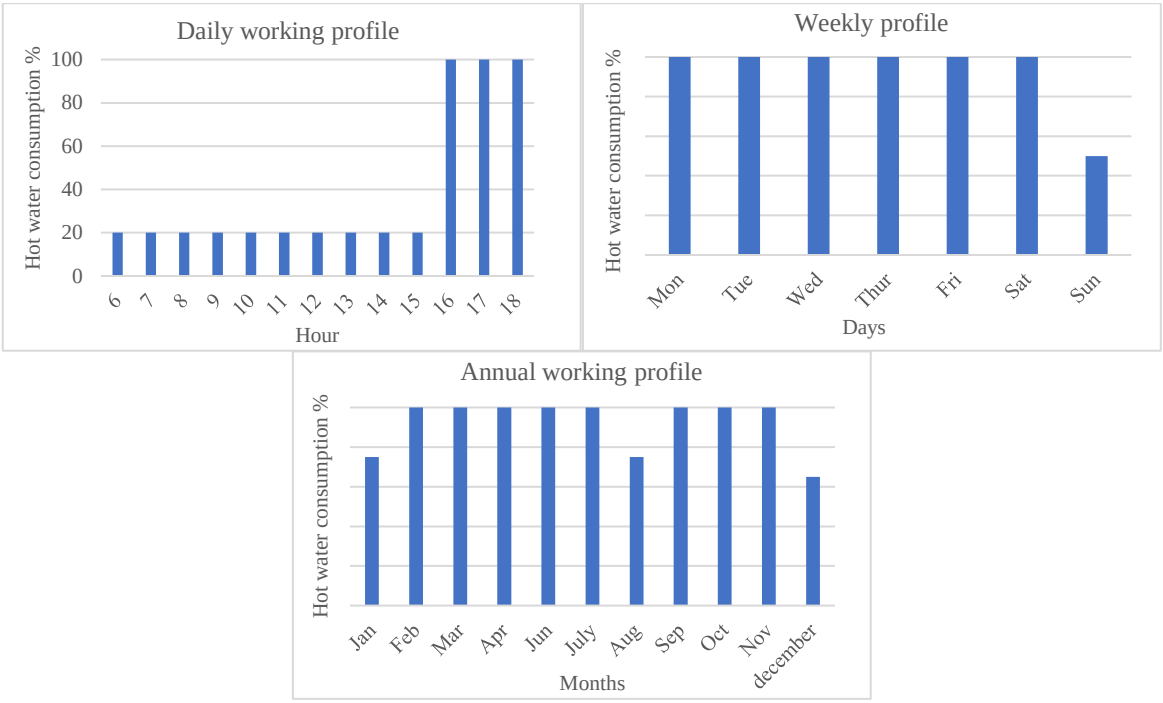

Fig. 3.8. Daily, weekly, and monthly pasteurising profiles

The solar thermal system is simulated using the following parameters:

Different numbers of Evacuated-tube collectors

An Evacuated-tube collector (ETC) is chosen to choose the optimum collector number with an 87.8% conversion ratio and 1.43 W/m^2 K and 0.0038 W/m^2·K^2 linear and quadratic heat transfer coefficients. The collector's gross and active areas are 2.14 m^2 and 1.31 m^{2,} respectively, with 8000 J/m^2·K specific heat capacity. Since the study is in the northern hemisphere, the solar collectors face the south with a tilt angle (β) of 72º, the optimum angle for Budapest under winter weather according to the solar electricity handbook. In this manner, factor A (collector area) has a -1 coded value corresponding to a 5 m^2 collector area and +1 as 100 m^2.

Collector loop heat exchanger

The maximum heat transferred by the heat exchanger depends on the size of the system, such as the collector area and the process heat demand. For our study, the mean logarithmic temperature difference (MLTD) is considered at 5 K for all scenarios.

Buffer tank

The buffer tank is an unstratified tank with 100 mm insulation thickness, 0.065 W/m·K thermal conductivity, and an average daily heat loss of 7.10 kWh/day. The studied variable considering the buffer tank is the height-to-diameter ratio H_T/D. For this, factor C (relative flow rate) has a -1 coded value corresponding to 5 l/h·m^2 and +1 as 100 l/h·m^2. Similarly, factor D (relative tank capacity) has a -1 coded value corresponding to 10 l/m^2 and +1 as 100 l/m^2. Also, factor E (relative tank height-to-diameter ratio) has a -1 coded value corresponding to 0.2 m/m and +1 as 2.4 m/m.

Auxiliary heater

53.1 kW gas-fired boiler is connected in parallel with the buffer tank or series with the secondary loop before the process heat section. The capacity of the auxiliary heater is oversized since it is not only needed for the process heat demand but also for space heating and domestic hot water

supply. The boiler's efficiency is 85%, measured based on the low heat value. The studied variable here is the connection type, in series or parallel.

Flow circulation pumps

Several pumps are mounted in the system to circulate the running medium fluid. The first is mounted in the primary loop in two places, the first between the solar collector and the external heat exchanger. The second circulates the fluid between the buffer tank and the external heat exchanger. The secondary loop has a circulating pump between the process heat and the buffer tank. In addition, an extra pump is needed in the parallel mode between the boiler and the buffer tank. For each pump, there is an on/off controlling system that generates the signals for each pump. In the primary loop, the controlling system generates an on signal if the collector's output temperature is above the tank's reference temperature by +8 K and an off signal if it is +3 K. It should be noted that two variables are studied in this section, which is the volumetric glycol ratio and the volume flow rate. For this manner, factor B (volumetric glycol ratio) has a -1 coded value corresponding to 5% and +1 as 80%.

Internal and external piping system

The external piping system is the part between the buffer tank and the solar collectors. At the same time, the internal ones are between the buffer tank and the process heat. The sizing of the pipes is chosen relatively based on 0.5 m/s fluid velocities. A thermal insulator surrounds the piping system with 0.045 W/m·K thermal conductivity and 100% relative thickness to the nominal pipe's diameter.

Weather and meteorological data

T*sol uses an external weather acquisition program as an external Typical Meteorological Year (TMY) file for the studied location. Budapest is the chosen city in our case study, and the weather data were acquired between 1986 and 2005.

Ultimately, the whole comparison and analysis of the inputs and outcomes can be described using the following flowchart as in Fig. 3.9.

Finally, the RSM method can be done using the five factors abovementioned with both -1 and +1 values, resulting in 5^2 equals 32 experiments and an extra experiment in 0 coded value to illustrate the system linearity or non-linearity as in Table 3.3.

Table 3.3. RSM method coded and real values

	Coded value		**Real value**	
A – collector area (m^2)	-1	+1	5	100
B – glycol ratio (%)	-1	+1	5	80
C – relative flow rate (l/h m^2)	-1	+1	5	100
D – relative tank capacity (l/m^2)	-1	+1	10	100
E - tank height-to-diameter ratio (m/m)	-1	+1	0.2	2.4

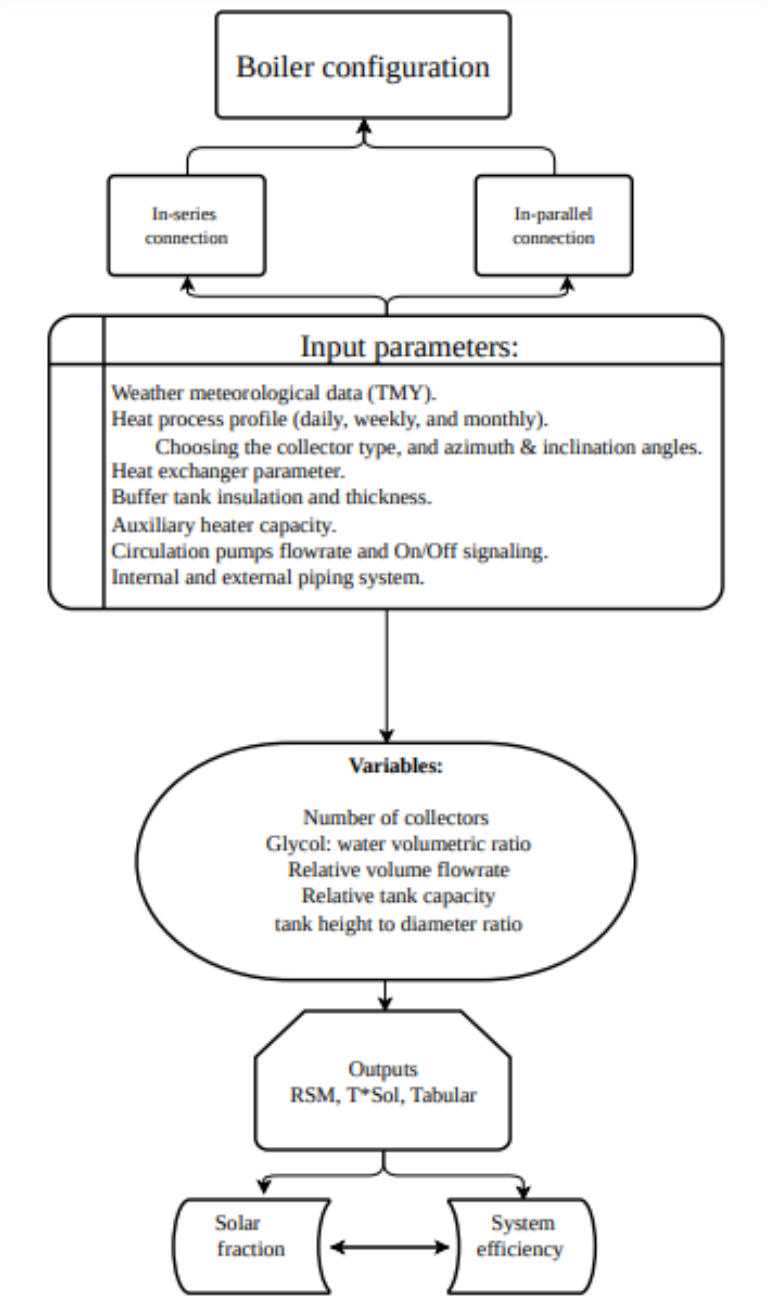

Figure 3.9. The flowchart describes the comparison process between the in-series and in-parallel boiler configurations.

4. RESULTS AND DISCUSSION

The experiments' results are presented in this chapter, and the discussions suggest new findings. The solar TES and tankless SHIP mentioned in the previous section were tested in different conditions and working cases in the Hungarian University of Agriculture and Life Sciences lab. The achieved results served as a basis for the new scientific results.

4.1. Experimental results of integrating PCM Soy wax into TES

This segment presents experimental and mathematical modelling of an encapsulated PCM material in a thermal tank, clearly showing that it plays a substantial role in solar thermal and heat process systems. We can see significant heat loss in the tank in cold countries to a greater extent. So, integrating PCMs in the thermal tank used as capsules or insulating layers will give a better performance and, as a result, reduce CO_2 emissions. By using PCMs, we can conserve more energy and create better utilisation. In our work, we investigated a matrix of three variables: Temperature, Quantity, and Sample number of both Soy wax 52℃ and Soy wax 62℃. We conducted eight experiments to optimise the performance in a specific thermal tank, as in Tables 4.1 and 4.2. Each experiment at the beginning uses the heater with the corresponding starting temperature, as in Tables 4.1 and 4.2. In contrast, the ambient temperature for all experiments was 25.23℃, and the maximum and minimum ambient temperatures were 26.5℃ and 24.2℃, respectively. The main aim is to let the thermal energy tank cool down till the difference between the average tank temperature and the ambient temperature is one Celsius degree. Then, we measure the time, represented by the y function, as in equations 4.1 and 4.2. Based on the R script results, we generated the mathematical second-degree, non-linear, 3-factors interaction equation. Moreover, to generate the second-order coefficients, more experiments were needed. Furthermore, to have a better visualisation, the Pareto plot illustrates the most influential factors of the non-linear equation, where for Soy wax 52℃, the temperature has the most significant positive magnitude, followed by sample and quantity of PCM as in Fig. 4.1.

On the contrary, the temperature has the most potent negative magnitude, proving the non-linearity. For Soy wax at 62℃, the second-degree interaction between samples and temperature has the highest positive magnitude, followed by the first-degree temperature effect. In contrast, the three interactions between samples, quantity and temperature have the most extensive negative magnitude. The applied method is the least-squares method, attributed to Carl Friedrich Gauss in 1795 and provides the overall rationale for the best-fit line placement among the studied data points. In our experiment, the non-linear model is solved using iterations. The following equations (4.1 and 4.2) represent the generated models:

$$y_{Soy\ wax\ 52℃} = 9.33 + 0.95(0.5\,S - 3) + 0.38(0.4\,Q - 3) + 3.16(0.2\,T - 7) - 0.38(0.2\,T - 7)^2 + 0.29(0.5\,S - 3)^2 - 0.05(0.5\,S - 3)(0.4\,Q - 3) + 0.23(0.5\,S - 3)(0.2\,T - 7) - 0.11(0.4\,Q - 3)(0.2\,T - 7) - 0.04(0.5\,S - 3)(0.4\,Q - 3)(0.2\,T - 7) \quad (4.1)$$

The 4.1 equation is valid for the Soy wax 52 ℃ for the following domains:

S ∈ [0-8] samples, Q ∈ [0-10] g, and T ∈ [30 – 60] ℃.

$$y_{Soy\ wax\ 62℃} = 15.03 + 0.84(0.5\,S - 3) + 0.18(0.4\,Q - 3) + 1.62(0.67\,T - 4) - 0.21(0.67\,S - 4)^2 + 0.07(0.4\,Q - 3)(0.5\,S - 3) + 2.04(0.5\,S - 3)(0.67\,T - 4) + 0.85(0.4\,Q - 3)(0.67\,.T - 4) - 1.16(0.4\,Q - 3)(0.5\,S - 3)(0.67\,T - 4) \quad (4.2)$$

The 4.2 equation is valid for the Soy wax 62 ℃ for the following domains:

S ∈ [0-8] samples, Q ∈ [5-10] g, and T ∈ [45 – 75] ℃.

Where:

y_i – The studied outcome (cooling time) according to the $_i$ PCM type (h)
S – The PCM sample numbers (Samples)
Q – The PCM quantity (g)
T – The tank temperature (℃)

Table 4.1 Experiment parameters and results of Soy wax 52℃

Number of experimental setups	S – Samples	Q – Quantity (g)	T -Temperature (℃)	y (hour)
1	-1=4	-1=5 g	-1=30 ℃	**4.86**
2	+1=8	-1=5 g	-1=30 ℃	**6.33**
3	-1=4	+1=10 g	-1=30 ℃	**5.87**
4	+1=8	+1=10 g	-1=30 ℃	**7.28**
5	-1=4	-1=5 g	+1=40 ℃	**10.88**
6	+1=8	-1=5 g	+1=40 ℃	**13.4**
7	-1=4	+1=10 g	+1=40 ℃	**11.58**
8	+1=8	+1=10 g	+1=40 ℃	**13.75**
9_extra_pre	-3=0	-3=0 g	-1=30 ℃	**4.68**
10_extra_post	+1=8	+1=10 g	+5=60 ℃	**17.62**

Table 4.2 Experiment parameters and results of Soy wax 62 ℃

Number of experimental setups	S – Samples	Q – Quantity (g)	T -Temperature (℃)	y (hour)
1	-1=4	-1=5 g	-1=45 ℃	**16.3**
2	+1=8	-1=5 g	-1=45 ℃	**11.43**
3	-1=4	+1=10 g	-1=45 ℃	**12.5**
4	+1=8	+1=10 g	-1=45 ℃	**12.56**
5	-1=4	-1=5 g	+1=75 ℃	**11.43**
6	+1=8	-1=5 g	+1=75 ℃	**19.38**
7	-1=4	+1=10 g	+1=75 ℃	**15.68**
8	+1=8	+1=10 g	+1=75 ℃	**19.28**
9_extra_centre	0=6	0=7.5 g	0=60 ℃	**15.03**

The Pareto plot is conducted to understand the relationship between the factors and the objective, as in Fig. 4.1.

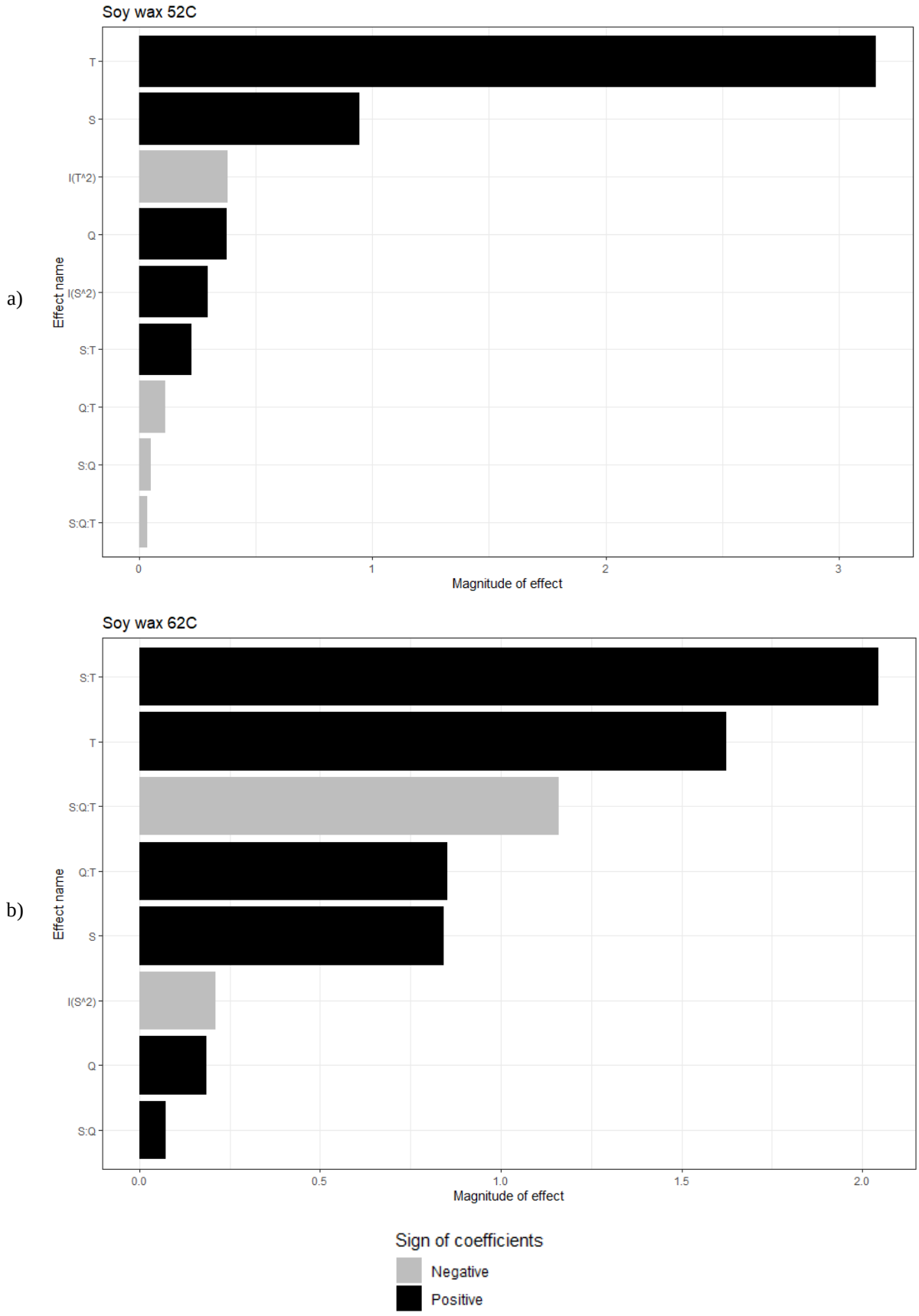

Fig. 4.1 Pareto plot a) Soy wax 52℃ and b) Soy wax 62℃

S – Samples; Q – Quantity (g); T – Temperature (℃)

4.1.1. Soy wax 52℃

The magnitude of each parameter is easily observed using the Pareto plot, while **t**emperature has the most significant positive magnitude, followed by **s**ample numbers. In the third place, contrariwise, the second-degree temperature coefficient has a negative magnitude due to the non-linear behaviour. Ultimately, the quantity of first and second-degree has a low positive magnitude on the overall result. Adding to the fact that the 3-factor interaction S·Q·T or any three-factor interaction does not exist in nature, as shown in the Pareto plot in Fig. 4.1, it has almost zero magnitudes. Similarly, this magnitude influence is similar to the interaction`s magnitude of S·Q and Q·T, which have a low influence.

On the other hand, the contour plot of each two-factor interaction shows the curves where the overall result can be better, as seen in Fig. 4.2, 4.3 and 4.4, paying attention to some coded values that may have no meaning on the chart. For instance, Q = -3 or S = -3 matches 0 g and 0 samples, so below the -3 value in the chart has no meaning in real-world values. As we can see in the chart, we should increase the samples and the PCM quantity, as in the referring arrow, to increase the storing time (y), which is the core target. On the other hand, the coefficient of S, Q and T in equation 4.1 shows the plot's direction. In other words, by analysing the equation 4.1 factors, moving from a 0-coded value to a coded value of ΔT 0 → [+1] will add 3.16 hours to the overall result. Similarly, ΔQ 0 → [+1] will add 0.38 hours, and ΔS 0 → [+1] will add 0.95 hours.

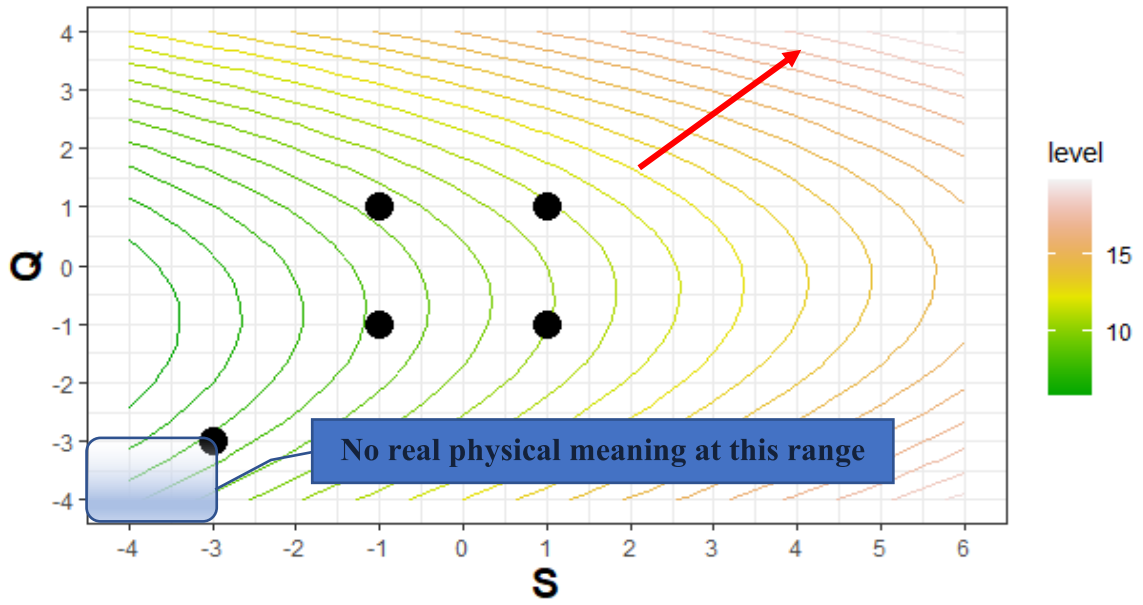

Fig. 4.2. Correlation of Parameters Q and S

(Q= -3; S= -3) means 0 (g) and 0 samples; (Q= +1; S= +1) means 10 (g) and 8 samples.

On the other hand, the T·Q interaction shows better results (as shown in Fig. 4.3), using more PCM materials and no more than 3.5 coded value temperature equaling 52.5℃, which is very close to the melting temperature of the PCM. This result proves that the PCM's melting point is around 52.5℃ compared to 52℃, as mentioned in the material description. The black dots in the graph represent the 4 corners of the cube from a 2D Q·T perspective. In addition, two pre- and post-experiments were needed to identify the second-order coefficients. The interpretations of those factors corresponding with the coefficients, as in equation 4.1, are 0.38Q, 3.16T, $-0.38T^2$, and $0.29Q^2$.

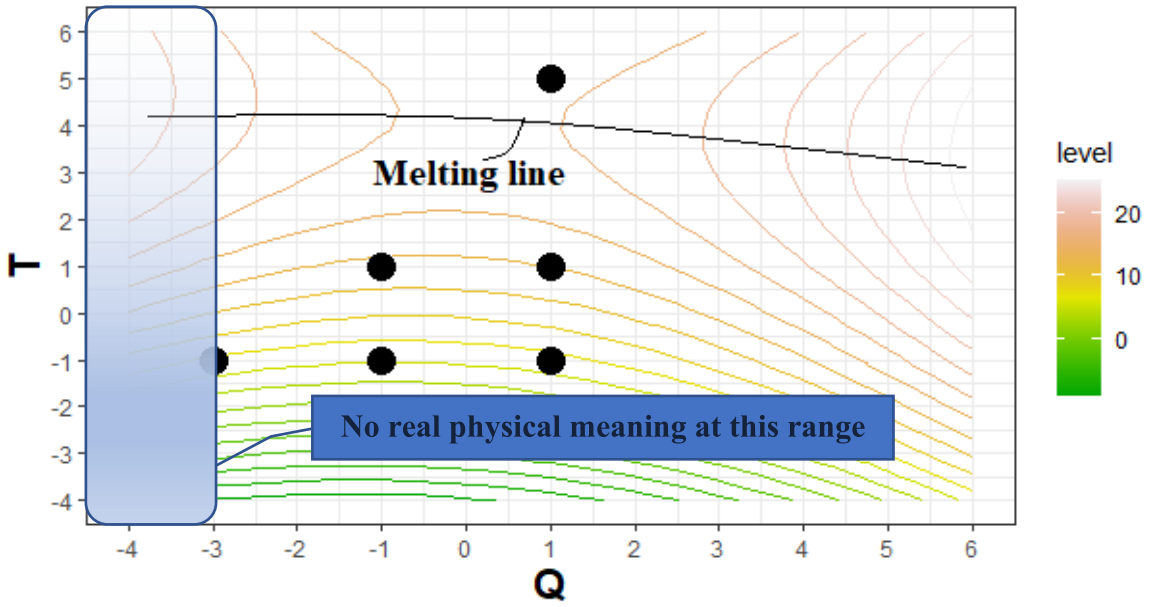

Fig. 4.3. Correlation of parameters T and Q

(T=-1; Q=-3) means 30 (°C) and 5 (g); (T=+5; Q=+1) means 60 (°C) and 10 (g)

Like the T·Q contour, the T·S contour has similar results (as in Fig. 4.4). They show that we should obtain better results at a near-code value of 4, corresponding to 55°C temperature, with extra samples. The black dots show the cube corners adding to two pre- and post-measurement values from 2D projection.

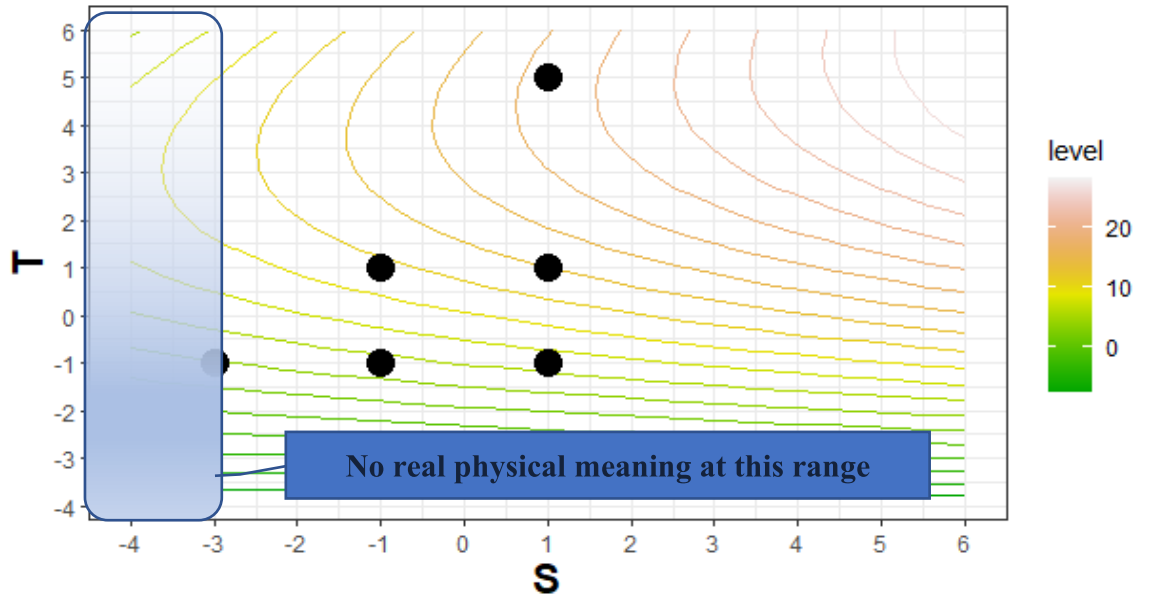

Fig. 4.4. Correlation of parameters T and S

(T=-1; S=-3) - means 30 (°C) and 0 sample number; (T=+5; Q=+1) - means 60 (°C) and 8 sample number

4.1.2. Soy wax 62°C

The magnitude of each parameter is easily observed using the Pareto plot, while the interaction of sample and temperature (S·T) and temperature (T) have the most significant positive magnitude. In the third, the third-degree interaction between all factors (S·Q·T) has the most significant negative magnitude. Ultimately, the quantity temperature interaction (Q·T) and sample numbers

(S) have a low positive magnitude. Finally, the second-degree sample (S^2) and quantity (Q) and sample quantity interaction (S·Q) do not have a significant influence on the system. The result is similar to a temperature that has a low influence. On the other hand, the contour plot of each two-factor interaction shows the curves where the overall result can be better, as seen in Fig 4.5.

a)

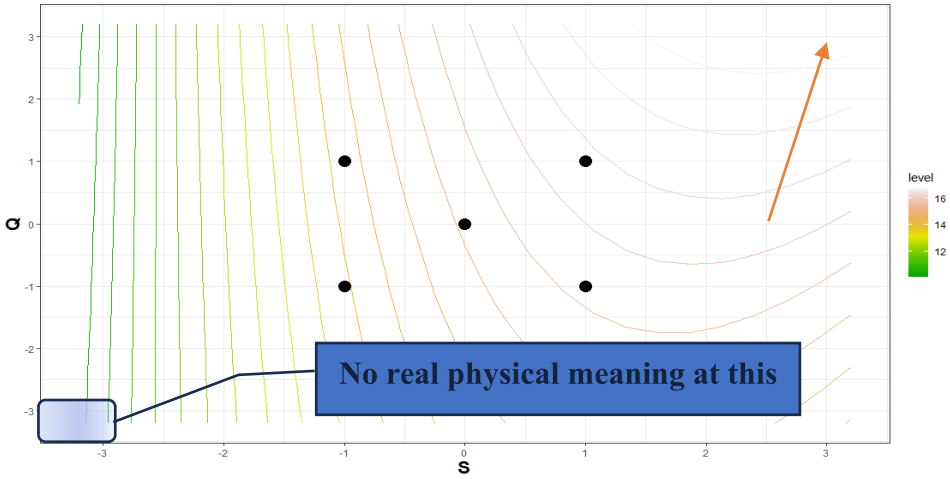

b)

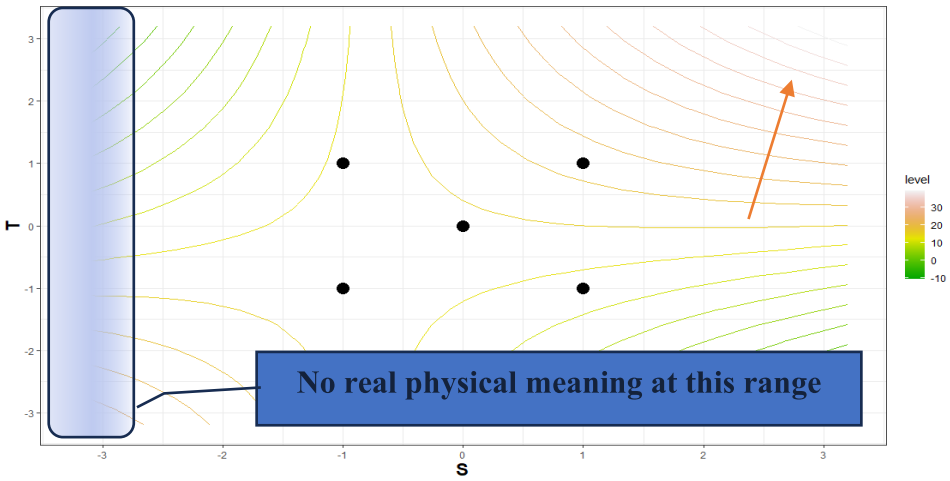

c)

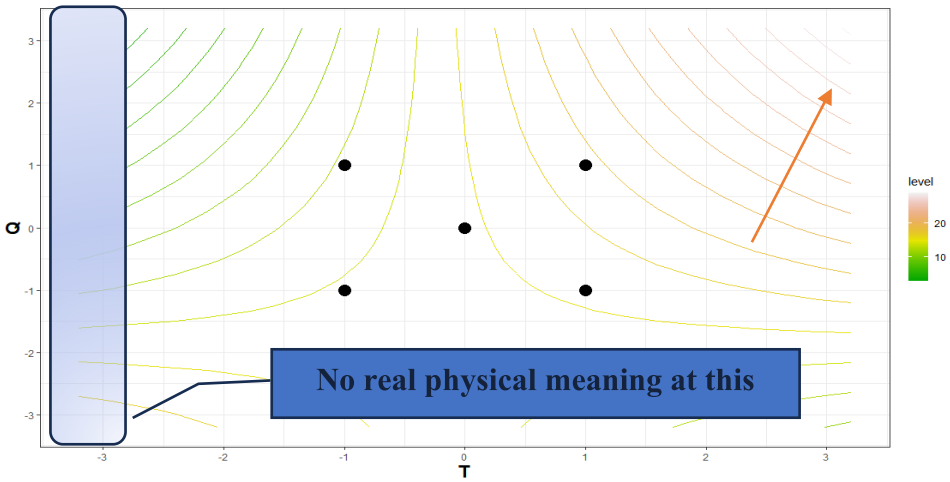

Figure 4.5. Soy wax 62°C two factors of interaction

a) Q-S correlation; b) T-S correlation; c) Q-T correlation

It must be highlighted that regular statistical tests, like ANOVA, do not provide information on the differences between the levels of one categorical variable at different levels/values of another variable, illustrating the importance of the chosen approach RSM.

It should be noted that some coded values may have no meaning on the chart. For instance, S(A) = 0 or Q(B) = 0 matches 0 samples and 0 (g), so below -3 values in the chart have no meaning in real-world values. As we can see in the chart, we should increase the temperature, samples and quantity of the PCM, as in the referring arrow, to increase the storing time (y), which is the core target as in equations 4.1 and 4.2, since all single factors have a single positive magnitude on the system. On the other hand, the most significant interaction of (S·T) has a positive magnitude, meaning that either the factors should be negative or both positive to have an overall positive magnitude. A similar sign of the samples and temperature will result in 2 hours of extra storage time. The equation's S, Q and T coefficients show the plot's direction. In other words, moving from a 0-coded value to a coded value of ΔT 0 → [+1] will add 1.6 hours to the overall result. Similarly, ΔQ 0 → [+1] will add 0.2 hours, and ΔS 0 → [+1] will add 0.8 hours, as in Fig. 4.1 b.

On the other hand, the S·Q interaction shows better results in the contour plot, as shown in Fig. 4.5 a. It is observed that when Q (quantity) and S (sample number) are positive, it will result in more than 15 hours of storing time (y). This result can be checked if S = Q = +1 coded values are substituted in equation 4.2, where these two variables have positive magnitudes (0.84S and 0.18Q). The black dots in the graph represent the 4 corners of the cube from a 2D Q·T perspective, adding to a central point at 0 coded value (6 samples, 7.5 g PCM, and 60℃ degree) were needed to identify the second-order coefficients. The contour plots are significant since in the Pareto plot Fig 4.1 b), it was concluded that samples and temperature interaction (T·S) could result from the two factors being at the same sign (either positive or negative). In contrast, from the contour plots as in Fig. 4.5 b, it is clear that the system will result in higher storing time (y) only if both factors are positive. Finally, the two interactions of quantity and temperature (Q·T) showed that both factors should be positive for higher storing time (y), as in Fig. 4.5 c.

By conducting eight trials to optimize the performance in a specific thermal tank, a matrix set of three variables was studied: temperature, quantity, and sample number of Soy wax 52℃ in Table 4.1 and 62℃ as in Table 4.2. The mathematical first-degree, non-linear, 3-factors interaction equation was created using R script based on the data—furthermore, one or more different experiments were to determine non-linear coefficients.

4.1.3. Statistical analysis of the soy waxes results

A statistical test was conducted to identify the linearity or non-linearity results significance from the two mathematical models as in equations 4.1 and 4.2. The two equations were tested with and without the two factors' interactions to measure the mean, standard deviation and R^2 values. Equations 4.1 and 4.2, in their forms, represent the non-linear models since it has two-factor interaction and parameters from the second degree. At the same time, linear models will be generated by omitting the second-degree factors. The mean value represents the sum of all values divided by the total number of values. For Tables 4.3 and 4.4, the mean value represents the centre point of the measurement points. It is noticed in both tables that the non-linear solution is the closest to the original experiment. In Soy wax 52℃, the experiment has a 9.63 mean value, while 9.62 and 10.39 are the mean values for the non-linear and linear solutions, respectively.

Similarly, for Soy wax 62℃, the mean measurement value is 14.84, the same as the non-linear mean value, while 15.03 for the linear solution. The best-fitting curve is the one which has the closest mean value to the measurement mean value. On the other hand, the standard deviation SD

(σ) measures how dispersed the data concerns the mean. From Table 4.3, the SD value of the Soy wax 52℃ measurement is 4.45 (h), the same as the non-linear curve, while it is 6.92 (h) for the linear curve. From Table 4.4, the Soy wax 62℃ measurement SD value is 3.11 (h), and both the linear- and non-linear curves showed the exact value of 3.10 (h). The best-fit solution is the one that has the closest mean value to the original measurement and the smallest SD value.

On the other hand, the R^2 value represents the coefficient of determination, a statistical measure in a regression model that shows how well the data fit the regression model. As a result, from Table 4.3, the Soy wax 52℃ showed slight differences in mean and standard deviation values. However, the non-linear behaviour seems to be the best-fitting curve since the R^2 values drop from 99.99% to 94.78%. It is also noted that the linear and non-linear predictions are pretty close from experiments 1 to 8 (representing the cube's edges). On the contrary, the two extra experiments (before and after the cube's edge, experiments 9 and 10) differ significantly, which shows why the non-linear model best fits this type of wax, as in Fig. 4.6 and 4.7.

Table 4.3. Soy wax 52℃ statistical results of the best fitting curve

Measurement points	**1**	**2**	**3**	**4**	**5**	**6**	**7**	**8**	**9**	**10**	**Mean (h)**	**SD (h)**	**R^2 (%)**
y (Wax 52℃)	4.86	6.33	5.87	7.28	10.88	13.4	11.58	13.75	4.68	17.62	9.63	4.45	
y (non-linear 52℃)	4.86	6.32	5.86	7.28	10.86	13.4	11.58	13.76	4.68	17.6	9.62	4.45	0.9999
y (linear 52℃)	4.95	6.41	5.95	7.37	10.95	13.49	11.67	13.85	2.45	26.81	10.39	6.92	0.9478

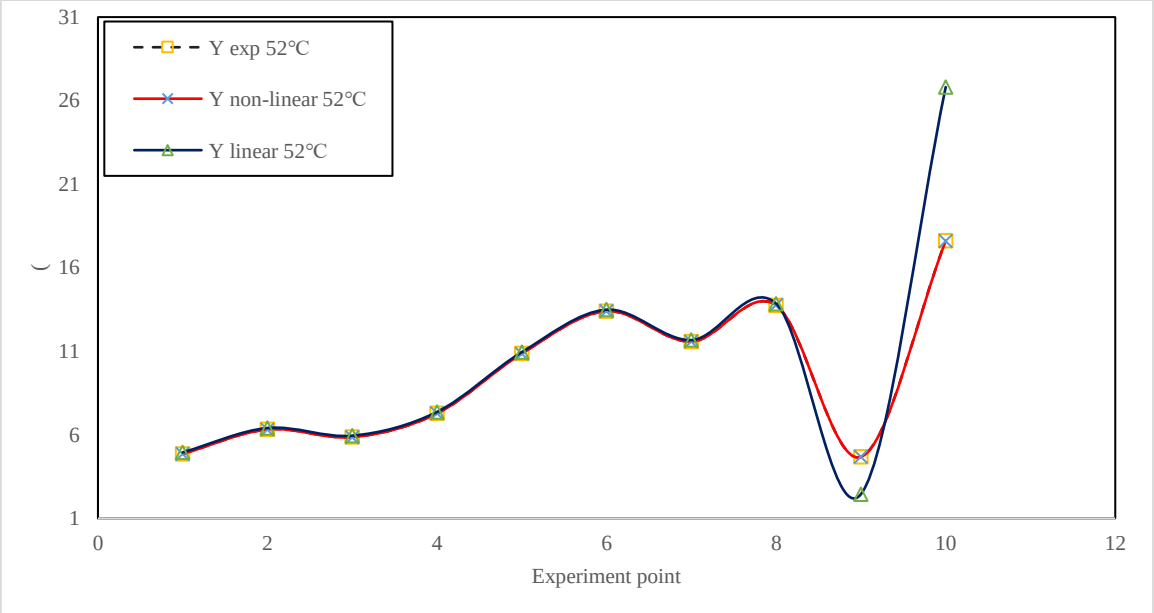

Fig. 4.6 Soy wax 52℃ linear and non-linear best fitting curve

Table 4.4. Soy 62℃ statistical results

Measurement points	**1**	**2**	**3**	**4**	**5**	**6**	**7**	**8**	**9**	**Mean (h)**	**SD (h)**	**R^2 (%)**
y exp 62℃	16.3	11.43	12.5	12.56	11.43	19.38	15.68	19.28	15.03	14.84	3.11	
y non-linear 62℃	16.16	11.58	12.64	12.42	11.3	19.52	15.82	19.12	15.03	14.84	3.10	0.9989
y linear 62℃	16.37	11.79	12.85	12.63	11.51	19.73	16.03	19.33	15.03	15.03	3.10	0.9987

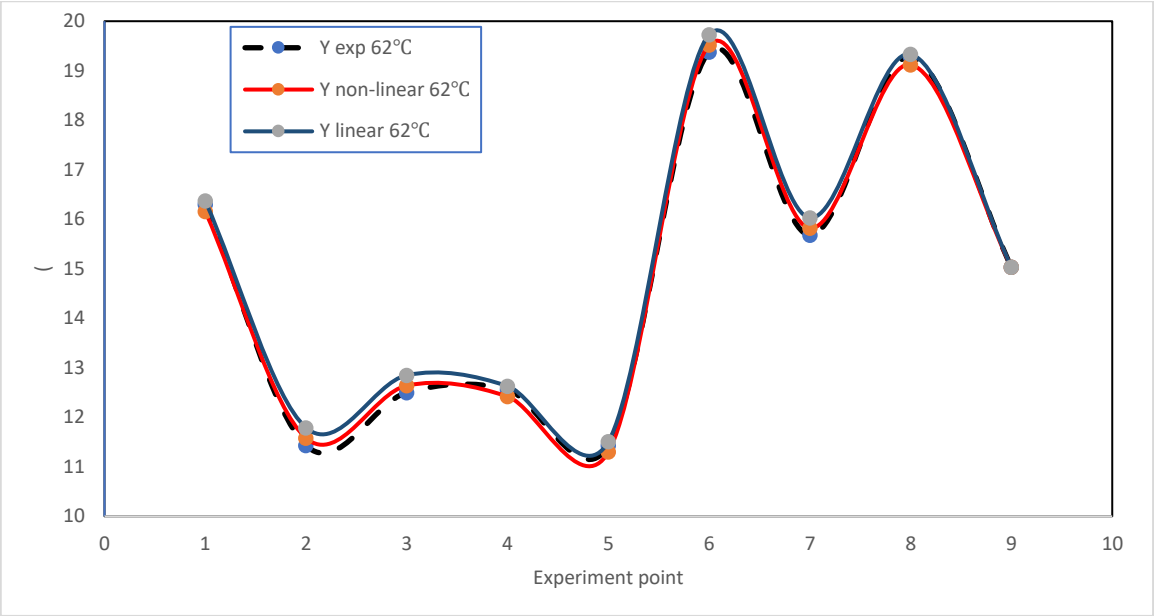

Fig. 4.7. Soy wax 62℃ linear and non-linear best fitting curve

Applying the Lagrange multiplier equations to unconstrained optimisation, the objective function y is a function of S, Q, and T as described by equation 4.3. It should be noted that the unconstrained conditions mean no predefined constraints for optimisation.

$$y = y\,(S, Q, T) \tag{4.3}$$

Since there are no conditions for the optimisation, the Lagrange condition for optimum is as in equation 4.4.

$$\nabla y = 0 \tag{4.4}$$

Equation 4.4 can be rewritten as in equation 4.5.

$$\frac{\partial y}{\partial S} = \frac{\partial y}{\partial Q} = \frac{\partial y}{\partial T} = 0 \tag{4.5}$$

By solving the two Soy wax equations 4.1 and 4.2 by deriving them according to S, Q, and T, we obtain three equations with three unknowns for both Soy wax 52℃ and 62℃, and we get the optimum solutions as in Table 4.5. It should be noted that these two equations were derived once with only first-order factors (linear model) and once with second-order factors included (non-linear model). The solution of these three equations, either manually or using software, will result in one solution, as described in Table 4.5. These two solutions are coded values, and equation 3.2 can be converted back to real values. The two new functions, $y_{wax\ 52℃}$ and $y_{wax\ 62℃,}$ using the optimum generated values, will result in the new optimum highest y function (15.6 (h) for the soy wax 52℃ and 16.36 (h) for soy wax 62℃). It should be noted that the linear model gave higher storing time than the non-linear model. However, on the other hand, the converted temperature outputs are not optimum since the non-linear temperature values are the same as the melting temperature, so we consider the non-linear model the best fit.

Table 4.5. Optimum values for Soy wax 52℃ and 62℃ using linear and non-linear models

Factors	Non-linear model				linear model			
	Soy wax 52℃ value		Soy wax 62℃ value		Soy wax 52℃ value		Soy wax 62℃ value	
	Coded	Real	Real	Coded	Coded	Real	Coded	Real
S	-0.090	5.82	3.2809	12.56	4.275	14.55	1.535	9.07
Q	3.587	16.46 g	2.1824	12.956 g	14.74	44.35 g	5.103	20.257 g
T	3.616	53℃	0.1385	62.07℃	0.592	37.96℃	0.3086	64.629℃
New y	15.6 (h)		16.36 (h)		15.84 (h)		17.78 (h)	

Concerning the Soy wax 52℃, during the approximation, the coefficients of determination were 99.99% and 94.78% for the nonlinear and linear models, respectively, as described in Fig. 4.6 and 4.7. On the other hand, the standard deviations were 4.45 and 6.92 hours for the nonlinear and linear models, respectively.

Similarly, in the Soy wax 62℃, the coefficients of determination were 99.89% and 99.87% for the nonlinear and linear models, respectively, while the standard deviation was 3.1 for both models. These models represent the closest expression of the relationship between samples, quantity, temperature, and the storage time of the TES.

Consequently, it was proven that the improvement of the storage time using the Lagrange multipliers optimisation process results in 15.6 (h) for the Soy wax 52℃ and 16.36 (h) for the Soy wax 62℃, which means more extended storing capacity as shown in Table 4.6 and 4.7.

Table 4.6. Soya wax 52℃

Non-linear model	Linear model
R^2 = 99.99%	R^2 = 94.78%
SD = 4.45 hours	SD = 6.92 hours
t = 15.6 hours	t = 16.36 hours

Table 4.7. Soya wax 62℃

Non-linear model	Linear model
R^2 = 99.89%	R^2 = 99.87%
SD = 3.1 hours	SD = 3.1 hours
t = 16.36 hours	t = 17.78 hours

4.2. Optimum boiler configurations into SHIP

4.2.1. Required collector area

The modelling for 20 collector areas varies from 5 to 100 m^2 with an incremental step of 5 m^2. Both in-series and parallel systems were modelled while fixing the other variables at 50 l/m^2 tank volume to the solar collector area recommended for solar heat for industrial processes under the climate of central Europe (Franco, 2020) to make the comparison. The relative volume flow rate

to each square meter of the collector area is 50 l/m^2·h, as the literature recommends (Duffie & Beckman, 2013). In the primary loop, the volumetric glycol ratio is 30%, which has 3736 J/kg·K specific heat capacity. It can stand at -13 °C freezing temperature and -30°C for burst protection according to the Hungarian climate. Finally, the height-to-diameter ratio of the buffer tank was chosen to be 1.8 m/m. Above this value, the daily heat losses from the tank will be relatively higher due to the larger exposed surface to the ambient.

As in Fig. 4.8, the results show that, in general, in-series boiler connection has higher results than in parallel configuration. It is noted that the difference reaches its maximum value of 5.8% when the collector area is 65 m^2. At this value, a series connection delivers 65.48% solar fraction while, in parallel, delivers 59.68% only. According to the design recommendations from financial aspects, the best feasible design should deliver between 40 – 60% solar fraction in winter and summer conditions, respectively. As for average design value, 50% annual solar fraction is the optimum, representing 40 – 45 m^{2,} which equals 20 ETC collectors. This design is adequate since it provides more than 50% monthly solar fraction between April and October.

Nevertheless, it does not fall below 25% monthly solar fraction for the entire year. Considering the required space, costs, and potential reliability issues attributed to large systems (in our case, between 40 – 45 m^2), this system is a good design for the studied plant in Budapest, Hungary. For the assumed recommendations, the solar thermal system consists of a 40 m^2 solar collector field that provides 49.05% and 51.72% in parallel and series configuration, respectively. In contrast, a system consisting of a 45 m^2 solar collector field provides 52.27% and 55.41% in parallel and series, respectively. In conclusion, the differences between 40 m^2 and 45 m^2 solar collector fields are 2.67% and 3.14% more solar fraction in series mode than in parallel.

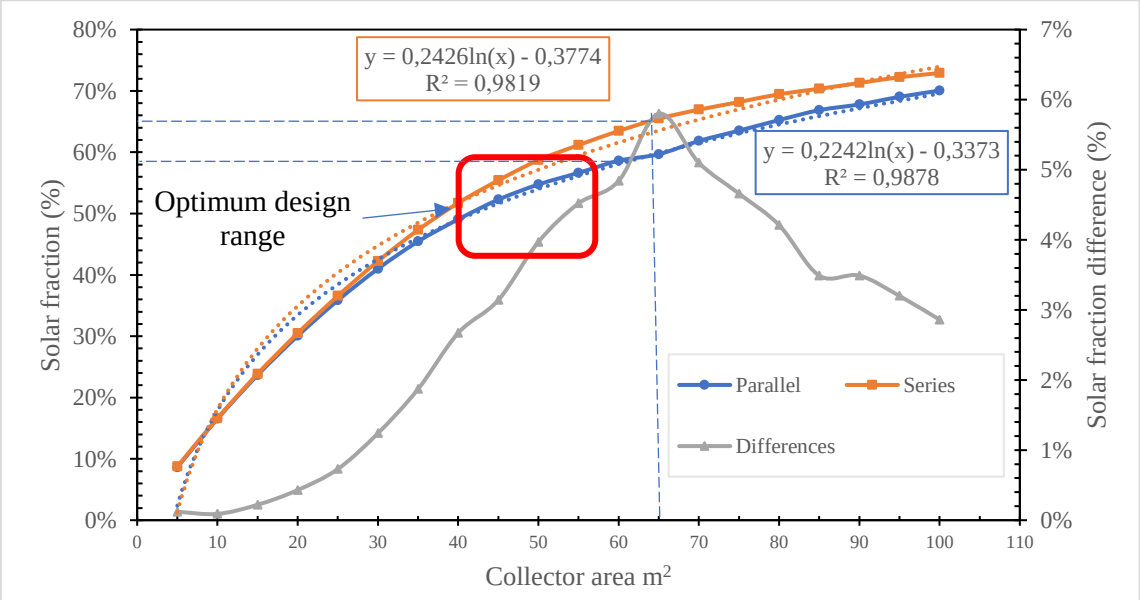

Fig. 4.8. Collector area versus solar fraction

4.2.2. Glycol ratio configurations

In the primary loop of the solar thermal systems, the solution of a polypropylene glycol-water mixture is used to avoid bursts and freezing situations in relatively cold climates. As the glycol volumetric ratio increases in water, the specific heat decreases of the whole mixture since the specific heat of the glycol is less than the water. For the comparison, the other variables were set at fixed values similar to our first model while changing the volumetric glycol ratio. The fixed variables were 50 l/m^2 tank volume to solar collector area, 50 l/m^2·h relative volume flow rate and

the height-to-diameter ratio of the buffer tank chosen to be 1.8 m/m and 35 m^2 collector area. The glycol ratio varies from 0% (thoroughly water solution) to 60% with an incremental step of 5%.

The results show, as in Fig. 4.9, that the series boiler configuration has a higher solar fraction than the parallel one. Nevertheless, the difference does not exceed 0.5% solar fraction at the best scenarios. This concludes that the glycol ratio does not severely affect the solar fraction in both modes, parallel and series. A glycol mixture is necessary for cold climate conditions to avoid freezing and burst problems that may stop the entire system. We can say that the glycol ratio does not affect the results from an energetic aspect, but we still have to consider the mechanical and hydraulic aspects. For the 30% glycol volumetric ratio, we noted that the solar system provides 40.07% solar fraction in parallel mode compared to 40.48% in series mode. This concludes that series configurations have a 0.42% solar fraction than parallel ones. Also, it is noted that the maximum difference is at a 15% glycol ratio of 0.5% more solar fraction, but this is below the recommended values from hydraulic and mechanical aspects.

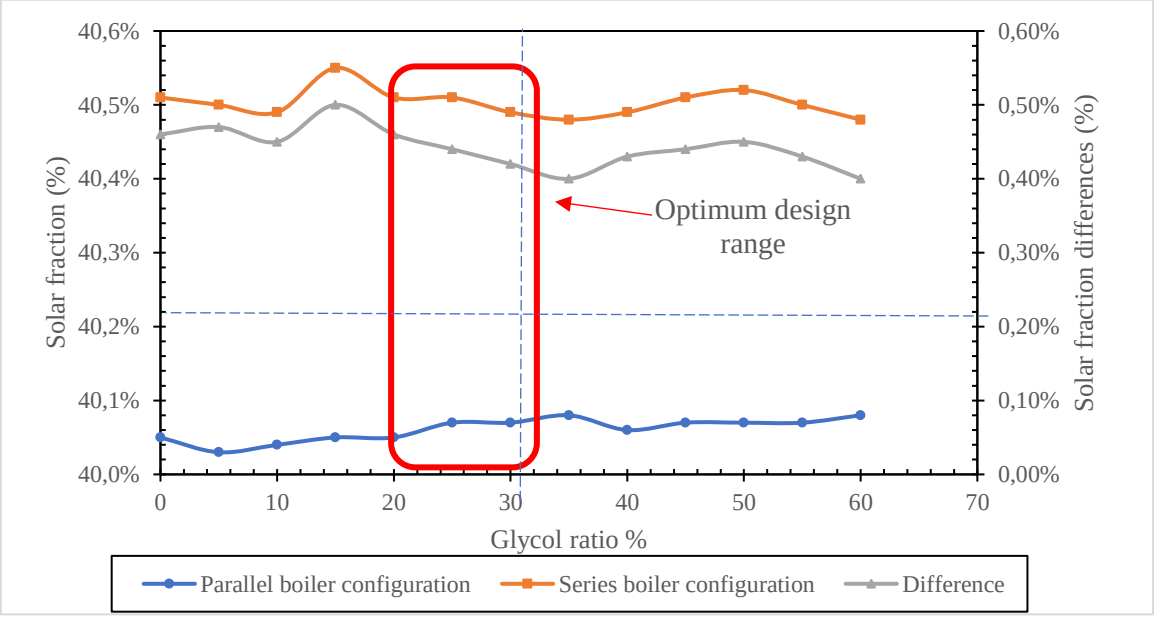

Fig. 4.9. Glycol ratio effect on the solar fraction

4.2.3. Collector flow rate configuration

The effect of the relative flow rate in the collector $\frac{\dot{m}}{A_C}$ Varies between 5 to 100 litres per hour for each square meter of the gross collector area with an incremental step of 5 l/h·m^2. The annual and monthly solar fraction was modelled for both systems, in series and parallel, to conduct the comparison. The other variables were fixed at 35 m^2 solar collector area, 50 l/m^2 relative tank volume to solar collector area, 30% volumetric glycol ratio and finally, the height-to-diameter ratio of the buffer tank chosen to be 1.8 m/m.

The results show in Fig. 4.10 that an in-series boiler connection generally provides a higher annual solar fraction. The differences between the two systems are more significant when the relative flow rate is significant at 5 – 15 l/h·m^2, while it is almost constant between 20 – 90 l/h·m^2. The difference in the results is more than 2.05% when the flow rate is 5 l/h·m^2, while it is around 0.5% between 20 – 90 l/h·m^2. According to the recommendation of using 50 l/h·m^2 in the central European climate, the difference is 0.42 – 0.56%.

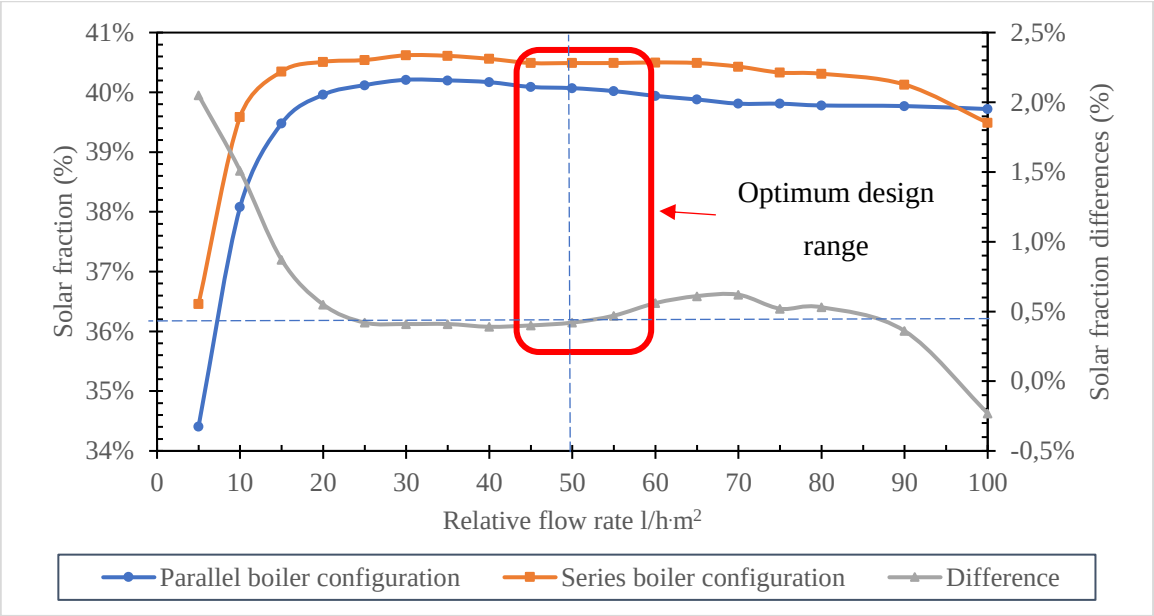

Fig. 4.10. Relative flow rate effect on the solar fraction

4.2.4. Relative tank volume configuration

Considered one of the most influential factors in the solar system, relative solar tank volume V_C/A_C is measured at different ratios from 10 to 300 litres buffer tank volume for each collector's gross square meter area. Meanwhile, the other variables were fixed at a 35 m^2 solar collector area, 50 $l/h \cdot m^2$ relative volume flow rate, 30% volumetric glycol ratio and finally, the height-to-diameter ratio of the buffer tank chosen to be 1.8 m/m.

As in Fig. 4.11, the results show that, in general, series boiler configurations provide higher solar yield than parallel connections. The maximum difference occurs when V_C/A_C equals 20 litres/m^2 with a 5.1% annual solar fraction difference. According to the central and southern Europe recommendations for industrial heat process, 50 – 75 litres/m^2 is a good design. In-series connection provides between 0.93 – 2.05% annual solar fraction for this range.

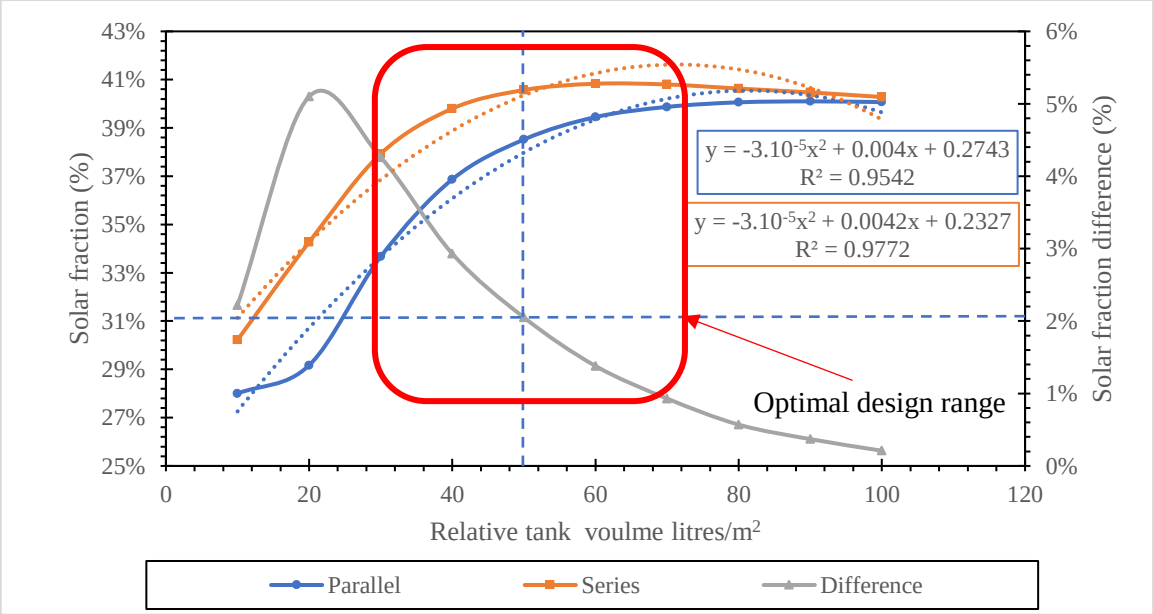

Fig. 4.11. Relative tank volume effect on the solar fraction

4.2.5. Tank height-to-diameter configuration

Both systems were studied using the tank height-to-diameter ratio as the variable to compare the two configurations. At the same time, the other parameters were fixed at a 35 m^2 solar collector area, 50 $l/h \cdot m^2$ volume flow rate, and 30% volumetric glycol ratio.

The results show, as in Fig. 4.12, that, in general, a series connection delivers more solar yield than a parallel connection. The variations between the two configurations are 0.44% on average. For recommended designs at a 1.8 m/m tank height-to-diameter ratio, the difference is 0.42% annual solar fraction. For horizontal design at 0.2 m/m, which is not common because it utilises more space to mount, the difference is 0.57%.

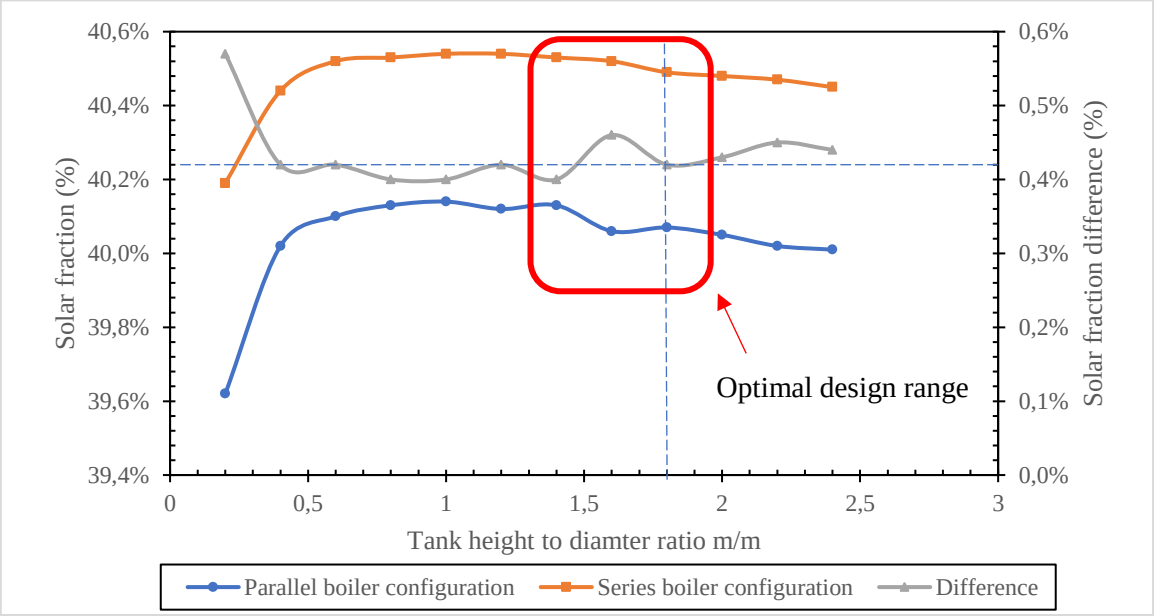

Fig. 4.12. Tank height-to-diameter ratio effect on the solar fraction

The results showed (Fig 4.8 - 4.12) that in-series boiler configuration yields between 2.67% and 3.14% more solar fraction than in-parallel configuration. On the other hand, considering the glycol ratio as the main factor, in-series boiler configuration delivers 0.42% more solar fraction than in-parallel configuration. For this aspect, hydraulic and mechanical prospects must be considered for safe operating conditions. Similarly, the relative flow rate harvests more than 2.05% solar fraction when the ratio is between 5 - 15 $l/h \cdot m^2$ and 0.42 – 0.56% at the recommended central European conditions. The relative tank volume is crucial since the maximum difference occurs when the value equals 20 litres/m^2 with a 5.1% solar fraction difference. While for the optimum values between 50 – 75 litres/m^2, I noticed that in-series configuration provides 0.93 – 2.05% more annual solar fraction for this range. Finally, the same observation for the tank height-to-diameter ratio is noticed. On average, an in-series configuration provides 0.44% more solar fraction than an in-parallel one. On the contrary, for the recommended value of 1.8 m/m, the difference is 0.42% annual solar fraction. I noticed that the highest difference of 0.57% occurred at 0.2 m/m, which means that the tank is horizontal and utilises a more extensive area to be mounted.

4.2.6. Overall system response to changing factors using RSM method

Many studies consider the final output of their research as one factor changing the result. For example, if the solar collector area changes from 5 to 10 m^2, the solar fraction will increase from 15% to 20%. This argument is not necessarily correct in a real system due to the interaction

between the studied factors. According to the same example, changing the collector area will definitely result in extra tank capacity, higher glycol content in the collector loop, and a higher volume flow rate. These facts are explained as follows:

- Generally, we need between 50-75 litres per square meter collector area.
- When having more collectors, we need to have an immense water volume in the collector loop, resulting in larger amounts of glycol.
- When having more collectors, we need a flow rate corresponding to the collector's area, around 75 litres per hour per collector's square area.

From the abovementioned facts, we deduce that we cannot get a final result before checking the interaction of the total factors. The modelling process takes place using T*Sol and R-Script software. The results were shown using Pareto plots, two factors' interactions, and tabular results.

It is clear from the parallel system in Fig. 4.13 that factors A, D, and C are the most dominant single factors, while A: D and A: C are the most significant two factors' interactions. The most substantial factor is A, representing the collector area and is times stronger than the other factors, around 28%, while the D factor is 3.15%. This output illustrates that the collector area is critical when planning a solar thermal system, considering the other factors' variations. On the contrary, in Fig. 4.8, changing the solar collector area from 5 to 100 m^2 will result in a 61.3% higher solar fraction when one-factor changes and the others remain the same. At the same time, according to Fig. 4.13, the change in the solar fraction will not be more significant than 28.52%, which is more realistic.

Similarly, factor D, which represents the relative tank volume, has a positive magnitude with a 3.15% solar fraction, as in Fig. 4.13. In comparison, Fig. 4.11 showed a 12% improvement when moving from 10 to 100 litres per square meter collector's area. In the third place, the two factors interaction A: D, as in Fig. 4.13, is the most internuncial at around 3% positive magnitude, which cannot be found in the analytical method. Similar to the D factor, the C factor has a positive magnitude of 3%, representing the relative flow rate. In Fig. 4.10, moving from 10 to 100 litres per hour per square meter collector area will improve the system by 3%, while in Fig. 4.13, only 1.64%. Finally, as in Fig. 4.13, C: D two-factor interaction will reduce the solar fraction by around -0.7%, while it cannot be observed by the analytical method. The in-parallel system performance is described in Equation 4.1, where y represents the solar fraction %.

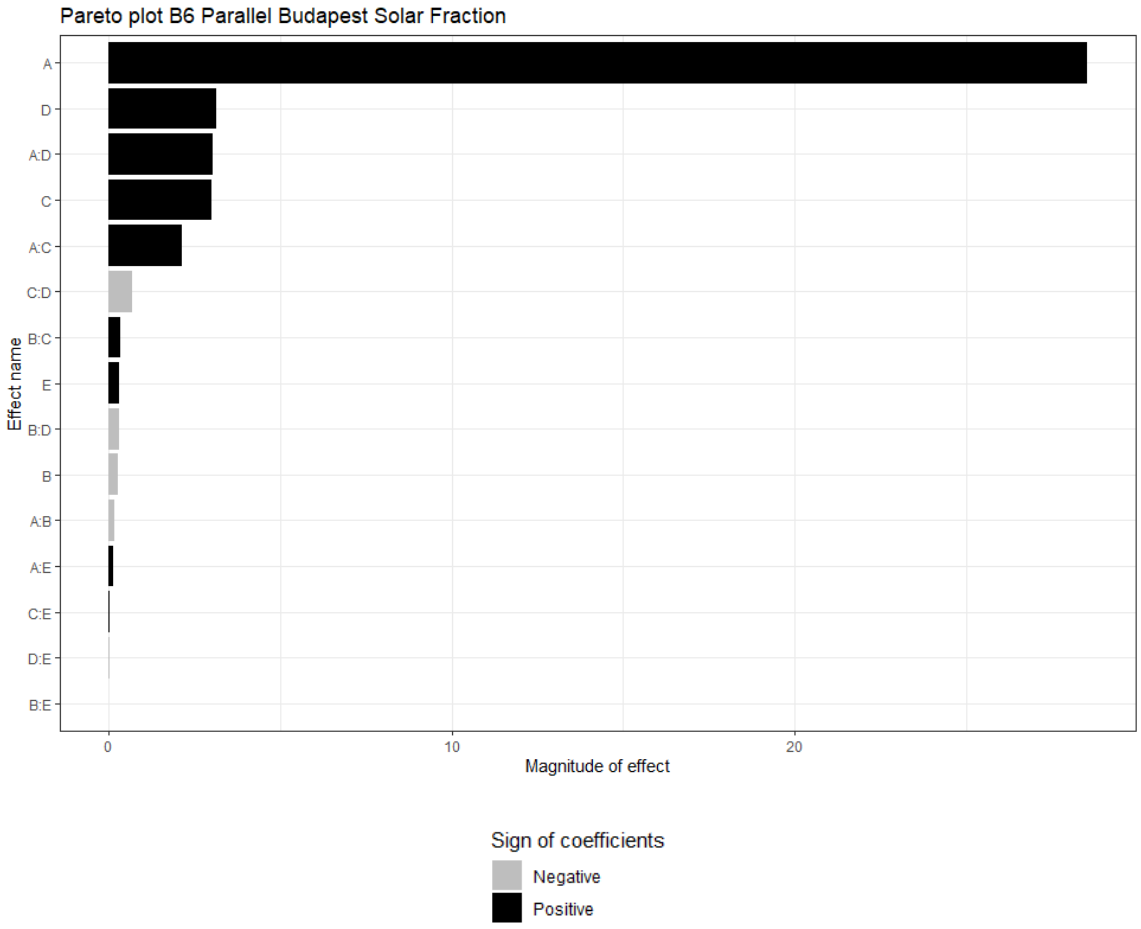

Figure 4.13. Pareto plot in parallel solar fraction.

A- Collector area (m^2); B - Glycol ratio (%); C - Relative flow rate ($l/h \cdot m^2$);

D - relative tank capacity (l/m^2); E - tank height-to-diameter ratio (m/m).

The contour plot of the A: D interaction 3% in Fig. 4.14 showed the optimum orientation of the model where both A and D factors are at a positive magnitude. Values higher than one coded value for A (100 m^2) and D (100 litres/m^2) will result in a 100% solar fraction or more. This result from the energetic aspect is optimum, but financially, systems with solar fractions between 40 – 60% are the best fit from an economic prospect. Also, the area on the left-hand side of the contour with dark green having negative solar fraction results is not a practical result, which leaves us with the highlighted optimum area. As seen from the key level indicator on the right side of the graph, the red colour means a higher solar fraction. So, moving to the upper right corner of the graph will lead us to the highest outcome.

Moreover, from the contour lines, it is evident that the lines tend towards the upper right side, meaning that both A (collector area) and D (relative tank capacity) factors should be positive coded values as indicated by the arrow. On the other hand, the highlighted area on the bottom left of the graph with coded values lower than -1 for A and D factors has no representatives in the real or practical world values. Using equation 3.2, we can obtain that A = +2 coded values correspond to 147.5 m^2 collector area, and D = +2 corresponds to 150 litres per collector square area.

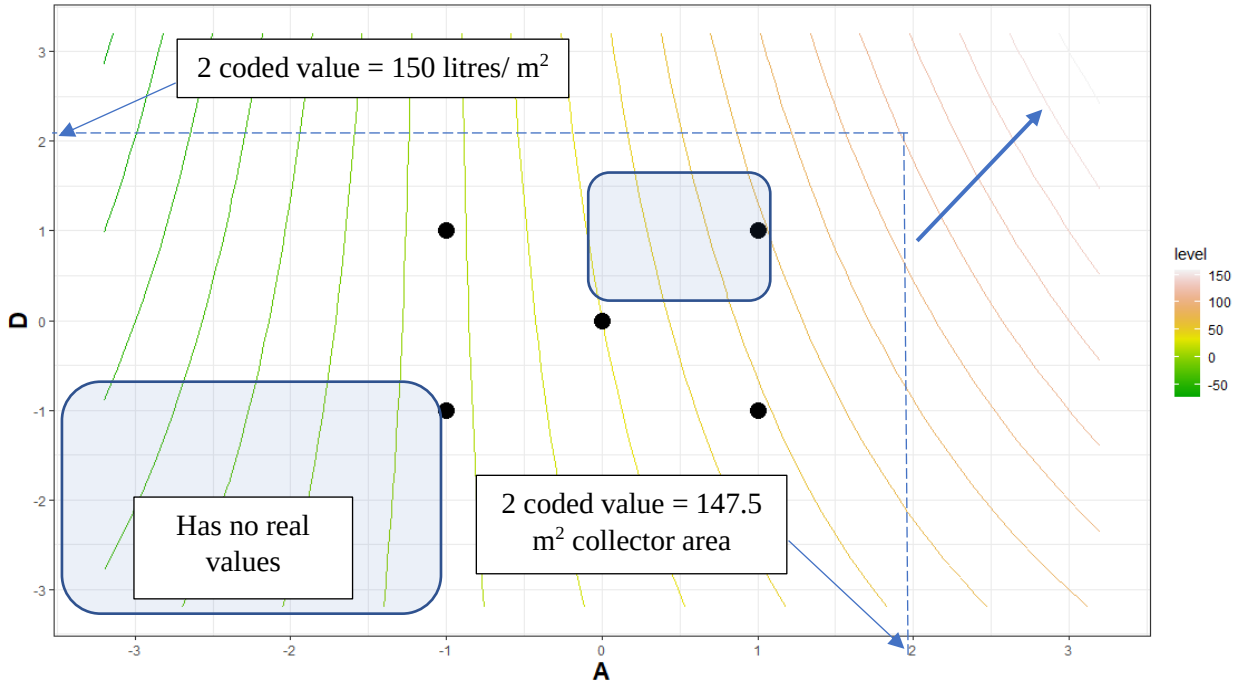

Fig. 4.14. Collector area (A (m^2))) and relative tank capacity (D (l/m^2)) two-factor interaction

Where A= -1 = 5 m^2 and A= +1 = 100 m^2; D=-1 = 10 l/m^2 and D= +1 = 100 l/m^2

On the other hand, the contour plot of the A: C interaction 2.13% in Fig. 4.15 between the collector area and the relative flow rate showed values higher than 100% solar fraction when the values of the factors are higher than one coded value (100 m^2 collector area, and 100 litres/hour·m^2 volume flow rate). Again, the extraordinarily high and negative solar fraction results are neither economical nor practical, leaving the optimum area, as highlighted in the contour plot.

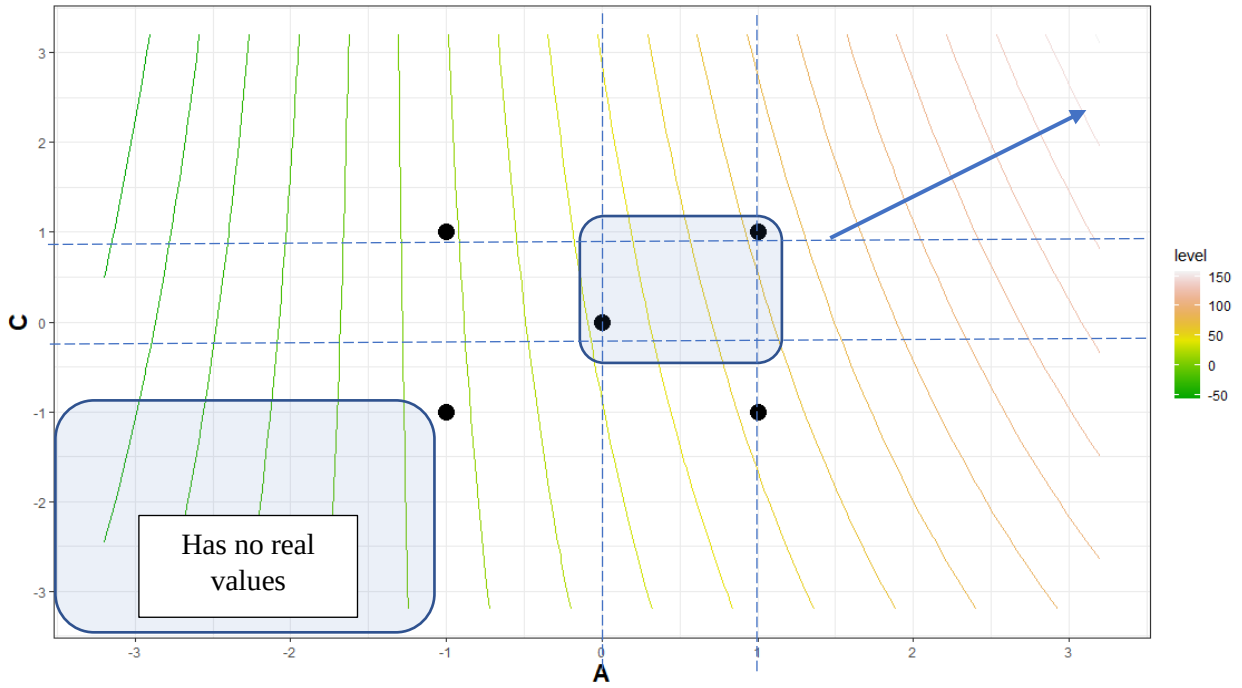

Figure 4.15. Collector area (A (m^2)) and relative flow rate (C ($l/h\ m^2$)) two-factor interaction

Where A = 0 = 52.5 m^2; A= +1 = 100 m^2; C = 0 = 52.5 $l/h·m^2$; C = +1 = 100 $l/h·m^2$

Finally, the C: D two-factor interaction -0.69% as in Fig. 4.16 between the relative flow rate and the relative tank capacity showed a negative magnitude. As represented on the right side of the graph, the level difference is minor, and the highest possible outcome can be obtained by moving to the upper right corner of the graph. This result means that both the C factor (relative flow rate) and D factor (relative tank capacity) should be at a positive magnitude. On the other hand, the lower left corner represents no real values near C = -1 = 5 litres per hour per collectors' square area and D = -1 = 50 litres per collectors' square meter. Finally, the optimum solar fraction values can be obtained by moving in the direction of the arrow to the upper right corner of the graph.

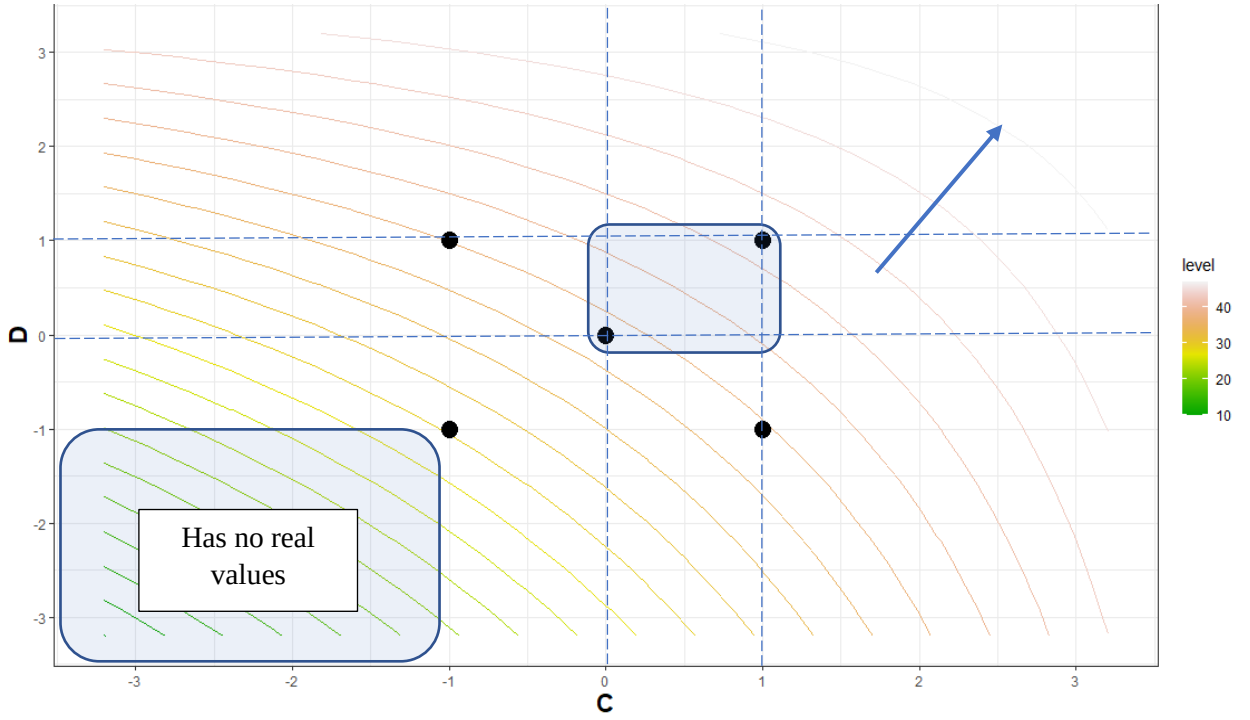

Figure 4.16. Relative flow rate (C (l/h· m^2)) and relative tank capacity (D (l/m^2)) Two factors interact in a parallel system.

Where C = 0 = 52.5 l/h· m^2; C = +1 = 100 l/h· m^2; D = 0 = 55 l/m^2 and D = +1 = 100 l/m^2

It is concluded from the two factors' interaction graphs that A (collector area), C (relative flow rate) and D (relative tank capacity) factors are essential, while B (Glycol ratio) and E (tanks height-to-diameter ratio) are to a lesser degree. The two-factor contours show that factors A, C, and D should be at a positive magnitude to obtain a higher solar fraction. The lower left corner has no corresponding real values since values lower than C = D = -1 can not be lower than 0 flow rate or tank capacity.

According to Table 4.8, we can identify the statistical aspects of the model (factors estimate, standard deviation, t-value- and p-value). The intercept value is the value that stands without any factor, meaning that if all factors are zero-coded values, then the system's output is the intercept value. For example, the solar fraction would be 36.59% if all factors equal zero. As high as the estimated value of factors, it has a higher magnitude on the overall performance. As in Table 4.8, the highest magnitudes are as follows: the set intercept, A, D, A: D, C, and A: C, respectively. At the same time, the standard error measures the discrepancy amount that can be expected in a sample compared to the actual population value. The standard deviation represents how scattered the data is with the mean value; therefore, as more minor, the standard error is better.

On the other hand, the t-value indicates the reliability of the predictive power of the coefficient. Generally, any value more excellent than +2 or lesser than -2 is acceptable; the higher the t-value, the greater the confidence of the predictor coefficient. Finally, if the p-value is less than 0.05, the predictor variable has a statistically significant relationship with the response variable in the model. In Table 4.8, it is observed with stars, meaning that the intercept and A values have a significant relationship with the solar fraction value as signed with three stars <0.0001. Similarly, factors C and D and A: D have a significant relationship with the solar fraction signed with two stars <0.001, and finally, A: C has a two-factor interaction with one star <0.05. The single factors that have no significant relationship with the solar fraction must be mentioned: B and E. The glycol ratio B has no observed influence on the solar fraction from energetic aspects. Nevertheless, this factor should be considered from mechanical aspects since it causes bursts or frozen pipes when the temperature falls below zero degrees. Similarly, for the E factor, it is concluded that the tank's orientation (horizontal or vertical) will not result in a significant energetic influence but should be considered if the stratification is favourable for the heat process.

Table 4.8. Statistical coefficients for the parallel boiler configuration system.

Coefficients for the Parallel system				
(Intercept)	**Estimate**	**Std. Error**	**t value**	**p-value (>|t|)**
	36.596970	0.896050	40.843	< 2e-16 ***
A - collector area (m^2)	28.528125	0.909943	31.352	< 2e-16 ***
B - Glycol ratio (%)	-0.259375	0.909943	-0.285	0.77905
C - relative flow rate ($l/h \cdot m^2$)	3.003125	0.909943	3.300	0.00423 **
D - Relative tank capacity (l/m^2)	3.146875	0.909943	3.458	0.00300 **
E - Tank height-to-diameter ratio (m/m)	0.284375	0.909943	0.313	0.75845
A: B	-0.153125	0.909943	-0.168	0.86835
A: C	2.134375	0.909943	2.346	0.03139 *
A: D	3.015625	0.909943	3.314	0.00410 **
A: E	0.115625	0.909943	0.127	0.90038
B: C	0.321875	0.909943	0.354	0.72789
B: D	-0.284375	0.909943	-0.313	0.75845
B: E	0.003125	0.909943	0.003	0.99730
C: D	-0.696875	0.909943	-0.766	0.45427
C: E	0.015625	0.909943	0.017	0.98650
D: E	-0.015625	0.909943	-0.017	0.98650

According to Table 4.9, we can identify the statistical aspects of the model (factors estimate, standard deviation, t-value- and p-value). The intercept value is the value that stands without any factor, meaning that if all factors are zero-coded values, then the system's output is the intercept value. For example, the solar fraction would be 39.72% if all factors equal zero, which is higher than the parallel model by approximately 3.13%. As in Table 4.9, the highest magnitudes are as follows: the set intercept, A, D, A: D, and C, respectively, as also referred to in Fig. 4.17.

In Table 4.9, it is observed with stars, meaning that the intercept and A, D, and A: D values have a significant relationship with the solar fraction value as signed with three stars <0.0001. The single factors that have no significant relationship with the solar fraction must be mentioned: B and E. The glycol ratio B has no observed influence on the solar fraction from energetic aspects. Nevertheless, this factor should be considered from mechanical aspects since it causes bursts or frozen pipes when the temperature falls below zero degrees. Similarly, for the E factor, it can be

concluded that the tank's orientation as horizontal or vertical, to avoid stratification, will not result in a significant energetic influence but should be considered if the stratification is favourable for the heat process or not.

It is noted that the difference between the magnitudes of the parallel and series systems is in the series system's favour. In the series system, the set intercept was higher by 3.13%, the A factor by 3.01%, the D factor by 0.37%, and the A: D interaction by 0.47%. On the contrary, the C factor estimate was higher in the parallel system than the series by 2.14% and the A: C interaction was higher by 2.09%. This difference showed that the volume flow rate in the parallel configuration matters because, in a parallel system, both the boiler and the collector loops are parallelly connected to the buffer tank, resulting in no final interference from the boiler into the heat process temperature. For the in-series system, the boiler is connected to the heat process directly before this service, resulting in direct interference from the boiler if the volume flow rate of the collector loop is not suitable. Moreover, Equation 4.2 represents the in-series configuration results.

Table 4.9. Statistical coefficients for the series boiler configuration system.

Coefficients for Series system				
(Intercept)	**Estimate**	**Std. Error**	**t value**	**p-value (>|t|)**
	39.72121	0.84898	46.787	< 2e-16 ***
A - collector area (m^2)	31.54375	0.86214	36.588	< 2e-16 ***
B - Glycol ratio (%)	-0.06875	0.86214	-0.080	0.937373
C - relative flow rate ($l/h \cdot m^2$)	0.85625	0.86214	0.993	0.334555
D - Relative tank capacity (l/m^2)	3.51250	0.86214	4.074	0.000790 ***
E - Tank height-to-diameter ratio (m/m)	0.08125	0.86214	0.094	0.926019
A: B	-0.00625	0.86214	-0.007	0.994300
A: C	0.04375	0.86214	0.051	0.960120
A: D	3.47500	0.86214	4.031	0.000868 ***
A: E	0.04375	0.86214	0.051	0.960120
B: C	0.26875	0.86214	0.312	0.759041
B: D	-0.1250	0.86214	-0.145	0.886425
B: E	-0.01875	0.86214	-0.022	0.982902
C: D	0.37500	0.86214	0.435	0.669060
C: E	0.03125	0.86214	0.036	0.971508
D: E	0.02500	0.86214	0.029	0.977204

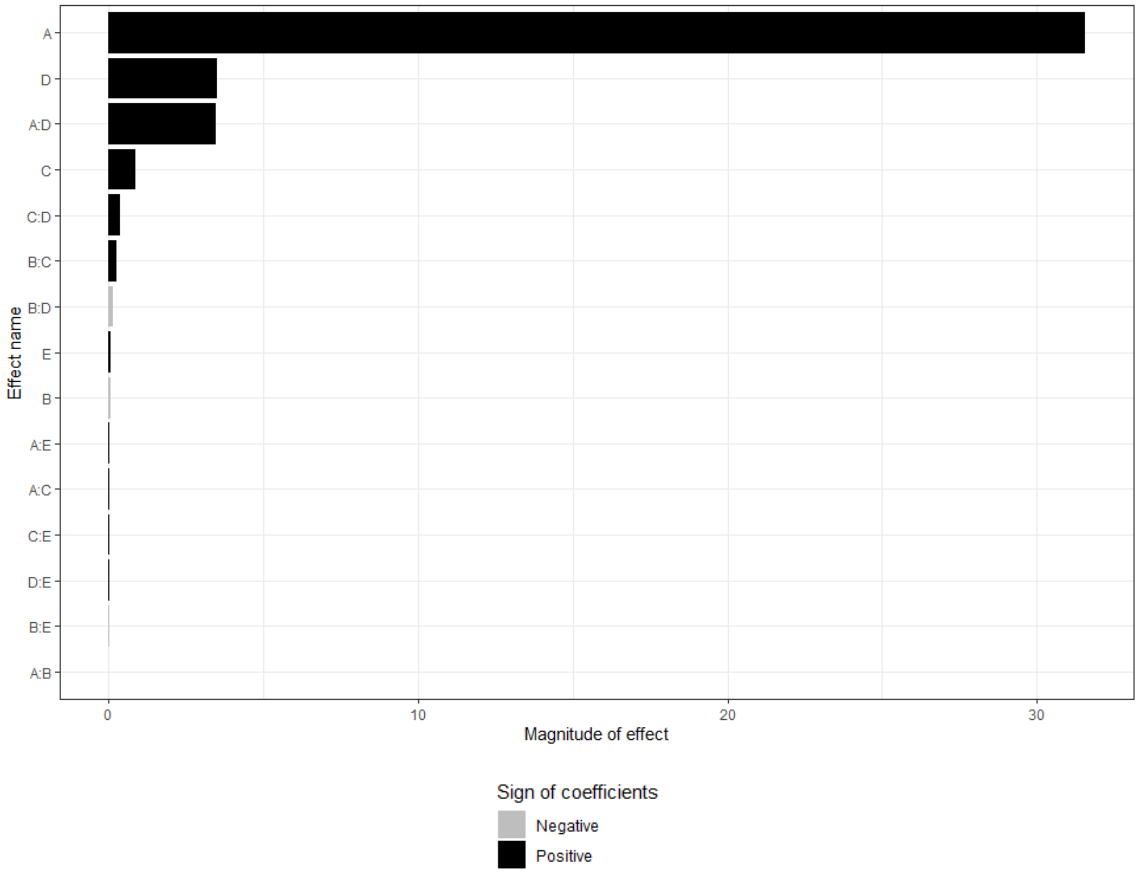

Figure 4.17. Pareto plot in a series solar system.

A- Collector area (m^2); B - Glycol ratio (%); C - Relative flow rate ($l/h \cdot m^2$);

D - relative tank capacity (l/m^2); E - tank height-to-diameter ratio (m/m).

The contour plot of the A: D interaction, in Fig. 4.18, 3.47%, showed the optimum orientation of the model where both A and D factors are at a positive magnitude. Values higher than one coded value for A (100 m^2) and D (100 litres/m^2) will result in a 100% solar fraction or more. This result from the energetic aspect is optimum, but financially, systems with solar fractions between 40 – 60% are the best fit from an economic prospect. Also, the area on the left-hand side of the contour with dark green having negative solar fraction results is not a practical result, which leaves us with the highlighted optimum area.

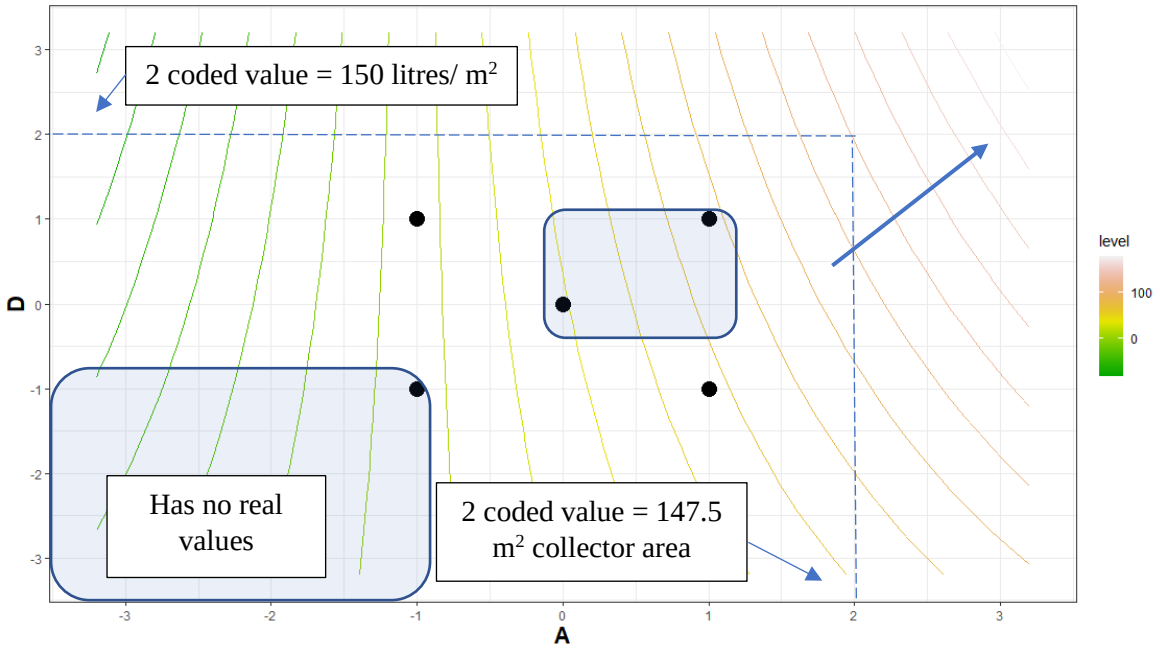

Figure 4.18. Collector area (A (m^2)) and relative tank capacity (D (l/m^2)) two factors' interaction in a series boiler configuration system

Where A= -1 = 5 m^2 and A= +1 = 100 m^2; D=-1 = 10 l/m^2 and D= +1 = 100 l/m^2

Similarly, the C: D two-factor interaction of 0.37%, as in Fig.4.19, between the relative flow rate and the relative tank capacity showed a positive magnitude. The optimum outcome can be gained if both factors move towards the upper right corner. It is also observed that the lower left corner of the graph has no corresponding real values since values lower than -1 for both C and D factors have no physical meaning.

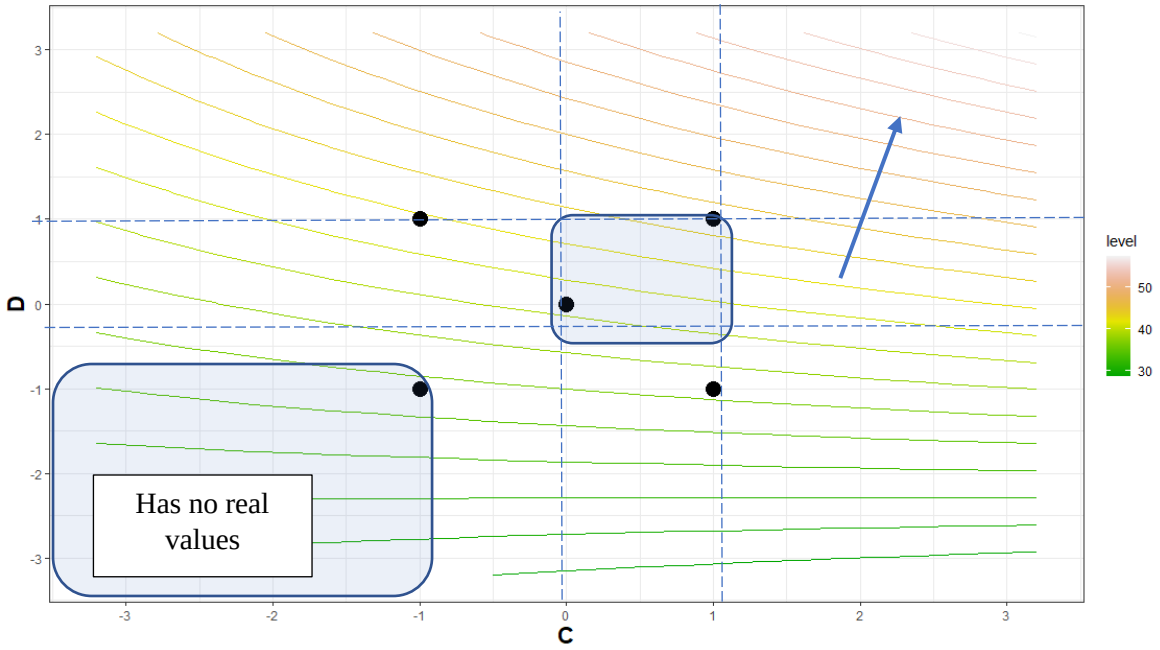

Figure 4.19. Relative tank capacity (D (l/m^2)) and relative flow rate (C ($l/h \cdot m^2$)) are two factors that interact in a series system

Where C = 0 = 52.5 $l/h \cdot m^2$; C = +1 = 100 $l/h \cdot m^2$; D = 0 = 55 l/m^2 and D = +1 = 100 l/m^2

On the other hand, the contour plot of the B: C interaction of 0.26%, as in Fig. 4.20, between the glycol ratio and the relative flow rate showed a low influence on the solar fraction when the values of the factors are higher than one coded value (80% glycol ratio, and 100 litres/hour·m^2 volume flow rate). As indicated by the level key indicator on the right side of the graph, the higher value can be obtained by moving towards the upper right corner.

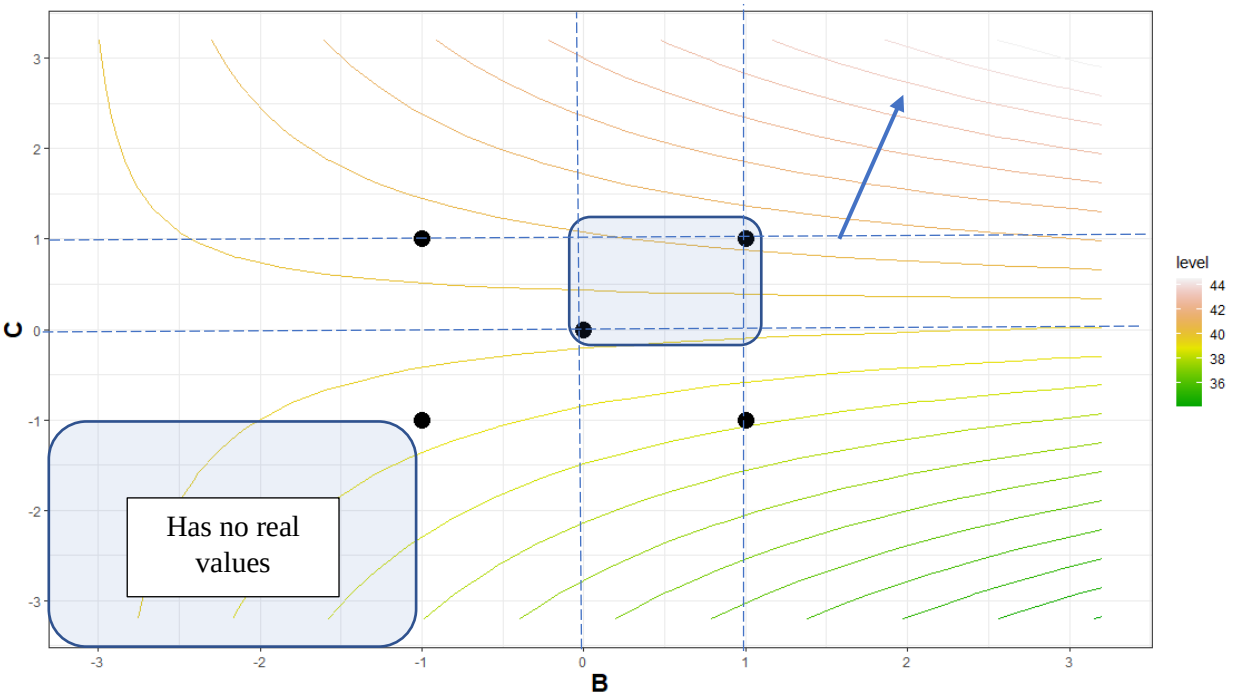

Figure 4.20. Glycol ratio (B (%)) and relative flow rate C (l/h·m^2)) two factors interaction in a series system

Where B = 0 = 42.5%; B = 1 = 80%; C = 0 = 52.5 l/h·m^2; C = +1 = 100 l/h·m^2

On the other hand, analysing the RSM results, I noted that the magnitude differences are in the series system's favour. Moreover, comparing the two systems in Fig. 4.12 and 4.16, I found out that in the series system, the set intercept was higher by 3.13%, the A factor by 3.01%, the D factor by 0.37%, and the A: D interaction by 0.47%. On the contrary, the C factor estimate was higher in the parallel system than the series by 2.14% and the A: C interaction was higher by 2.09%. This difference showed that the volume flow rate in the parallel configuration matters because, in a parallel system, both the boiler and the collector loops are parallelly connected to the buffer tank, resulting in no final interference from the boiler into the heat process temperature. For the in-series system, the boiler is connected to the heat process directly before this service, resulting in direct interference from the boiler if the volume flow rate of the collector loop is not suitable. It is also evident from the results that factors B: Glycol ration and E: tank height-to-diameter ratio have very little influence on the overall results, as illustrated by the summary results in Table. 4.10.

In conclusion, I proved that in-series boiler configuration provides higher annual solar yields (solar fraction) than in-parallel configuration from the most significant aspects using RSM and analytical methods. On the other hand, the results showed that choosing the RSM method will lead to more actual results than the traditional analytical method, since RSM provide real correlations between the studied factors. In contrast, the analytical method deals with it as independent factors. Due to these results, in-series configurations should be considered when installing solar thermal system technology in industrial plants for a higher outcome and results.

It must be noted that when analysing one factor, the other factors are set at recommended values: 50 l/m^{2}· h relative volume flow rate and 30% glycol ratio suggested for the Hungarian or central European climates, 50 l/m^{2} relative tank capacity, 1.8 m/m tank height-to-diameter ratio, and 35 m^{2} collector area.

Table 4.10. Differences summary between RSM and the analytical methods for Parallel configurations.

Factor	Change	In- parallel results		In-series results	
		Analytical method (%)	RSM method (%)	Analytical method (%)	RSM method (%)
A - Collector area (m^{2})	From 5 to 100	61.3	28.52	64.16	31.54
B - Glycol ratio (%)	From 5 to 80	-0.05	0.26	0.02	-0.07
C - Relative flow rate (litres/h m^{2})	From 10 to 100	1.64	3	0.1	0.86
D - Relative tank volume (litres/m^{2})	From 10 to 100	12.07	3.15	10.06	3.51
E - Tank height-to-diameter ratio (m/m)	From 0.2 to 2.4	-0.39	0.28	-0.26	0.08
A:D - two-factor interaction	-	-	3.02	-	3.48
C:D - two-facto interaction	-	-	-0.7	-	0.37

4.3. Tankless SHIP

The outcomes of this research, along with the corresponding physical explanations, are described in this paragraph. Data were collected for the continual flow of hot water at different process heat temperatures, 35 - 60 ℃ for preheating water and 60 litres per hour configurations of flow rates in the primary and secondary loop and actual solar radiation from the sun.

4.3.1. Hungarian weather profile

The Hungarian climate is continental, with cold, snowy, frigid winters and low humid hot summers. The average annual temperature is 9.70℃ based on long-term statistics and 11.25℃ based on the software outputs. In comparison, temperature extremes can reach down to -29℃ in winter which require 30% of glycol mixture in order to avoid burst and freeze. The minimum and maximum variation of the annual ambient temperatures obtained from the T*sol simulation compared to the actual data shown in Fig. 4.21 (a). In the same plot, the solar radiation's annual variation is also portrayed to show the interactive pattern between the two parameters, as in Fig. 4.21 (b). It is evident from the graph that the ambient temperature varies with the solar radiation, and the ambient temperature profile varies between -1 and 23℃ in average monthly rates.

The comparison is conducted between the T*sol weather data file, TMY, an average recorder between 1995 and 2012, and the actual experiment data at the site location. As a result, the average differences are more than one hundred kWh/m^{2,} and the error is 10% between the two yields, as in Fig. 4.22 (b). The average difference for the ambient air temperature profiles is less than 0.1℃, with approximately 0.8% error, as in Fig. 4.22 (a).

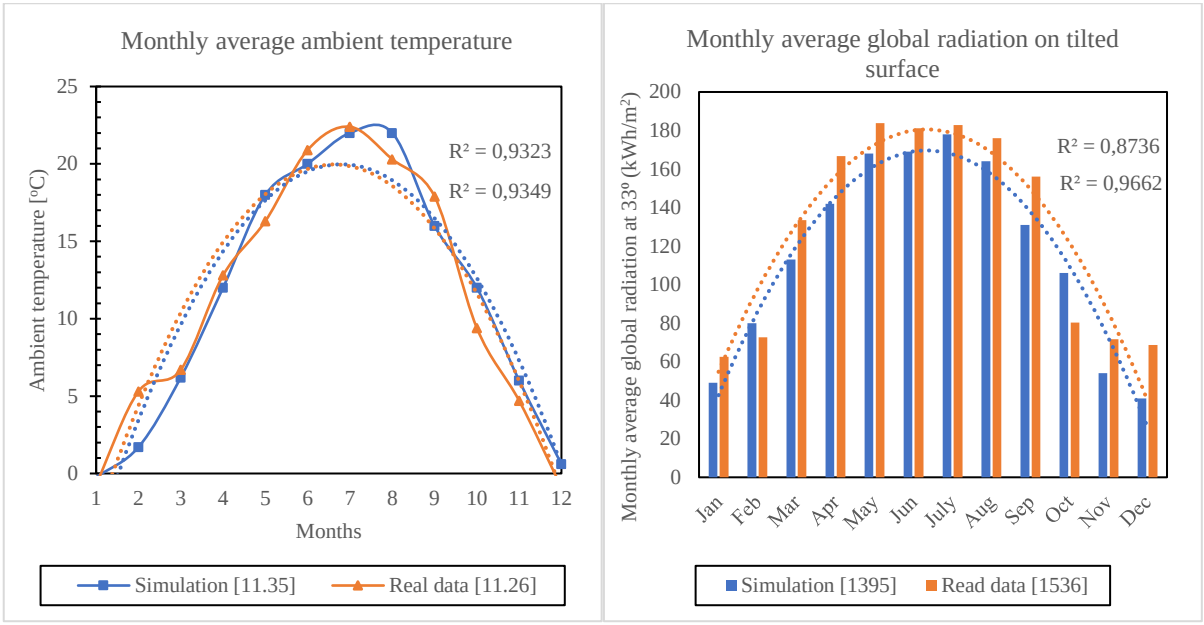

(a) (b)

Figure 4.21. Monthly average a) ambient temperature b) solar radiation

A comparison analysis was conducted to understand this difference. It was found that there is a linear correlation using (0,0) set intercept between the two ambient temperature profiles and the determination coefficient R^2= 0.9848. Similarly, for the global radiation profiles, it was found that the two profiles have a linear correlation with a determination coefficient R^2= 0.9874, as in Fig. 4.22. On the other hand, the equations representing the two graphs are linear models where y = 0.9863x and y = 0.9874x for the ambient temperature and the global radiation, respectively. Finally, the high coefficient of determination R^2 values showed that the modelled and real data are highly correlated, and the error is below 2%.

a)

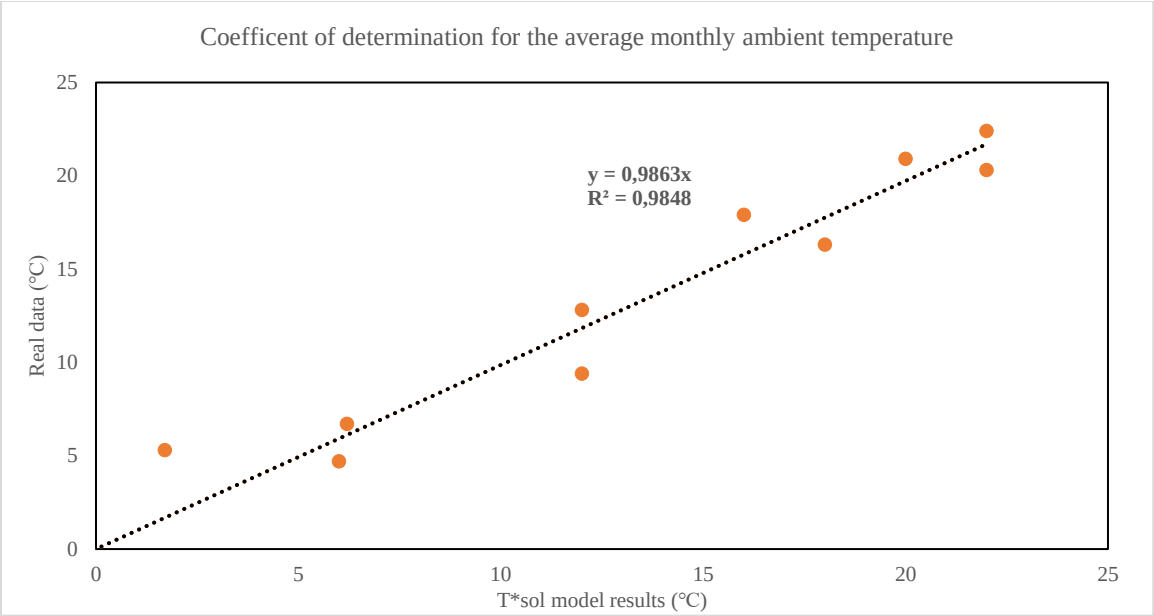

b)

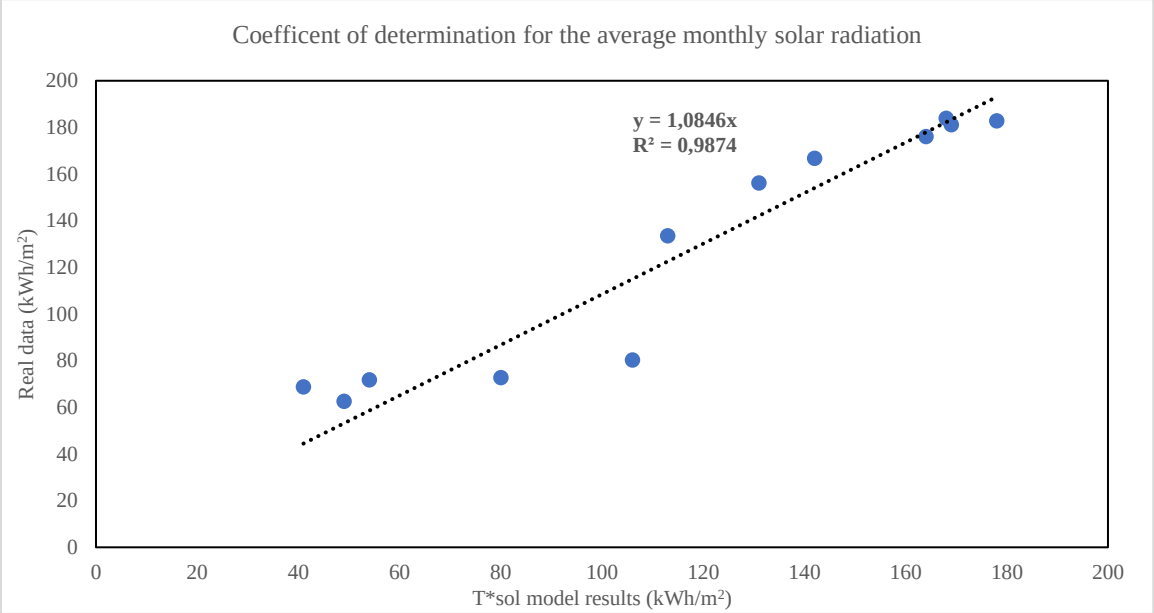

Figure 4.22. Coefficients of determination for linear average monthly weather data a) ambient temperature b) solar radiation

For a narrower vision of the weathering profile, we conducted the average hourly measurements of the three-month experiment (July, August, and September 2021). The ambient temperature and solar radiation are highly correlated, as well as in Fig. 4.23. The Least-square method is used, which is a statistical method to find the best-fit line of a particular equation in the form of Y = m X +b for a given set of data. Since we have hundreds of data sets, this method is ideal for generating the regression line. This method is generally used in data fitting, where we assume that the best-fit result is to reduce the sum of the squared errors, which is the difference between the observed values and the corresponding values.

It should be noted that (0,0) set intercept is a logical constraint since it can be assumed that where the real experiment's ambient temperature equals zero, the simulation must match these results. Similarly, it can be applied to global radiation results. In case of using a set intercept (0,0), the equation for the ambient temperature is y= 1.1773x and R^2 = 0.9769. Similarly, the equation for

the globarl solar radiation with a set intercept (0,0) is y = 1.085x and R^2 = 0.748. In the end, the higher the R^2 value showed us that this method is the best-fit line for the below-illustrated graphs.

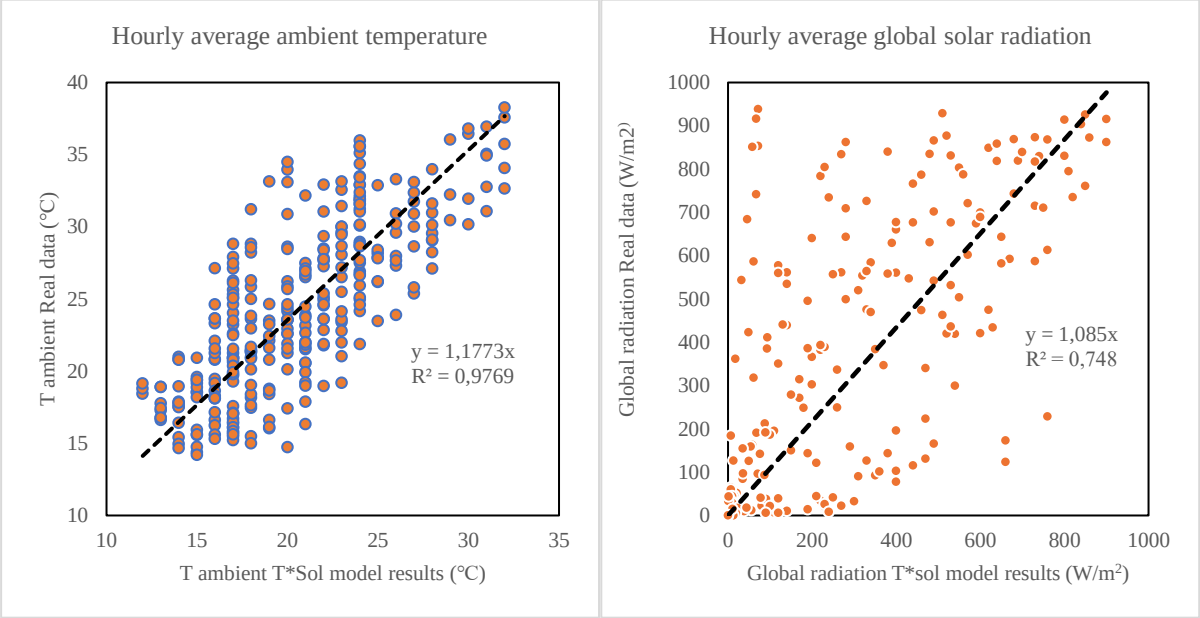

(a) (b)

Figure 4.23 Coefficients of determination of hourly average (a) Ambient temperature (b) Solar radiation

By comparing Fig. 4.22 and 4.23, it can be summed that real long-run data from 1992 - 2012 with the model resulted in high R^2 values, meaning that the two data sets are highly correlated, and the error is below 2% for both ambient temperature and global solar radiation. While by only comparing three months results, it shows that the ambient temperature is still highly correlated, and the error is below 3%, but the global solar radiation at around 25% error.

On the other hand, another conclusion was drawn to determine the correlation between solar radiation and the ambient temperature from two prospectives: long-term records from 1995 - 2012 generated by T*sol software and our experiment. The generated results were with a set intercept (0,0) and linear correlations trendlines. Regarding the long-term records and the experiment, the results show that the correlation between the ambient temperature and solar radiation is as in equations 4.6 and 4.7:

Long-term records: $T_{amb} = 0.1456Ra - 7.3775$ where $R^2 = 0.8288$ (4.6)

Based on one year of data in 2021, the validation curve is as follows:

Experiment validation result: $T_{amb} = 0.1552Ra - 6.6844$ where $R^2 = 0.8772$ (4.7)

The deviation between the two results, as in Fig. 4.24 a) and b), are minor, and the model can be used for further investigations.

a)

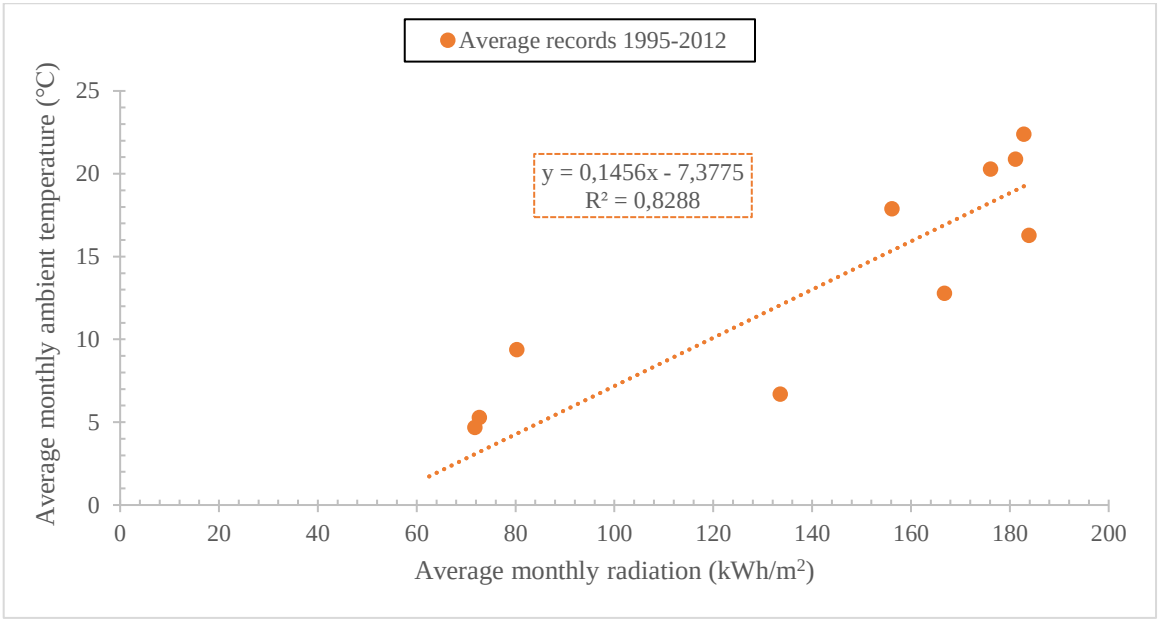

b)

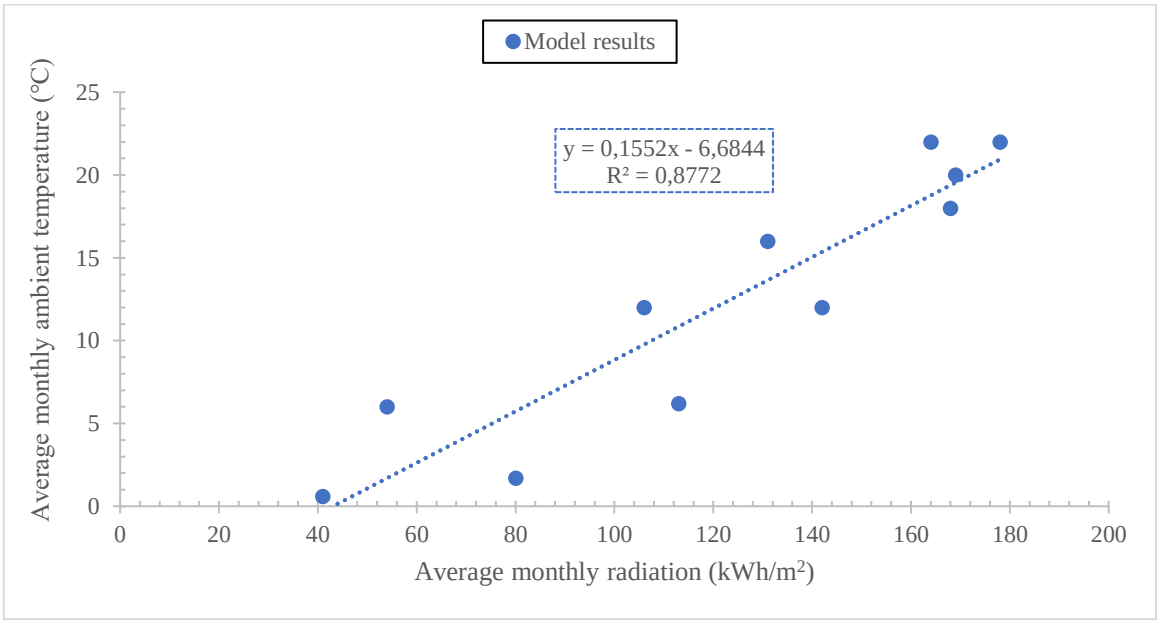

Figure 4.24. a) Long-term records (1995-2012) and b) Experiment model correlation between the average monthly ambient temperature and solar radiation.

4.3.2. Experiment model validation using LMTD approach

The authenticity of the dynamic simulation model using T*sol software of the tankless SHIP has been examined experimentally by real-time measurement for three months at 60/60 litres per hour for both loops (60 l/h primary and 60 l/h secondary). Fig. 4.25 shows the black dashed line, representing the heat process set temperature. It is pretty apparent from the graph that the orange line (representing the secondary output temperature) is always near the set temperature. Hence, the simulation model is appropriate for further predicting system performance. As illustrated in Fig. 4.25, each measurement took place for at least two successive days and was repeated if necessary due to the unexpected meteorological weather, if applicable. Each measurement's target temperature is set as required for the heat process (HX1_Sec_out), varying from 35°C to 60°C. This measurement aims at the low heat process temperatures that many food and beverage industry

processes need. The horizontal dashed line represents the target temperature in each graph with a notation above it mentioning the temperature value targeted. The most critical parameter is the HX1_Pr_in (as in grey), which represents the temperature coming from the solar collector.

On the other hand, the HX1_Sec_out (as in orange) represents the temperature used for the heat process. The two lines are further apart, so the solar collector can deliver more energy than required. If the grey line falls below the orange one, the heat process requires more energy than the solar system can provide. Nevertheless, it did not happen in all six measurements, which means this tankless solar system can provide direct energy for low-heat processes during summertime weather conditions in Budapest, Hungary. On the contrary, the HX1_Sec_in (as in blue) represents the post heating is needed. In the experiments, the grid water temperature is used for this purpose.

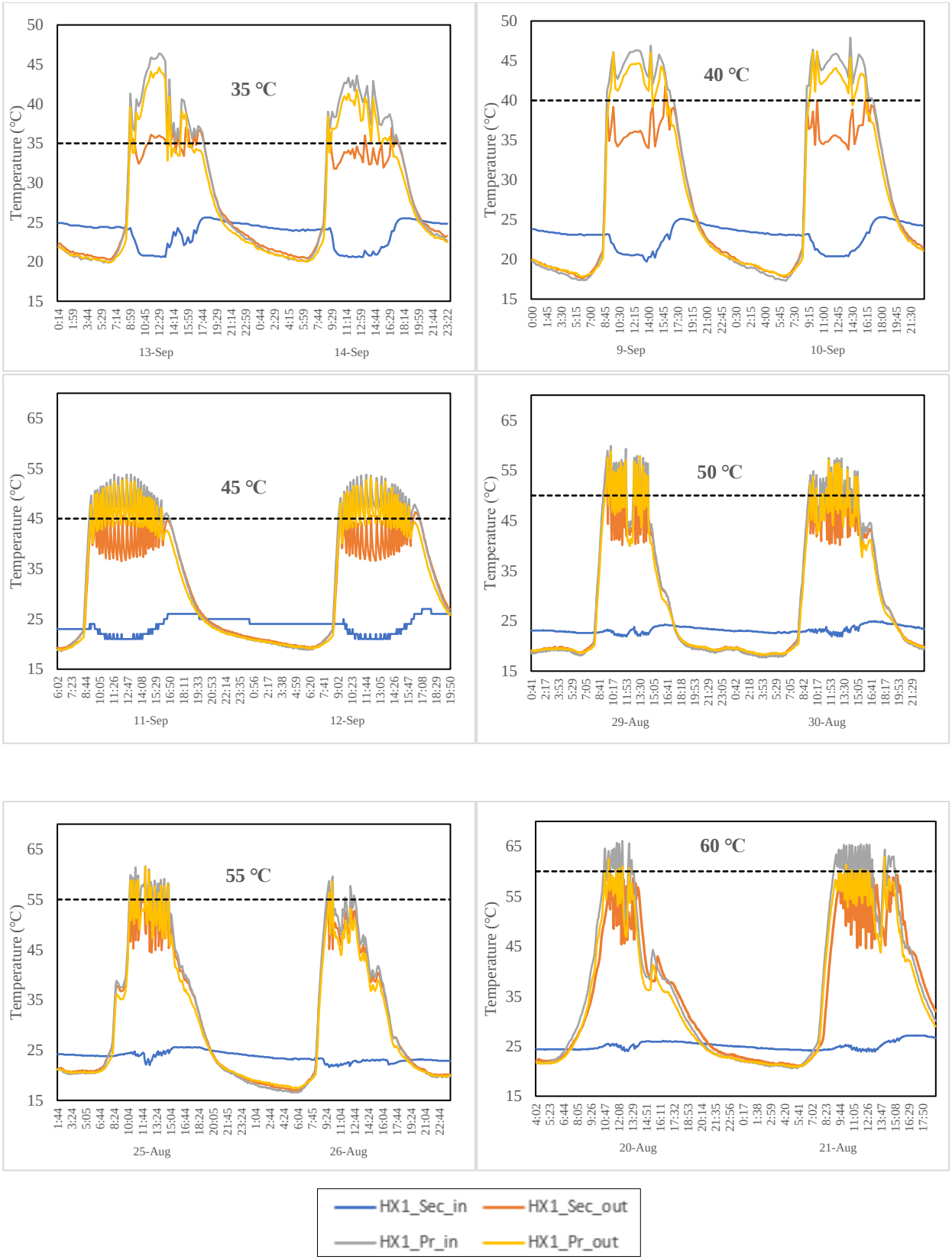

Figure 4.25. Actual experiments for a different set of output temperatures

HX1_Pr_in - primary input side temperature; HX1_Pr_out - primary output side temperature; HX1_Sec_in - secondary side input temperature; HX1_Sec_out - secondary output side temperature

The heat exchanger's secondary side output temperature as a function of the primary side input temperature was conducted in a linear correlation with a (0,0) set intercept to estimate the strength of the connection between the most critical parameters of the heat exchanger. As a result, in Fig. 4.26, the coefficients of determination are always higher than 0.9863, indicating the performance of the heat exchanger. It shows that the differences between the two parameters are as low as possible.

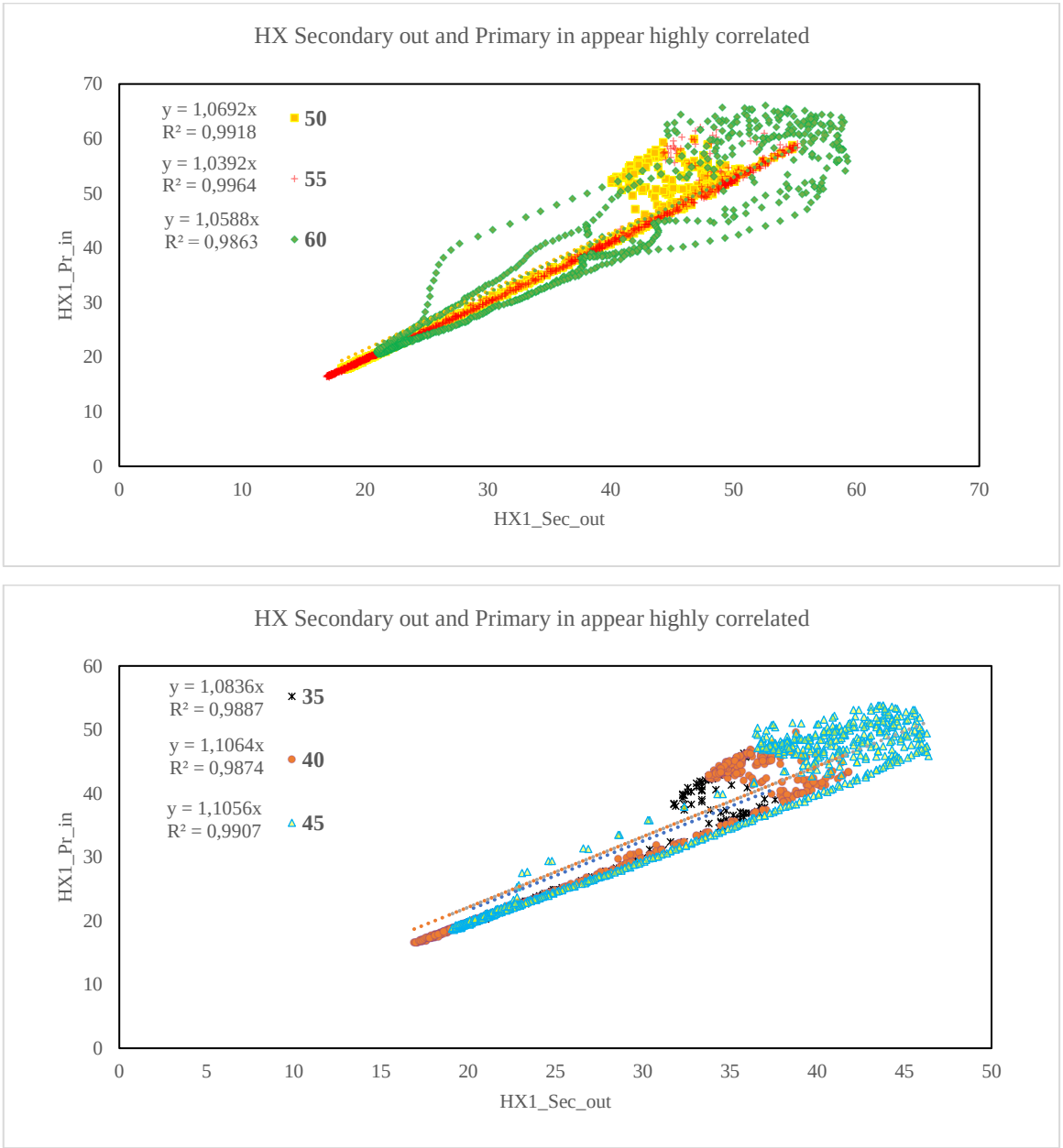

Figure 4.26. Heat exchanger primary input versus secondary output temperature

As in Fig. 4.26, the graphs show the black dashed line, representing the heat process set temperature. It is pretty apparent from the graph that the orange line (representing the secondary output temperature) is always near the set temperature. This measurement represents the efficiency of the extensive system represented by the four sides of the heat exchanger. Hence, the simulation model is appropriate for further predicting system performance. On the other hand, I conducted a linear correlation with a (0,0) set intercept of the heat exchanger's secondary side output temperature as a function of the primary side input temperature to estimate the strength of the

connection between the most critical parameters of the heat exchanger. As a result, I identified the coefficients of determination, which were consistently higher than 98.63%, indicating the performance of the heat exchanger as in the set equations 4.8:

$$\left.\begin{array}{lll} 60℃; & T_{pri\text{-}in} = 1.0588\ T_{sec\text{-}out}; & R^2 = 0.9863 \\ 55℃; & T_{pri\text{-}in} = 1.0392\ T_{sec\text{-}out}; & R^2 = 0.9964 \\ 50℃; & T_{pri\text{-}in} = 1.0692\ T_{sec\text{-}out}; & R^2 = 0.9918 \\ 45℃; & T_{pri\text{-}in} = 1.1056\ T_{sec\text{-}out}; & R^2 = 0.9907 \\ 40℃; & T_{pri\text{-}in} = 1.1064\ T_{sec\text{-}out}; & R^2 = 0.9874 \\ 35℃; & T_{pri\text{-}in} = 1.0836\ T_{sec\text{-}out}; & R^2 = 0.9887 \end{array}\right\} \quad (4.8)$$

In addition, the logarithmic mean temperature difference (LMTD) is a tool in flow systems, most notably in heat exchangers, to determine the temperature driving force for the heat transfer process (Li et al., 2021). For a heat exchanger with a specific heat transfer coefficient and constant area, the larger the LMTD the more heat is transferred. For a generic heat exchanger with two ends at which the cold and hot streams enter, the LMTD is defined by equation 4.9:

$$LMTD = \frac{\Delta T_p - \Delta T_s}{\ln\left(\frac{\Delta T_p}{\Delta T_s}\right)} \quad (4.9)$$

Where ΔT_s is the temperature changes in the heat exchanger's primary and secondary sides. In our case, the heat exchanger is a counter-current where the streams enter from different ends. It should be noted that the LMTD is a steady-state concept, and it cannot be applied to a dynamic analysis (Bálint et al., 2019).

Fig. 4.27 shows the LMTD of all real cases to estimate the average value. As LMTD is getting higher, better heat exchanger performance will be generated. It is noted that all cases have average LMTDs higher than eight, while the higher value means more heat has been transferred between the two sides. Each measurement temperature is plotted in a different colour from 35℃ to 60℃. The heat exchanger performs the best for cases in lower temperatures 30℃, 35℃ and 45℃ while the lowest performance was for the higher temperatures 50 - 60 ℃ where the measurement points are scattered far from the polynomial second order graph. On the other hand, the average LMTD value was the highest for the cases of 60℃ and 45℃, while it was not lower than 7.92 for the rest of the cases.

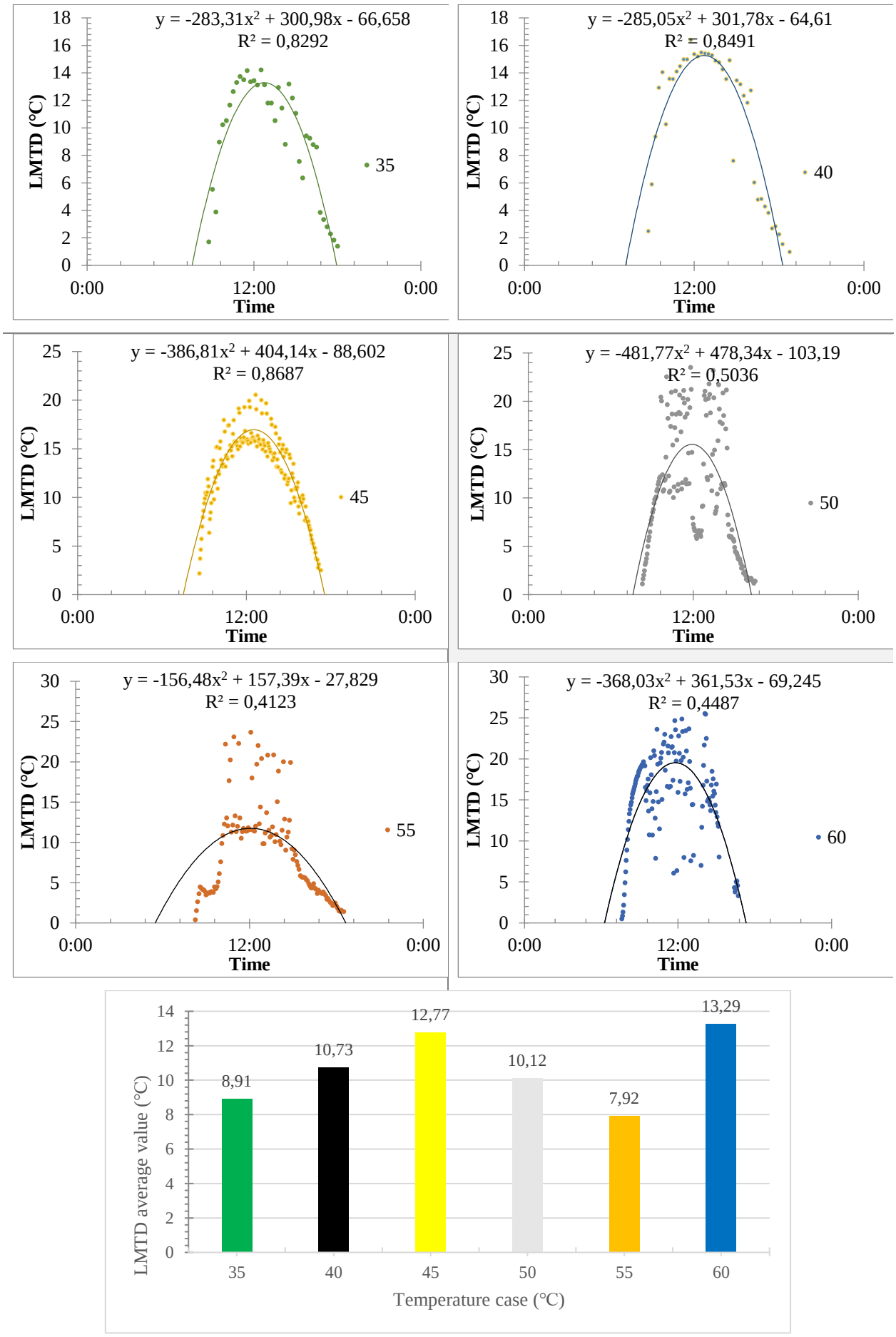

Figure 4.27. LMTD performance of the heat exchanger

On the other hand, the correlation between the LMTD and the specific solar radiation is plotted in Fig. 28. It can be seen that for temperature cases 60, 55, and 50℃, the correlation between the LMTD and the specific solar radiation on the inclined surface is polynomial from the second order with accelerated increase and set intercept (0,0). At the same time, the 45℃ case is a second-degree polynomial correlation with decelerated increase with also set intercept (0,0). On the contrary, 40 and 35℃ cases have more linear correlation with a set intercept of (0,0).

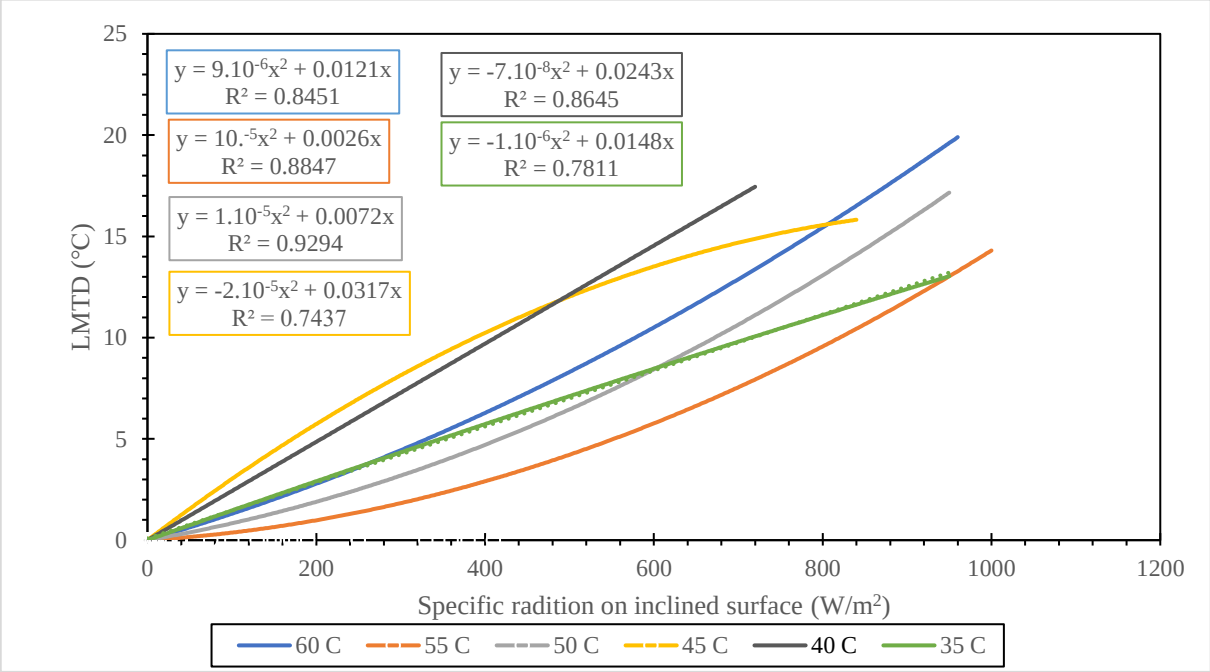

Figure 4.28. Correlation between LMTD and specific solar radiation on an inclined surface

4.3.3. Parametric analysis

4.3.3.1. Effect of solar radiation and mass flow rate on the outlet temperature

Fig. 4.29 shows the outlet temperature variation under varying solar radiations for three configurations, 30/30, 60/60 and 90/90 litres per hour per square meter mass flow rate. The left-hand side number represents the flow rate at the primary loop, while the right-hand side number represents the secondary loop flow rate. In contrast, the inlet water temperature of the secondary loop was relatively constant at 25℃ return temperature. The modelling was conducted in July 2021, and the results show that the 30/30 configuration has the highest output temperature for summertime compared to 60/60 and 90/90 l/h·m^2. It means obtaining the highest outlet temperature during the summer, 30/30 l/h· m^2 flow rate is the optimum configuration, followed by 60/60 and 90/90, respectively. It was also noted that the linear best-fitting lines are the linear trendlines where the coefficients of determination R^2 were 0.9332, 0.9521 and 0.9384 for configurations 30/30, 60/60, and 90/90, respectively. For example, 800 W/m^2 solar radiation will result in 56℃, 46℃, and 42℃ outlet temperatures for configurations 30/30, 60/60, and 90/90, respectively.

Similarly, higher solar radiation will result in broader temperature ranges between the configurations, while lower solar radiation will result in narrower temperature ranges. These results explain that when the flow rate is slower in the primary loop, this will allow the glycol-water (1:3) mixture to take more time to absorb the solar radiation from the solar collector and then convey it to the heat exchanger. In addition, the slow flow rate will have lesser friction losses. Finally, it can be concluded that depending on the outlet heat process temperature, the lowest the

flow rate, the highest the outlet heat process temperature. These results can be utilised in the solar controlling system to adjust the flow rate at the primary and secondary pumps to obtain the required temperature, as illustrated by equation 4.10.

$$\begin{aligned} &30/30: && T_{out} = 22.611\,\mathrm{Ra} + 23.986; && R^2 = 0.9332 \\ &60/60: && T_{out} = 28.248\,\mathrm{Ra} + 22.811; && R^2 = 0.9384 \\ &90/90: && T_{out} = 40.615\,\mathrm{Ra} + 22.194 && R^2 = 0.9521 \end{aligned} \quad (4.10)$$

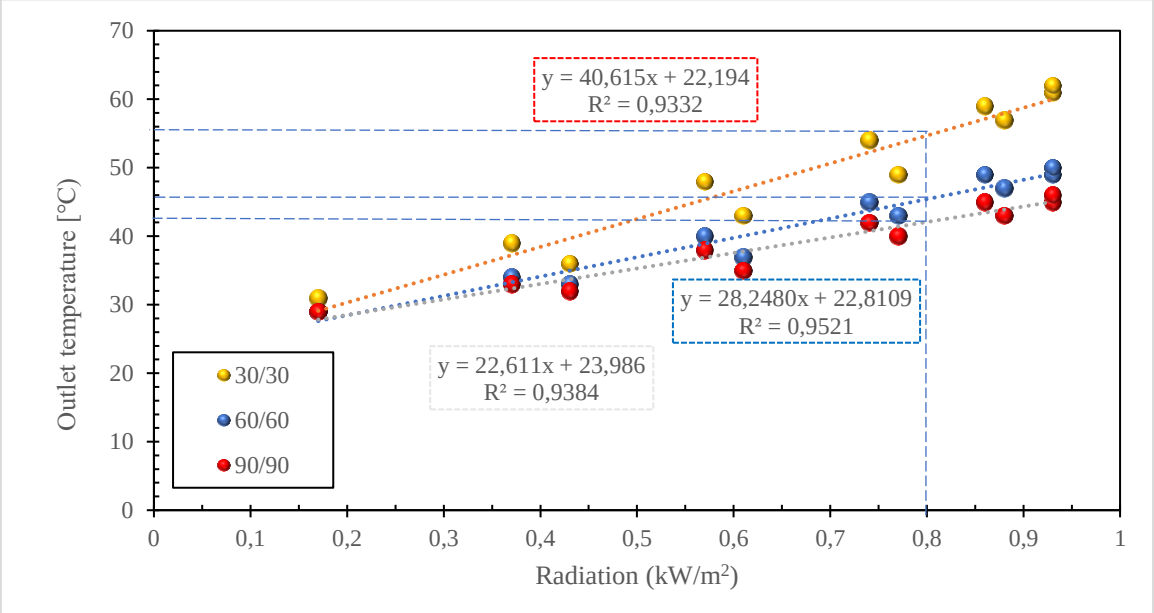

Figure 4.29. Effect of solar radiation on water outlet temperature for tankless SHIP system at different flow rates

4.3.3.2. Effect of solar gain under different mass flow rate

Fig. 4.30 illustrates the variation of the generated thermal energy fraction from the tankless SHIP system for the specific industrial process under varying solar radiation and mass flow rates. The annual energy yield represents the valuable energy harvested by one square meter of the solar collector and transported through the primary loop. Results show that the 30/90 configuration has the highest annual energy yield of 638.79 kWh/m^2. In other words, one square meter of the collector area generates 638.79 kWh per year. Similarly, the 30/60 and 60/90 configurations have 621.5 and 604.05 kWh/m^2 annual energy yield, respectively. The remaining configurations have less than 600 kWh/m^2 annual energy yield. It is noted from the graph that the second loop must have a higher flow rate compared to the primary loop, which is a result of choosing a closed loop on the primary side. At the same time, the open loop on the secondary side shows that a higher flow rate results in higher yields if we consider a fixed flow rate at the primary loop.

Using the R script, the annual energy gain can be generated using the primary and secondary flow rates with coded values -1 equals 30 litres per hour and +1 equals 90 litres per hour. As a result, 0 coded values will be 60 litres per hour. The following equation 4.11 represents the generated formula knowing that R^2 equals 0.9128:

$$E = 577.598 + 41.663\ Q_{pr} - 24.717\ Q_{sec} + 1.422\ Q_{pr}\ Q_{sec} \quad (4.11)$$

Coefficients	Estimate	Std. Error	t value	Pr(>|t|)
(Intercept)	577.598	5.470	105.600	1.44e-09***
A	41.663	6.699	6.219	0.00157**
B	-24.717	6.699	-3.690	0.01415*
A:B	1.422	8.204	0.173	0.86915

Signif. codes: 0 '***' 0.001 '**' 0.01 '*' 0.05 '.' 0.1 ' ' 1

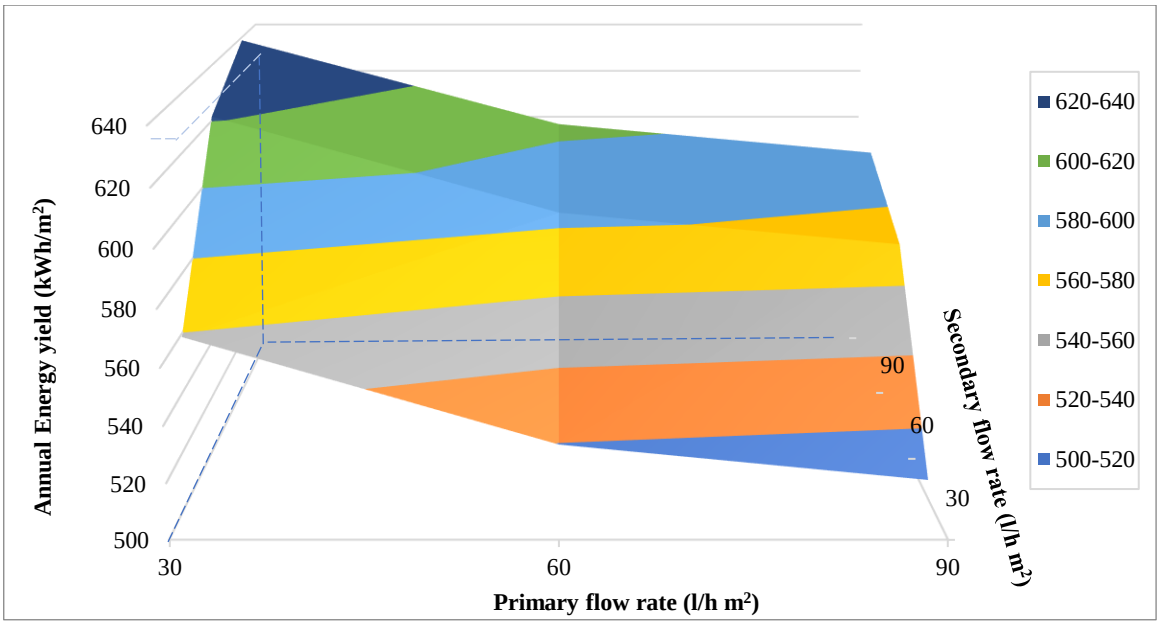

Figure 4.30. Annual energy yield considering different flow rate configurations

4.4. New scientific results

The results were comprehensively investigated in this study, and the following points are noteworthy to be mentioned:

1. Correlation between the phase change material Soy wax integrated into the Thermal Energy Storage

Based on the experimental results, I enhanced the solar thermal tank's storage time by integrating two types of Soy wax at two melting temperatures, 52℃ and 62℃. To justify this enhancement, I developed a non-linear model that can be applied to TES operating solar buffer tanks using encapsulated PCMs and considering the most influential factors, wax quantity (Q), sample quantity (S), and temperature (T). The Equations 4.12 and 4.13 represent the mathematical correlation using actual values:

$$y_{Soy\ wax\ 52℃} = 9.33 + 0.95(0.5\,S - 3) + 0.38(0.4\,Q - 3) + 3.16(0.2\,T - 7) - 0.38(0.2\,T - 7)^2 + 0.29(0.5\,S - 3)^2 - 0.05(0.5\,S - 3)(0.4\,Q - 3) + 0.23(0.5\,S - 3)\,(0.2\,T - 7) - 0.11(0.4\,Q - 3)\,(0.2\,T - 7) - 0.04(0.5\,S - 3)\,(0.4\,Q - 3)(0.2\,T - 7)$$

(hour); R^2= 99.99%; SD= 4.45 hours (4.12)

The 4.9 equation is valid for the Soy wax 52℃ for the following domains:

S ∈ [0-8] samples, Q ∈ [0-10] g, and T ∈ [30 – 60] ℃.

$$y_{Soy\ wax\ 62℃} = 15.03 + 0.84(0.5\,S - 3) + 0.18(0.4\,Q - 3) + 1.62(0.67\,T - 4) - 0.21(0.67\,S - 4)^2 + 0.07(0.4\,Q - 3)\,(0.5\,S - 3) + 2.04(0.5\,S - 3)\,(0.67\,T - 4) + 0.85(0.4\,Q - 3)\,(0.67\,T - 4) - 1.16(0.4\,Q - 3)\,(0.5\,S - 3)(0.67\,T - 4)$$

(hour); R^2= 99.89%; SD= 3.1 hours (4.13)

The 4.10 equation is valid for the Soy wax 62℃ for the following domains:

S ∈ [0-8] samples, Q ∈ [5-10] g, and T ∈ [45 – 75] ℃.

By applying the Lagrange multiplier method $\mathbf{y = y\,(S, Q, T)}$ using unconstrained optimisation $\boldsymbol{\nabla y = 0}$, I identified the optimum values for operating factors as in Equations 4.14 and 4.15:

S = 5.82 samples, Q = 16.46 g, and T = 53 ℃ for Soy wax 52 ℃

$$\rightarrow y_{Soy\ wax\ 52℃} = 15.6\ (h) \quad (4.14)$$

S = 12.56 samples, Q = 12.956 g, and T = 62.07 ℃ for Soy wax 62 ℃

$$\rightarrow y_{Soy\ wax\ 62℃} = 16.3\ (h) \quad (4.15)$$

2. Correlation between the solar fraction and the boiler configurations in the solar heat for industrial prcesses

Based on the analytical results, I proved that the in-series configuration is the most efficient and productive one to get the highest solar fraction. I have pointed out that the collector area, relative flow rate, and relative tank volume have a tangible influence on the overall yield. In contrast, the glycol and tank height-to-diameter ratios have a lesser impact. It is essential to mention that the targeted solar fraction domain is between 40 – 60% since lower than this value, the solar thermal system will not be effective and higher than this will not be feasible. Considering the analytical method, I calculated the solar fraction as a function of collector area A and relative tank volume D as in equations 4.16 and 4.17, valid for A ∈ [5-100] m^2 and D ∈ [5-100] litres/m^2:

$$\left.\begin{aligned} y_{in-series} &= 0.2426\ \ln(A) - 0.3774 \quad (\%); && R^2 = 0.9819 \\ y_{in-parallel} &= 0.2242\ \ln(A) - 0.3371 \quad (\%); && R^2 = 0.9878 \end{aligned}\right\} \quad (4.16)$$

$$\left.\begin{aligned} y_{in-series} &= -3.10^{-5}\ D^2 + 0.0042\ D + 0.2327 \quad (\%); && R^2 = 0.9772 \\ y_{in-parallel} &= -3.10^{-5}\ D^2 + 0.0040\ D + 0.2743 \quad (\%)\ ; && R^2 = 0.9542 \end{aligned}\right\} \quad (4.17)$$

While for the RSM method, the formula concerning the solar fraction in (%) unit concludes both factors: solar collector area, relative tank capacity, and their two-factor interaction as in equation 4.18 which are valid for A ∈ [5-100] m^2 and D ∈ [5-100] litres/m^2 as follow:

$$\left.\begin{aligned} y_{in-Parallel} &= 36.60 + 28.53\left(\frac{A-52.5}{47.5}\right) + 3.15\left(\frac{D-55}{45}\right) + 3.02\left(\frac{A-52.5}{47.5}\right) * \left(\frac{D-55}{4}\right)\ (\%) \\ y_{in-Series} &= 39.11 + 31.54\left(\frac{A-52.5}{47.5}\right) + 3.51\left(\frac{D-55}{45}\right) + 3.48\left(\frac{A-52.5}{47.5}\right) * \left(\frac{D-55}{4}\right)\ (\%) \end{aligned}\right\} \quad (4.18)$$

3. Tankless solar heat for industrial process system validation

I experimentally examined the authenticity of the dynamic simulation model using T*sol software of the tankless SHIP by real-time measurement for three months of the experiment at 60 litres per hour for both the primary and secondary loops. Firstly, I have found minimal deviation between my measured meterological data (for one year) and the applied model (data from 1995 - 2012), so my model is applicable well in practice. Furthermore, the following two equations represent the correlation between the monthly average solar radiation values and the ambient temperature for both the model and the long-term records as in equation 4.19, valid for T_{amb} ∈ [0 – 25] ℃, Ra ∈ [0 – 1000] W/m^2, 1.92 m^2 and 33º inclined FPC, and 960 W heat exchanger.

$$\left.\begin{aligned} &\text{Long-term records:} && T_{amb} = 0.1456\ Ra - 7.3775 \quad (℃); && R^2 = 0.8288 \\ &\text{Experiment validation result:} && T_{amb} = 0.1552\ Ra - 6.6844 \quad (℃); && R^2 = 0.8772 \end{aligned}\right\} \quad (4.19)$$

I also calculated the correlation between the simplified model LMTD efficiency indicator and the specific solar radiation of the inclined surface using six different temperature targets (35 – 60℃). The results show using a set intercept of (0,0) that for temperature cases 50, 55, and 60℃, the correlation is a second-degree polynomial correlation with accelerated increase. In contrast, case

45℃ is a second-degree polynomial with a decelerated increase. On the contrary, cases 40 and 35℃ showed a linear correlation with set intercept (0,0). The set Equation 4.20 shows the correlations for all cases with the appropriate trendline.

$$\left.\begin{array}{lll} 60℃; & LMTD= 9.\,10^{-6}\,Ra^2 + 0.012\,Ra; & R^2 = 0.8451 \\ 55℃; & LMTD= 10^{-5}\,Ra^2 + 0.0026\,Ra; & R^2 = 0.8847 \\ 50℃; & LMTD= -10^{-5}\,Ra^2 + 0.0072\,Ra; & R^2 = 0.9294 \\ 45℃; & LMTD= -2.\,10^{-5}\,Ra^2 + 0.0317\,Ra; & R^2 = 0.7437 \\ 40℃; & LMTD= -7.10^{-8}\,Ra^2 + 0.0243\,Ra; & R^2 = 0.8628 \\ 35℃; & LMTD= -1.10^{-6}\,Ra^2 + 0.0148\,Ra; & R^2 = 0.7811 \end{array}\right\} \quad (4.20)$$

4. The effect of solar radiation and mass flow rate on the solar heat for industrial process outlet temperature

For identifying the optimum flow rate in the primary and secondary loops of the solar heat for industrial process system, I calculated the outlet temperature variation under varying solar radiations for three different configurations, 30/30, 60/60 and 90/90 litres per hour per square meter mass flow rate. In contrast, the inlet water temperature of the secondary loop was relatively constant at 25℃ return temperature. The experiment was conducted in July, and the results show that the 30/30 configuration has the highest output temperature for summertime compared to 60/60 and 90/90 l/h·m^2. This result highlights that the lowest possible flow rate is the best for having the highest possible outlet temperature since the water-glycol mixture (1:3) will have a longer time absorbing the energy from the collector loop and then transfer it to the heat process. I identified the relationship between the rendition in (kW/m^2) and the outlet temperature in Celsius degrees (℃) and the coefficient of determination R^2 as in Equations 4.21, 4.22, and 4.23:

T_{out}= 40.615 Ra + 22.194 (℃); R^2=0.9332 30 litre/hour·m^2; if T_{in}=25℃=const. (4.21)

T_{out}= 28.248 Ra + 22.811 (℃); R^2=0.9521 60 litre/hour·m^2; if T_{in}=25℃=const. (4.22)

T_{out}= 22.611 Ra + 23.986 (℃); R^2=0.9384 90 litre/hour·m^2; if T_{in}=25℃=const. (4.23)

5. The impact of solar gain under different mass flow rates

I illustrated the variation of the generated thermal energy gain from the tankless SHIP system for the specific industrial process under varying solar radiation and mass flow rates. I noticed that the Q_{pr}=30 (l/h·m^2) for the primary loop and Q_{sec}=90 (l/h·m^2) for the heat process loop configuration has the highest annual energy yield (E) of 638.79 kWh/m^2. Similarly, the 30/60 and 60/90 configurations have 621.5 and 604.05 kWh/m^2 annual energy yield, respectively. I also noted from the graph that the second loop must have a higher flow rate than the primary loop, resulting in choosing a closed loop on the primary side as a favourable configuration. At the same time, the open loop on the secondary side shows that a higher flow rate results in higher yields if we consider a fixed flow rate at the primary loop. The boundary conditions were the secondary inlet water temperature (T_{Sec_In} = 25℃) was constant, the three selected specific primary/secondary mass flow rates were 30/30, 60/60 and 90/90 (litres/hour·m^2), water/glycol ratio (1:3) and solar radiation interpretation range 0.2 - 0.9 (kW/m^2).

The annual energy gain can be generated using the R script's primary and secondary flow rates when the coded values -1 equals 30 litres per hour, and +1 equals 90 litres per hour. As a result, 0 coded values will be 60 litres per hour. The following equation 4.24 represents the generated formula, knowing that this equation is valid for primary and secondary flow rates range (30 – 90) litres/hour·m^2:

$$E = 577.598 + 41.663.\left(\frac{Q_{pr}-60}{30}\right) - 24.717.\left(\frac{Q_{sec}-60}{30}\right) \quad \text{(kWh/year)}; \quad R^2 = 0.9128 \quad (4.24)$$

5. CONCLUSION AND SUGGESTIONS

In conclusion, a dynamic experimental and modelling investigation has been carried out of various types of solar thermal systems for industrial heat process objectives. A comparison between Soy wax 52℃ and 62℃ has studied the effect of integrating encapsulated specimens of PCMs into solar TES to extend the storage time and the thermal efficiency. Each experiment generates eight cases, and supplementary interior or exterior cases were used to rectify the contour lines using the RSM approach and R script coding. The results showed that non-linear behaviour is the best fit considering the most influential factors (wax quantity, sample quantity, and temperature). Both waxes showed in the Pareto plots that the temperature factor is the most substantial single factor magnitude, followed by samples and quantity. In contrast, the second-degree factors showed that temperature and samples are crucial for Soy wax 52℃ and the sample factor for Soy wax 62℃. Also, the two factors' interactions were illustrated using contour plots, and the S · T interaction is the most influential for both experiments. Then, the optimum operating values of both experiments were identified using the Lagrange multiplier method with unconstrained boundary conditions. Using the values will result in 15.6 (h) and 16.36 (h) for Soy wax 52℃ and 62℃, respectively.

The mechanical configuration of the solar heat for industrial processes significantly improves the solar fraction and system efficiency. The boiler can be connected to the heat process in series or parallel. The results were analysed using analytical and dynamic approaches. Both approaches showed that in-series configuration delivers higher solar fraction than in-parallel one. The studied factors are collector area, glycol ratio, relative tank volume, relative volume flow rate and tank height-to-diameter ratio. Analytically, collector area and relative tank volume are the most critical factors considering the optimum design of 40 – 60% solar fraction. On the other hand, RSM approaches showed that in-parallel configuration collector area, relative flow rate, and relative tank capacity are the most significant single factors. At the same time, the interaction of the collector area with relative tank capacity and collector area with relative flow rate are the most crucial two-factor interactions. The same applies to in-series configuration, except that relative flow rate has no significant influence on the overall solar fraction. It was concluded that the RSM approach gives more realistic and dynamic results than the analytical method.

The real-time measurement of the tankless SHIP compared to the dynamic simulation model was examined for three months at 60 litres per hour for both primary and secondary loops. Targeted temperatures (35 - 60℃) could be approached using the tankless SHIP during the measurement time for all target sets of the heat process. Also, the heat exchanger efficiency passing the heat from the primary side to the secondary one was conducted as a linear correlation with (0,0) set intercept. For all scenarios, the coefficient of determination was consistently higher than 98.63%, illustrating that the difference between the primary side inlet temperature and the secondary side outlet temperature is as minimum as possible. Similarly, the heat exchanger LMTD values were correlated with the specific radiation on the inclined surface using a second-degree polynomial correlation trendlines.

To evaluate the SHIP outlet temperature as a relationship between the solar radiation and the mass flow rate, three configurations, 30/30, 60/60 and 90/90 litres per hour per collector’s square area, were calculated. The experiment showed that the 30/30 configuration has the highest output temperature. In addition, the formula connecting the solar radiation (kW/m^2) with the output temperature (℃) was generated with a 93.32% coefficient of determination. In contrast, the 30/90 configuration has the highest annual energy yield of 638.79 (kWh/m^2). It is noted that the secondary loop must have a higher flow rate than the primary one.

This topic is fertile for further exploration since many aspects remain uncovered. To highlight some of the numerous recommendations, for example, the solar thermal heat processes can be tested using other simulations like MATLAB and ANSYS. Also, other types of solar collectors can be evaluated to improve the solar fraction, like black chrome FPC, FPC with selenium coating, and unglazed collectors. In addition, other types of integrated or encapsulated cheap PCMs can be tested to improve the TES or the solar collector. The solar thermal process can also be tested at a higher temperature for medium-temperature industrial processes.

6. SUMMARY

In this work, a comprehensive experimental and modelling investigation was carried out to evaluate solar heat's energetic and thermal performance for industrial process systems. The studied system consists of several parts: solar collector, storage tank, heat exchangers, boiler, and hydraulic system. The storage tank has been analysed to improve the storage time by integrating encapsulated PCMs Soy wax 52 ℃ and 62 ℃ into an 8.7 litre 42 x 13 x 16 (cm) storage tank. The tank is well insulated by 5 cm of expanded polystyrene (EPS) material, and the specimen tray comprises 7 x 3 specimens, each holding up to 50 mL of the PCM material. The most influential factors (sample quantity, samples, and temperature) have been analysed, generating $3^2 = 8$ experiments for each PCM (3- factors, 2-cases/factor) and supplementary interior and exterior experiments to rectify the contour lines. The used approach is RSM to identify the single and two-factor magnitudes using Pareto plots and contour lines, while R script was used for coding. The results showed different intercept values, 9.33 (h) and 15.03 (h), for Soy wax 52℃ and 62℃, respectively. In addition, temperature, samples, and quantity are the most influential factors, and its magnitudes for Soy wax 52℃ are higher than 62℃. On the contrary, samples and temperature have substantial second-degree magnitude on Soy wax 52℃ while only samples on Soy wax 62℃. It was noted that the non-linear behaviour is the best-fit solution for the two waxes with 99.99% and 99.89% coefficient of determination for Soy wax 52℃ and 62℃, respectively. The equations generated from the RSM process were used for obtaining the optimum parameters using a Lagrange multiplier with unconstrained boundary conditions. The results showed 15.6 and 16.36 (h) storing time for Soy wax 52 ℃ and 62 ℃, respectively.

A different aspect of the hydraulic configuration of the boiler was tested under two different conditions: in series and parallel. The boiler is an essential part of the solar thermal system, and the optimum configuration will result in higher solar fraction yield. Analytical and RSM approaches were used, and the five most important factors were analysed: collector area, glycol ratio, relative flow rate, relative tank capacity, and tank height-to-diameter ratio. Analytically and using the RSM method, collector area and relative tank capacity significantly impact the solar fraction on in-series configuration. In contrast, the RSM method showed that the relative flow rate has a magnitude of the in-parallel configuration. For two-factor interactions, the collector area with relative tank capacity has significant magnitude on both configurations and the collector area with relative flow rate only on in-parallel configuration.

Real-time measurement of the tankless SHIP took place for the whole summer with dynamic simulation models at 60 ($l/h \cdot m^2$) relative flow rate for primary and secondary loops. The experiments targeted several sets of outlet heat process temperatures for low-temperature industrial duties under Hungarian weather conditions, and all the temperature targets were reached. In addition, the heat exchanger efficiency was tested with a linear correlation using (0,0) set intercept with a 98.63% R^2 coefficient of determination. Similarly, the LMTD values were measured, and all scenarios showed more than eight, representing the high efficiency of the heat exchanger. Moreover, the correleation between the LMTD and the specific radiation on the inclined surface was drawn for all cases.

The heat process temperature due to the solar radiation and mass flow rate at different configurations was also estimated, showing that 30/30 ($l/h \cdot m^2$) is the optimum value. In contrast, while considering the highest annual energy, the 30/90 ($l/h \cdot m^2$) configuration can yield 638.79 (kWh/m^2) with a 93.32% coefficient of determination.

7. ÖSSZEFOGLALÁS (SUMMARY IN HUNGARIAN)

Ebben a munkámban átfogó kísérleti és modellezési vizsgálatokat végeztem a napenergia termikus teljesítményének értékelésére vonatkozóan, iparban alkalmazott rendszerek esetében. Az általam vizsgált rendszer több részegységből épült fel: napkollektor, tárolótartály, hőcserélő, kazán és a hidraulikai rendszer. A tárolási idő javítása érdekében elemeztem, hogy ha egy 8,7 literes, 42x13x16(cm) méretű tárolótartályba (52°C és 62°C-os olvadáspontú) szója viasz kapszulákat teszek, hogyan változik a tárolási idő, a különböző beállítások esetén. A tartály jól szigetelt 5 cm-es expandált polisztirol (EPS) anyaggal lett bevonva, a minta tartó tálcába 7x3db mintát helyeztem, amelyek mindegyike legfeljebb 50ml fázisváltó anyagot (PCM) tartalmazott. A kísérleti faktorok hatásainak vizsgálatára RSM (válaszfelületi-módszert) módszert alkalmaztam. Pareto-elemzés segítségével azonosítottam a legjelentősebb tényezőket, melyek befolyásolják a folyamatomat. R-script programot használtam a kódolt adatok feldolgozásához. A legjelentősebb tényezőket, a minta mennyiséget (Q), a minta darabszámát (S), a hőmérsékletet (T) változtattam és kísérleti eredmények alapján elemeztem a megkapott adatokat (52°C és 62°C-os olvadáspontú) szója viasz alkalmazása esetén. Az eredmények különböző értékeket mutattak, 9,33(h) és 15,03(h), a szójaviasz 52°C és 62°C esetében. Megállapítottam, hogy nem lineáris az összefüggés a két viasz esetében a három legjelentősebb tényező figyelembevétele esetén. A legjobban illeszkedő egyenletek a két szójaviasz esetében, 99,99%-os és 99,89%-os együtthatóval rendelkeztek. Az RSM-folyamatból generált egyenleteket "Lagrange multiplier" módszerrel az optimális paraméterek meghatározására használtam, és az eredmények 15,6 és 16,36 (h) tárolási időt mutattak a szójaviasz 52°C és 62°C esetében.

A napkollektoros rendszerekben is előszeretettel alkalmazott kazán hidraulikai konfigurációjának különböző összeállítását vizsgáltam: soros és párhuzamos. Az optimális konfiguráció kiválasztása nagyobb szoláris frakcióhozamot eredményez. Két megközelítést alkalmaztam, analitikus és RSM módszert, és az öt legfontosabb tényezőt elemeztem: kollektor felület, glikol arány, relatív áramlási sebesség, relatív tartálykapacitás és a tartály magasság és átmérő arány. Az RSM-módszerrel megállapítottam, hogy a kollektor felülete és a relatív tartálykapacitás jelentősen befolyásolja a szoláris frakció alakulását a soros konfiguráció esetén. Ezzel szemben ugyancsak az RSM-módszer azt mutatta, hogy a relatív áramlási sebességnek van nagyobb hatása a párhuzamos konfiguráció esetén. Ugyanakkor a kéttényezős kölcsönhatások esetében a kollektor felülete a relatív tartálykapacitással együttes hatása mindkét konfigurációnál jelentős, a kollektor felülete a relatív áramlási sebességgel együtt már csak a párhuzamos konfigurációnál jelentős.

A vizsgálataim során a tartály nélküli kollektoros rendszer valós idejű mérésével validáltam az általam felállított dinamikus szimulációs modelleket ismert relatív áramlási sebesség alkalmazása esetén, 2021. év nyár folyamán. A kísérletek magyarországi időjárási körülmények között történtek, alacsony hőmérsékletű ipari feladatokhoz szükséges kimeneti hőmérséklet előállítását céloztam meg. Megállapítottam több solar radiation és LMTD (logaritmikus átalgos hőmérséklet-különbség) összefüggést különböző kívánt technológiai kimeneti hőmérséklet esetére, sík kollektor alkalmazásával. Az általam megfogalmazott összefüggések 0,8–0,9 korrelációs együtthatókat mutattak.

A lemezes hőcserélő primer és szerkunder körében beállított tömegáramok alapján megállapítottam összefüggéseket, mellyel a global sugárzás ismeretében a technológiához szükséges hőmérsékletet lehet meghatározni.

Meghatároztam egy éves energiamennyiség összefüggését a primer és szekunder térfogatáramok függvényében.

8. APPENDICES

A1: Bibliography

1. Abdelsalam, M. Y., Teamah, H. M., Lightstone, M. F., & Cotton, J. S. (2020). Hybrid thermal energy storage with phase change materials for solar domestic hot water applications: Direct versus indirect heat exchange systems. *Renewable Energy*, *147*, 77–88. https://doi.org/10.1016/j.renene.2019.08.121
2. ABPS. (2011). *FINAL REPORT ON MARKET ASSESSMENT OF SOLAR WATER HEATING Submitted to MINISTRY OF NEW AND RENEWABLE ENERGY (Government of India) Prepared by : ABPS Infrastructure Advisory Private Ltd . May 2011 Final Report on Market Assessment of SWH Systems in Indust* (Issue May).
3. Abraham, J. P., Plourde, B. D., & Minkowycz, W. J. (2015). Continuous flow solar thermal pasteurization of drinking water: Methods, devices, microbiology, and analysis. *Renewable Energy*, *81*, 795–803. https://doi.org/10.1016/J.RENENE.2015.03.086
4. Al-Hilphy, A. R. S. (2013). Designing and manufacturing of a non thermal milk pasteurizer using electrical field. *American Journal of Agricultural and Biological Science*, *8*(3), 204–211. https://doi.org/10.3844/ajabssp.2013.204.211
5. Alktranee, M., & Bencs, P. (2020). Overview of the hybrid solar system. *Analecta Technica Szegedinensia*, *14*(1), 100–108. https://doi.org/10.14232/analecta.2020.1.100-108
6. Almsater, S., Saman, W., Bruno, F., Alemu, A. A., & Omaraa, E. (2019). Parametric analysis of PCM in vertical triplex tube thermal energy storage technology for concentrating solar power. *AIP Conference Proceedings*, *2126*(July). https://doi.org/10.1063/1.5117717
7. Anderson, M. (2017). *USING SOLAR THERMAL TO LOWER ENERGY COSTS FOR SMALL SCALE DAIRY PROCESSORS*.
8. Anderson, T. N., & Duke, M. (2007). Solar energy use for energy savings in dairy processing plants. *I P E N Z Engineering TreNz*, *2008*(001), 1–9.
9. Antoniadis, C. N., & Martinopoulos, G. (2019). Optimization of a building integrated solar thermal system with seasonal storage using TRNSYS. *Renewable Energy*, *137*, 56–66. https://doi.org/10.1016/j.renene.2018.03.074
10. Asgharian, H., & Baniasadi, E. (2019). A review on modeling and simulation of solar energy storage systems based on phase change materials. *Journal of Energy Storage*, *21*(November 2018), 186–201. https://doi.org/10.1016/j.est.2018.11.025
11. Bakyalakshmi Nisha, R., & Madhumitha, S. (2010). Solar food processor. *ICCCE 2010 - 2010 International Conference on Chemistry and Chemical Engineering, Proceedings*, *Iccce*, 381–385. https://doi.org/10.1109/ICCCENG.2010.5560407
12. Bálint, R., Fodor, A., & Magyar, A. (2019). Model-based power generation estimation of solar panels using weather forecast for microgrid application. *Acta Polytechnica Hungarica*, *16*(7), 149–165. https://doi.org/10.12700/APH.16.7.2019.7.9
13. Barba, F. J., Gavahian, M., Es, I., Zhu, Z., Chemat, F., Lorenzo, J. M., & Mousavi Khaneghah, A. (2019). Solar radiation as a prospective energy source for green and economic processes in the food industry: From waste biomass valorization to dehydration, cooking, and baking. *Journal of Cleaner Production*, *220*, 1121–1130. https://doi.org/10.1016/j.jclepro.2019.02.175
14. Başaran, A., Yılmaz, T., Azgın, Ş. T., & Çivi, C. (2021). Comparison of drinking milk production with conventional and novel inductive heating in pasteurization in terms of energetic, exergetic, economic and environmental aspects. *Journal of Cleaner Production*, *317*, 128280. https://doi.org/https://doi.org/10.1016/j.jclepro.2021.128280

15. Beikircher, T., Osgyan, P., Reuss, M., & Streib, G. (2014). Flat plate collector for process heat with full surface aluminium absorber, vacuum super insulation and front foil. *Energy Procedia*, *48*, 9–17. https://doi.org/10.1016/j.egypro.2014.02.003
16. Bie, Y., Li, M., Chen, F., Królczyk, G., Yang, L., Li, Z., & Li, W. (2019). A novel empirical heat transfer model for a solar thermal storage process using phase change materials. *Energy*, *168*, 222–234. https://doi.org/10.1016/j.energy.2018.11.107
17. Buzás, J., Bhave, A. G., Screed, F., Bajnóczy, G., Pálffy, E. G., Prépostffy, E., Zöld, A., Cabeza, L. F., Ibáñez, M., Solé, C., Roca, J., Nogués, M., Hoshi, A., Mills, D. R., Bittar, A., Saitoh, T. S., Schweiger, H., Mendes, J. F., Carvalho, M. J., … Krüger, D. (2005). Screening of high melting point phase change materials (PCM) in solar thermal concentrating technology based on CLFR. *Solar Energy*, *79*(3), 332–339. https://doi.org/10.1016/j.solener.2004.04.023
18. Cabeza, L. F., & Oró, E. (2016). Thermal Energy Storage for Renewable Heating and Cooling Systems. In *Renewable Heating and Cooling: Technologies and Applications* (pp. 139–179). Elsevier Inc. https://doi.org/10.1016/B978-1-78242-213-6.00007-2
19. Carielo da Silva, G., Tiba, C., & Calazans, G. M. T. (2016). Solar pasteurizer for the microbiological decontamination of water. *Renewable Energy*, *87*, 711–719. https://doi.org/10.1016/j.renene.2015.11.012
20. Carielo, G., Calazans, G., Lima, G., & Tiba, C. (2017). Solar water pasteurizer: Productivity and treatment efficiency in microbial decontamination. *Renewable Energy*, *105*, 257–269. https://doi.org/10.1016/j.renene.2016.12.042
21. Chandrasekaran, S., Ramanathan, S., & Basak, T. (2013). Microwave food processing-A review. *Food Research International*, *52*(1), 243–261. https://doi.org/10.1016/j.foodres.2013.02.033
22. Chantawong, P. (2019). Experimental Investigation of Thermal Performance of a Multipurpose PV Solar Collector Wall with Phase Change Material. *Journal of Solar Energy Engineering, Transactions of the ASME*, *141*(6), 1–7. https://doi.org/10.1115/1.4043712
23. Choubineh, N., Jannesari, H., & Kasaeian, A. (2019). Experimental study of the effect of using phase change materials on the performance of an air-cooled photovoltaic system. *Renewable and Sustainable Energy Reviews*, *101*(October 2018), 103–111. https://doi.org/10.1016/j.rser.2018.11.001
24. Cocco, D., Tola, V., & Petrollese, M. (2016). Application of Concentrating Solar Technologies in the Dairy Sector for the Combined Production of Heat and Power. *Energy Procedia*, *101*, 1159–1166. https://doi.org/10.1016/j.egypro.2016.11.157
25. Cottrel, N., & Menichetti, E. (2011). Solar Heat for Industrial Processes (SHIP) - State of the art in the Mediterranean region. *Observatoire Méditerranéen de l'Energie*, 64.
26. Crespo, A., Barreneche, C., Ibarra, M., & Platzer, W. (2019). Latent thermal energy storage for solar process heat applications at medium-high temperatures – A review. *Solar Energy*, *192*(June), 3–34. https://doi.org/10.1016/j.solener.2018.06.101
27. Daneshi, A., Esmaili-Sari, A., Daneshi, M., & Baumann, H. (2014). Greenhouse gas emissions of packaged fluid milk production in Tehran. In *Journal of Cleaner Production* (Vol. 80, pp. 150–158). https://doi.org/10.1016/j.jclepro.2014.05.057
28. Deng, S., Nie, C., Wei, G., & Ye, W. B. (2019). Improving the melting performance of a horizontal shell-tube latent-heat thermal energy storage unit using local enhanced finned tube. *Energy and Buildings*, *183*, 161–173. https://doi.org/10.1016/j.enbuild.2018.11.018
29. Desai, D. D., Raol, J. B., Patel, S., & Chauhan, I. (2013). Application of Solar energy for sustainable Dairy Development. *European Journal of Sustainable Development*, *2*(2), 131–140. https://doi.org/10.14207/ejsd.2013.v2n2p131

30. Duffie, J. A., & Beckman, W. A. (2013). *Wiley: Solar Engineering of Thermal Processes, 4th Edition - John A. Duffie, William A. Beckman*.
31. Dyduch, J., & Skorek, A. (2020). Go South! Southern dimension of the V4 states' energy policy strategies – An assessment of viability and prospects. *Energy Policy*, *140*(June 2019), 111372. https://doi.org/10.1016/j.enpol.2020.111372
32. Enebe, V., & Samuel, M. (2019). RE-DESIGING AND FABRICATION OF THE CONTACT AREA OF A SOLAR MILK PASTEURIZER. *Preprints*, *December*. https://doi.org/10.20944/preprints201912.0407.v1
33. Eswara, A. R., & Ramakrishnarao, M. (2013). Solar energy in food processing - A critical appraisal. *Journal of Food Science and Technology*, *50*(2), 209–227. https://doi.org/10.1007/s13197-012-0739-3
34. Farjana, S. H., Huda, N., Mahmud, M. A. P., & Saidur, R. (2018). Solar industrial process heating systems in operation – Current SHIP plants and future prospects in Australia. *Renewable and Sustainable Energy Reviews*, *91*(February), 409–419. https://doi.org/10.1016/j.rser.2018.03.105
35. Fathey Mohamed Atia, M., M Mostafa, M., A El-Nono, M., & F Abdel-Salam, M. (2011). Solar Energy Utilization for Milk Pasteurization. *Misr Journal of Agricultural Engineering*, *28*(October 2011), 729–744.
36. Flysjö, A. (2012). *Greenhouse gas emissions in milk and dairy product chains. Improving the carbon footprint of dairy products Greenhouse gas emissions in milk and dairy product chains improving the carbon footprint of dairy products*.
37. Föste, S., Giovannetti, F., Ehrmann, N., & Rockendorf, G. (2014). Performance and reliability of a high efficiency flat plate collector - Final results on prototypes. *Energy Procedia*, *48*, 48–57. https://doi.org/10.1016/j.egypro.2014.02.007
38. Franco, A. (2020). Methods for the sustainable design of solar energy systems for industrial process heat. *Sustainability (Switzerland)*, *12*(12). https://doi.org/10.3390/su12125127
39. Frasquet, M. (2016). SHIPcal: Solar Heat for Industrial Processes Online Calculator. *Energy Procedia*, *91*, 611–619. https://doi.org/10.1016/j.egypro.2016.06.213
40. Frein, A., Calderoni, M., & Motta, M. (2014). Solar thermal plant integration into an industrial process. *Energy Procedia*, *48*, 1152–1163. https://doi.org/10.1016/j.egypro.2014.02.130
41. Frey, P., Fischer, S., Drück, H., & Jakob, K. (2015). Monitoring Results of a Solar Process Heat System Installed at a Textile Company in Southern Germany. *Energy Procedia*, *70*, 615–620. https://doi.org/10.1016/j.egypro.2015.02.168
42. Fuller, R. J. (2011). Solar industrial process heating in Australia - Past and current status. *Renewable Energy*, *36*(1), 216–221. https://doi.org/10.1016/j.renene.2010.06.023
43. Gallego, A. J., Ruíz-Pardo, A., Cerezuela-Parish, A., Sánchez, J., Martín-Macareno, C., Cabeza, L. F., Camacho, E. F., & Oró, E. (2013). Mathematical modeling of a PCM storage tank in a solar cooling plant. *Solar Energy*, *93*, 1–10. https://doi.org/10.1016/j.solener.2013.03.026
44. Harald Mehling; Luisa F. Cabeza. (2008). Heat and cold storage with PCM. In *Journal of Visual Languages & Computing* (Vol. 11, Issue 3).
45. Hermanucz, P., & Benécs, J. (2019). APPLYING THE INTELLIGEN MEASURING SYSTEM (IMRe) TO A COOLING SYSTEM USED IN THE FOOD INDUSTRY. In F. Istvá & V. Piroska (Eds.), *BioPhys Spring 2019*. Szent István Egyetemi Kiadó.
46. Huang, X., Chen, X., Li, A., Atinafu, D., Gao, H., Dong, W., & Wang, G. (2019). Shape-stabilized phase change materials based on porous supports for thermal energy storage

applications. *Chemical Engineering Journal*, *356*(June 2018), 641–661. https://doi.org/10.1016/j.cej.2018.09.013
47. Hungarian Ministry of National Development. (2012). National Energy Strategy 2030. In *Hungarian Ministry of National Development. p. 7*.
48. Ilchmann, C., Hess, S., & Klatt, M. (2015). Open Source Modeling of Solar Process Heat Systems. *Sterg.Sun.Ac.Za*.
49. Ivancic, A., Mugnier, D., Stryi-Hipp, G., & Weiss, W. (2014). Solar Heating and Cooling Technology Roadmap. *European Technology Platform on Renewable Heating and Cooling*, 1–32. https://doi.org/10.13140/2.1.3594.9764
50. Jaber, J., & Khraiwish, A. S. (2019). Emissions Reduction Resulting from Renewable Energy Projects in Jordan. *Journal of Energy Technologies and Policy*, *October*. https://doi.org/10.7176/jetp/9-6-06
51. Jahangiri, M., Akinlabi, E. T., & Sichilalu, S. M. (2021). Assessment and Modeling of Household-Scale Solar Water Heater Application in Zambia: Technical, Environmental, and Energy Analysis. *International Journal of Photoenergy*, *2021*. https://doi.org/10.1155/2021/6630338
52. Jahangiri, M., Alidadi Shamsabadi, A., & Saghaei, H. (2018). Comprehensive Evaluation of Using Solar Water Heater on a Household Scale in Canada. *Journal of Renewable Energy and Environment*, *5*(1), 35–42.
53. Jitjaroen, W., Suvannakita, A., Jitjaroen, A., & Bunthawong, O. (2011). *Coefficiency of Pasteurization and Incubation Systems of Prototype In-Line-Stirred Yogurt Machine for Small Scale Industry*. *22*, 15–19.
54. Jouhara, H., Żabnieńska-Góra, A., Khordehgah, N., Ahmad, D., & Lipinski, T. (2020). Latent thermal energy storage technologies and applications: A review. *International Journal of Thermofluids*, *5–6*. https://doi.org/10.1016/j.ijft.2020.100039
55. József, B., Péter, H., & Zoltán, D. (2018). *EXAMINATION OF INTELLIGENT MEASUREMENT SYSTEM (IMRE) APPLICATIONS* (I. Bíró., S. Beszédes, J. Gá, G. Hampe, S. Kertész, S. Mária, & K. Sziládi, Eds.; Issue October).
56. Kádár, P. (2014). Pros and cons of the renewable energy application. *Acta Polytechnica Hungarica*, *11*(4), 211–224. https://doi.org/10.12700/aph.25.04.2014.04.14
57. Kalbasi, R., Jahangiri, M., Mosavi, A., Jalaladdin Hosseini Dehshiri, S., Shahabaddin Hosseini Dehshiri, S., Ebrahimi, S., Al-Sadat Etezadi, Z., & Karimipour, A. (2021). Finding the best station in Belgium to use residential-scale solar heating, One-year dynamic simulation with considering all system losses: Economic analysis of using ETSW. *Sustainable Energy Technologies and Assessments*, *45*(February), 101097. https://doi.org/10.1016/j.seta.2021.101097
58. Kalogirou, S. (2003). The potential of solar industrial process heat applications. *Applied Energy*, *76*(4), 337–361. https://doi.org/10.1016/S0306-2619(02)00176-9
59. Kalogirou, S. (2006). *THE POTENTIAL OF SOLAR ENERGY IN FOOD-INDUSTRY PROCESS HEAT APPLICATIONS*. 1–9.
60. Kalogirou, S. A. (2001). Use of TRYNSYS for modeling and simulation of a hybrid PV–thermal solarsys tem for Cyprus. *Renewable Energy*, *23*, 247–260.
61. Kanimozhi, B., & Bapu, B. R. R. (2012). Experimental study of thermal energy storage in solar system using PCM. *Advanced Materials Research*, *433–440*, 1027–1032. https://doi.org/10.4028/www.scientific.net/AMR.433-440.1027
62. Karagiorgas, M., & Botzios-Valaskakis, A. (2000). *Solar Systems Applications in the Dairy Industry* (p. 8).

63. Kasibhatla, R. R. (2015). *Compact Thermal Energy Storage IEA SHC Position Paper*. *42*(August).
64. Kempener, R. (2015). *Solar heat for industrial processes -Technology Brief* (Issue January).
65. Kempener, R., & Saygin, D. (2014). Renewable Energy in Manufacturing-A technology roadmap for REmap 2030. *The International Renewable Energy Agency*, *June*, 6.
66. Khan, M. M. A., Saidur, R., & Al-Sulaiman, F. A. (2017). A review for phase change materials (PCMs) in solar absorption refrigeration systems. *Renewable and Sustainable Energy Reviews*, *76*(February), 105–137. https://doi.org/10.1016/j.rser.2017.03.070
67. Khan, Z., Khan, Z. A., & Sewell, P. (2019). Heat transfer evaluation of metal oxides based nano-PCMs for latent heat storage system application. *International Journal of Heat and Mass Transfer*, *144*, 118619. https://doi.org/10.1016/j.ijheatmasstransfer.2019.118619
68. Khanam, T., Rahman, A., Mola-Yudego, B., Pelkonen, P., Perez, Y., & Pykäläinen, J. (2017). Achievable or unbelievable? Expert perceptions of the European Union targets for emissions, renewables, and efficiency. *Energy Research and Social Science*, *34*(July), 144–153. https://doi.org/10.1016/j.erss.2017.06.040
69. Korzenszky, P., & Adebayo, S. (2018). *COOLING AND STORING ENERGETIC ANALYSIS IN FOOD TECHNOLOGY*. 59–66.
70. Korzenszky, P., & Géczi, G. (2016). Heat Pump Application in Food Technology. *Journal of Microbiology, Biotechnology and Food Sciences*, *2016*(vol. 6), 493–500.
71. Korzenszky, P., Kovács, Á., Meixner, R., & Pettkó, C. (2017). Food safety and energetics analysis of the heat treatment of milk. *Elelmiszervizsgalati Kozlemenyek*, *63*(3), 1680–1691.
72. Korzenszky, P., Meixner, R., & Sembery, P. (2018). THE POSSIBILITY OF USE OF RENEWABLE ENERGY IN THE PASTEURIZATION SYSTEM. *Researched Risk Factor of Food Chain*, 26–28.
73. Korzenszky, P., Sembery, P., & Géczi, G. (2013). Microwave milk pasteurization without food safety risk. *Potravinarstvo*, *7*(1), 45–48. https://doi.org/10.5219/260
74. Kumar, B., Szepesi, G., Čonka, Z., Kolcun, M., Péter, Z., Berényi, L., & Szamosi, Z. (2021). Trendline assessment of solar energy potential in hungary and current scenario of renewable energy in the visegrád countries for future sustainability. *Sustainability (Switzerland)*, *13*(10). https://doi.org/10.3390/su13105462
75. Kylili, A., Fokaides, P. A., Ioannides, A., & Kalogirou, S. (2018). Environmental assessment of solar thermal systems for the industrial sector. *Journal of Cleaner Production*, *176*, 99–109. https://doi.org/10.1016/j.jclepro.2017.12.150
76. Lados, M., Somossy, É. S., & Tóth, T. (2020). Financial subsidies and the location decision of solar power plants in Hungary: An empirical investigation. *Regional Statistics*, *10*(2), 166–185. https://doi.org/10.15196/RS100207
77. Lauterbach, C., Schmitt, B., Jordan, U., & Vajen, K. (2012). The potential of solar heat for industrial processes in Germany. *Renewable and Sustainable Energy Reviews*, *16*(7), 5121–5130. https://doi.org/10.1016/j.rser.2012.04.032
78. Lauterbach, C., Schmitt, B., & Vajen, K. (2014). System analysis of a low-temperature solar process heat system. *Solar Energy*, *101*, 117–130. https://doi.org/10.1016/j.solener.2013.12.014
79. Leong, K. Y., Abdul Rahman, M. R., & Gurunathan, B. A. (2019). Nano-enhanced phase change materials: A review of thermo-physical properties, applications and challenges. *Journal of Energy Storage*, *21*(October 2018), 18–31. https://doi.org/10.1016/j.est.2018.11.008

80. Li, Q., Huang, X., Tai, Y., Gao, W., Wenxian, L., & Liu, W. (2021). Thermal stratification in a solar hot water storage tank with mantle heat exchanger. *Renewable Energy*, *173*, 1–11. https://doi.org/10.1016/j.renene.2021.03.105
81. Lian, J., Zhang, Y., Ma, C., Yang, Y., & Chaima, E. (2019). A review on recent sizing methodologies of hybrid renewable energy systems. *Energy Conversion and Management*, *199*(April), 112027. https://doi.org/10.1016/j.enconman.2019.112027
82. Liew, P. Y., Wan Alwi, S. R., Klemeš, J. J., Varbanov, P. S., & Abdul Manan, Z. (2014). Algorithmic targeting for Total Site Heat Integration with variable energy supply/demand. *Applied Thermal Engineering*, *70*(2), 1073–1083. https://doi.org/10.1016/j.applthermaleng.2014.03.014
83. Ling, D., Mo, G., Jiao, Q., Wei, J., & Wang, X. (2016). Research on Solar Heating System with Phase Change Thermal Energy Storage. *Energy Procedia*, *91*, 415–420. https://doi.org/10.1016/j.egypro.2016.06.277
84. Liu, C., Hu, P., Xu, Z., Ma, X., & Rao, Z. (2019). Experimental investigation on thermal properties of sodium acetate trihydrate based phase change materials for thermal energy storage. *Thermochimica Acta*, *674*(August 2018), 28–35. https://doi.org/10.1016/j.tca.2019.02.002
85. Matsuda, K. (2014). Low heat power generation system. *Applied Thermal Engineering*, *70*(2), 1056–1061. https://doi.org/10.1016/j.applthermaleng.2014.03.037
86. McMichael, A. J., Powles, J. W., Butler, C. D., & Uauy, R. (2007). Food, livestock production, energy, climate change, and health. *Lancet*, *370*(9594), 1253–1263. https://doi.org/10.1016/S0140-6736(07)61256-2
87. Medrano, M., Yilmaz, M. O., Nogués, M., Martorell, I., Roca, J., & Cabeza, L. F. (2009). Experimental evaluation of commercial heat exchangers for use as PCM thermal storage systems. *Applied Energy*, *86*(10), 2047–2055. https://doi.org/10.1016/j.apenergy.2009.01.014
88. Milani, F. X., Nutter, D., & Thoma, G. (2011). Invited review: Environmental impacts of dairy processing and products: A review. *Journal of Dairy Science*, *94*(9), 4243–4254. https://doi.org/10.3168/jds.2010-3955
89. Mo, J. P. T. (2016). Design of solar energy system in food manufacturing environment. *Cogent Engineering*, *3*(1). https://doi.org/10.1080/23311916.2016.1233613
90. Mølgaard, K., Søndergård, T., Prof, A., Mølgaard, K., Vej, F. B., Ø, D.-A., Prof, A., & Søndergaard, T. (2001). *Solar Panel based Milk Pasteurization Solar Panel based Milk Pasteurization*.
91. Müller, H., Brandmayr, S., & Zörner, W. (2014). Development of an evaluation methodology for the potential of solar-thermal energy use in the food industry. *Energy Procedia*, *48*, 1194–1201. https://doi.org/10.1016/j.egypro.2014.02.135
92. Muster, B., Ben Hassine, I., Helmke, A., Heß, S., Kavouras, M., & Kokla, M. (2015). Integration Guidelines. *Theories of Geographic Concepts*, *February*, 253–292. https://doi.org/10.1201/9781420004670.ch16
93. Muthukumar, P. (2005). Thermal Energy Storage : Methods and Materials. *Mechanical Engineering*.
94. Najafian, A., Haghighat, F., & Moreau, A. (2015). Integration of PCM in domestic hot water tanks: Optimization for shifting peak demand. *Energy and Buildings*, *106*, 59–64. https://doi.org/10.1016/j.enbuild.2015.05.036
95. Neumann, C. (2018). *Roadmap for industrial solar heat supply in combination with emerging technologies*.

96. Noro, M., Lazzarin, R. M., & Busato, F. (2014). Solar cooling and heating plants: An energy and economic analysis of liquid sensible vs phase change material (PCM) heat storage. *International Journal of Refrigeration*, *39*(0), 104–116. https://doi.org/10.1016/j.ijrefrig.2013.07.022
97. Pahlavana, S., Jahangirib, M., Shamsabadic, A., & Khechekhouched, A. (2018). Feasibility study of solar water heaters in Algeria, a review. *Journal of Solar Energy Research (JSER)*, *3*(August), 135–146.
98. Pietruschka, D., Hassine, I. Ben, Cotrado, M., Fedrizzi, R., & Cozzini, M. (2016). Large Scale Solar Process Heat Systems -planning, Realization and System Operation. *Energy Procedia*, *91*, 638–649. https://doi.org/10.1016/j.egypro.2016.06.223
99. Prieto, C., & Cabeza, L. F. (2019). Thermal energy storage (TES) with phase change materials (PCM) in solar power plants (CSP). Concept and plant performance. *Applied Energy*, *254*(January), 113646. https://doi.org/10.1016/j.apenergy.2019.113646
100. Putra, N., Rawi, S., Amin, M., Kusrini, E., Kosasih, E. A., & Indra Mahlia, T. M. (2019). Preparation of beeswax/multi-walled carbon nanotubes as novel shape-stable nanocomposite phase-change material for thermal energy storage. *Journal of Energy Storage*, *21*(June 2018), 32–39. https://doi.org/10.1016/j.est.2018.11.007
101. Qiu, L., Ouyang, Y., Feng, Y., & Zhang, X. (2019). Review on micro/nano phase change materials for solar thermal applications. *Renewable Energy*, *140*, 513–538. https://doi.org/10.1016/j.renene.2019.03.088
102. Quijera, J. A., Alriols, M. G., & Labidi, J. (2014). Integration of a solar thermal system in canned fish factory. *Applied Thermal Engineering*, *70*(2), 1062–1072. https://doi.org/10.1016/j.applthermaleng.2014.04.012
103. Rawlins, J., & Ashcroft, M. (2013). Small-scale Concentrated Solar Power - A review of current activity and potential to accelerate deployment. *Carbon Trust*, *March*, 50.
104. Rivett-Carnac, K., & Scholtz, L. (2018). *Solar thermal technologies : clean fit for food and beverage industries: Emerging climate-smart business opportunities*.
105. Sabiha, M. A., Saidur, R., Mekhilef, S., & Mahian, O. (2015). Progress and latest developments of evacuated tube solar collectors. *Renewable and Sustainable Energy Reviews*, *51*, 1038–1054. https://doi.org/10.1016/j.rser.2015.07.016
106. Sandey, K. K., Agrawal, A. K., & Nikam, P. (2015). Solar Water Heating- Potential use in Dairy Industry. *INTERNATIONAL JOURNAL OF ENGINEERING RESEARCH & TECHNOLOGY (IJERT) ISNCESR – 2015 (Volume 3 – Issue 20)*, *3*(20), 3–4.
107. Schmitt, B. (2016). Classification of Industrial Heat Consumers for Integration of Solar Heat. *Energy Procedia*, *91*, 650–660. https://doi.org/10.1016/j.egypro.2016.06.225
108. Schramm, S., & Adam, M. (2014). Storage in solar process heat applications. *Energy Procedia*, *48*, 1202–1209. https://doi.org/10.1016/j.egypro.2014.02.136
109. Sheng, N., Zhu, C., Sakai, H., Akiyama, T., & Nomura, T. (2019). Synthesis of Al-25 wt% Si@Al2O3@Cu microcapsules as phase change materials for high temperature thermal energy storage. *Solar Energy Materials and Solar Cells*, *191*(June 2018), 141–147. https://doi.org/10.1016/j.solmat.2018.11.013
110. Sierra, I., & Vidal-Valverde, C. (2000). Influence of heating conditions in continuous-flow microwave or tubular heat exchange systems on the vitamin B1 and B2 content of milk. *Lait*, *80*(6), 601–608. https://doi.org/10.1051/lait:2000147
111. Singh, G., Tyagi, V. V., Singh, P. J., & Pandey, A. K. (2020). Estimation of thermodynamic characteristics for comprehensive dairy food processing plant: An energetic and exergetic approach. *Energy*, *194*, 116799. https://doi.org/10.1016/j.energy.2019.116799

112. Suman, S., Khan, M. K., & Pathak, M. (2015). Performance enhancement of solar collectors - A review. *Renewable and Sustainable Energy Reviews*, *49*, 192–210. https://doi.org/10.1016/j.rser.2015.04.087
113. Tolnay, A., Nath, A., & Koris, A. (2020). *CHALLENGES OF SUSTAINABLE FOOD TECHNOLOGY - A REVIEW*. *14*(1), 118–129. https://doi.org/10.14232/analecta.2020.1.118-129
114. TÓTH, L., ŠLIHTE, S., ÁDÁM, B., PETRÓCZKI, K., Korzenszky, P., & GERGELY, Z. (2017). Solar assisted ground source heat pump. *SpringerBriefs in Applied Sciences and Technology*, 17–29. https://doi.org/10.1007/978-3-319-49698-6_3
115. Urbán, K., Bíró-szigeti, S., & Pataki, B. (2022). *Technology Road-Mapping of Final-Energy Generator Technologies , for the Industrial Sector , in Developed European Economies Basic Concepts of the Final-Energy Industry*. *19*(4), 65–84.
116. Wallerand, A. S., Kermani, M., Voillat, R., Kantor, I., & Maréchal, F. (2017). Optimal design of solar-assisted industrial processes considering heat pumping: Case study of a dairy. *Renewable Energy*, *128*, 565–585. https://doi.org/10.1016/j.renene.2017.07.027
117. Walmsley, T. G., Walmsley, M. R. W., Atkins, M. J., & Neale, J. R. (2014). Integration of industrial solar and gaseous waste heat into heat recovery loops using constant and variable temperature storage. *Energy*, *75*, 53–67. https://doi.org/10.1016/j.energy.2014.01.103
118. Walmsley, T. G., Walmsley, M. R. W., Tarighaleslami, A. H., Atkins, M. J., & Neale, J. R. (2015). Integration options for solar thermal with low temperature industrial heat recovery loops. *Energy*, *90*, 113–121. https://doi.org/10.1016/j.energy.2015.05.080
119. Wang, Z., Zhang, H., Dou, B., Zhang, G., & Wu, W. (2019). Influence of inlet structure on thermal stratification in a heat storage tank with PCMs: CFD and experimental study. *Applied Thermal Engineering*, *162*(July). https://doi.org/10.1016/j.applthermaleng.2019.114151
120. Wang, Z., Zhang, H., Dou, B., Zhang, G., Wu, W., & Zhou, L. (2020). An experimental study for the enhancement of stratification in heat-storage tank by equalizer and PCM module. *Journal of Energy Storage*, *27*(October 2019), 101010. https://doi.org/10.1016/j.est.2019.101010
121. Wang, Z., Zhang, H., Huang, H., Dou, B., Huang, X., & Goula, M. A. (2019). The experimental investigation of the thermal stratification in a solar hot water tank. *Renewable Energy*, *134*, 862–874. https://doi.org/10.1016/j.renene.2018.11.088
122. Wayua, F. O., Okoth, M. W., & Wangoh, J. (2013). Design and performance assessment of a flat-plate solar milk pasteurizer for arid pastoral areas of kenya. *Journal of Food Processing and Preservation*, *37*(2), 120–125. https://doi.org/10.1111/j.1745-4549.2011.00628.x
123. Yadav, R. H., Jadhav, V. V., & Chougule, G. A. (2016). *EXPLORING THE SCOPE OF RENEWABLE ENERGY TECHNOLOGIES IN DAIRY SECTOR*. *5*(7), 439–450.
124. Yildirim, N., & Genc, S. (2015). Thermodynamic analysis of a milk pasteurization process assisted by geothermal energy. *Energy*, *90*, 987–996. https://doi.org/10.1016/j.energy.2015.08.003
125. Yuan, H., Bai, H., Lu, X., Zhang, X., Zhang, J., Zhang, Z., & Yang, L. (2019). Size controlled lauric acid/silicon dioxide nanocapsules for thermal energy storage. *Solar Energy Materials and Solar Cells*, *191*(August 2018), 243–257. https://doi.org/10.1016/j.solmat.2018.11.019
126. Zahira, R., Akif, H., Amin, N., Azam, M., & Zia-ul-Haq. (2009). Fabrication and performance study of a solar milk pasteurizer. *Pakistan Journal of Agricultural Sciences*, *46*(2), 162–168.

127. Zalba, B., Marin, J., Cabeza, L. F., & Mehling, H. (2003). Review on thermal energy storage with phase change: materials, heat transfer analysis and applications. In *Applied Thermal Engineering* (Vol. 704). https://doi.org/10.1017/jfm.2012.219
128. Zhang, L., Zhou, K., Wei, Q., Ma, L., Ye, W., Li, H., Zhou, B., Yu, Z., Lin, C. Te, Luo, J., & Gan, X. (2019). Thermal conductivity enhancement of phase change materials with 3D porous diamond foam for thermal energy storage. *Applied Energy*, *233–234*(October 2018), 208–219. https://doi.org/10.1016/j.apenergy.2018.10.036
129. Zhou, F., Ji, J., Yuan, W., Zhao, X., & Huang, S. (2019). Study on the PCM flat-plate solar collector system with antifreeze characteristics. *International Journal of Heat and Mass Transfer*, *129*, 357–366. https://doi.org/10.1016/j.ijheatmasstransfer.2018.09.114

A2: Publications related to the dissertation

Refereed papers in foreign languages:

1. **Ghabour, R.**, Korzenszky, P. (2020): Mathematical modelling and experimentation of soy wax PCM solar tank using response surface method, *Analecta Tech. Szeged*, 14 (2), 35–42, ISSN: 2064-7964, https://doi.org/10.14232/analecta.2020.2.35-42.
2. **Ghabour, R.**, Josimović, L., Korzenszky, P. (2021): Two analytical methods for optimising solar process heat system in pasteurising plant, *Applied Engineering Letters*, 6, 166–174, 2021, ISSN: 2466-4847. https://doi.org/10.18485/aeletters.2021.6.4.4, (Scopus: Q3).
3. **Ghabour, R.**, Korzenszky, P. (2021): Technical and non-technical difficulties in solar heat for industrial process. *ACTA Tech CORVINIENSIS – Bulletin of Engineering*, 3, 11–8, ISSN: 2067-3809, https://acta.fih.upt.ro/pdf/archive/ACTA-2021-3.pdf.
4. **Ghabour, R.**, Korzenszky, P. (2021): Effect of series and parallel flow heater configuration of industrial solar heat processes, *Science, technology and innovation*, 14 (3), 18-26, 2021, ISSN: 2544-9125, https://doi.org/10.55225/sti.315.
5. **Ghabour, R.**, Korzenszky, P. (2021): Identifying the optimum tilting angles for solar thermal collectors using four different modelling factors in Hungary. *Hungarian agriculture research*.,21, 51-64, ISSN: 2060-3789.
6. **Ghabour, R.**, Korzenszky, P. (2021): Optimal design and configuration for pasteurizing heat demand supported by solar thermal system using T * sol, ANNALS of faculty engineering Hunedoara – International journal of engineering, 2, 105-110, ISSN: 2601-2332, https://annals.fih.upt.ro/pdf-full/2022/ANNALS-2022-2-16.pdf.
7. **Ghabour, R.**, Korzenszky, P. (2021) Assessment and Modelling of Industrial-Scale Solar Thermal System Application in Hungary. *Hungarian Agriculture Engineering*, 40, 70-77, ISSN: 2415-9751, https://doi.org/10.17676/HAE.2021.40.70.
8. **Ghabour, R.**, Korzenszky, P. (2022): Economic and energetic assessment of industrial-scale solar thermal energy in the Visegrád region, *Analecta Technica Szegedinensia*, 17 (1), 1-9, ISSN: 2064-7964, https://doi.org/10.14232/analecta.2023.1.1-9.
9. **Ghabour, R.**, Korzenszky, P. (2022): Feasibility study of using solar thermal energy for heating swimming pools in central European climate (Hungary as a case study), *Hungarian Agriculture engineering*, 41, 72-78, ISSN: 2415-9751, https://doi.org/10.17676/HAE.2022.41.72.
10. **Ghabour, R.,** Korzenszky, P. (2022): Linear Model of DHW System Using Response Surface Method Approach**,** Tehnički *vjesnik*, 29 (1), 66-72, ISSN: 1848-6339, https://doi.org/10.17559/TV-20201128095138, (IF: 0,783; Scopus: Q2).
11. **Ghabour, R.**, Korzenszky, P. (2022): Dynamic modelling and experimental analysis of tankless solar heat process system for preheating water in the food industry, *Acta polytechnica Hungarica*, 20 (4), 65-83, ISSN: 1785-8860, (IF: 1.806; Scopus: Q2)

International conference abstracts:

12. **Ghabour, R.**, Korzenszky, P. (2018): Studying the possibility of providing the thermal requirements of pasteurization by PV/T solar system in Hungary, *International Conference on Science, Technology, Engineering and Economy*: ICOSTEE 2018: Book of Abstracts Szeged, Hungary: University of Szeged Faculty of Engineering (2018) pp. 20, ISBN:9789633066201.
13. **Ghabour, R.**, Korzenszky, P. (2018): Study of renewable energies within the industrial sector in Hungary: energetic and economic analysis, *Tudományos Diákköri Konferencia előadásainak összefoglalói 2018* Gödöllő, Hungary: Szent István Egyetemi Kiadó (2018) pp. 48, ISBN: 9789632697857
14. **Ghabour, R.**, Korzenszky, P. (2019): Optimum solar thermal energy utilization in food industry: case study of a dairy plant, *SYNERGY - Engineering, Agriculture and Green Industry Innovation*: ABSTRACTS of the VI. International Conference of CIGR Hungarian National Committee and the Szent István University, Faculty of Mechanical Engineering and the XXXIX. R&D Conference of Hungarian Academy of Sciences, Committee of Agricultural and Biosystems Engineering, Gödöllő, Hungary, pp. 22. November 2019. Gödöllő, Hungary: Szent István University Faculty of Mechanical Engineering, ISBN: 9789632698540
15. **Ghabour, R.**, Korzenszky, P. (2021): Effect of in-series and in-parallel flow heater configuration of solar heat system for industrial processes, *Risk Factors of Food Chain*: XXIst International Conference: Book of abstract Iwonicz, Poland: Uniwersytet Rzeszowski (2021) pp. 15, ISBN:9788379969326
16. **Ghabour, R.**, Korzenszky, P. (2021): Mathematical modelling and experimentation of Soy wax PCM solar tank using response surface method, *XXIV. Tavaszi Szél Konferencia (2021)*: Absztrakt kötet Budapest, Hungary: Association of Hungarian PHD and DLA Students (2021) pp. 440, ISBN:9786155586996
17. **Ghabour, R.**, Korzenszky, P. (2021): Design optimisation and configuration of solar heating system used for pasteurising heat demand in two different regions, *Efficiency, solar and thermal energy for the human comfort*: Book of Abstracts Gödöllő, Hungary: Hungarian University of Agriculture and Life Science (2021) pp. 33-34, ISBN: 9789632699585
18. Hossain, S., **Ghabour, R.**, Korzenszky, P. (2021): Potential application and system optimization of solar domestic swimming pool heating system in cold climates, *Efficiency, solar and thermal energy for the human comfort*: Book of Abstracts Gödöllő, Hungary: Hungarian University of Agriculture and Life Science (2021) pp. 19-20, ISBN: 9789632699585
19. **Ghabour, R.**, Korzenszky, P. (2022): Economic and energetic assessment of industrial-scale solar thermal energy in the Visegrád region, *Risk Factors of Food Chain: Book of Abstracts Węgierska Górka, Poland (2022)*, pp. 17, ISBN:9789632698540

Book chapter in foreign languages:

20. **Ghabour, R.**, Korzenszky, P. (2018): Optimal design of solar-assisted industrial processes considering solar energy hybridized with pasteurizer, *Risk Factors of Food Chain*, 93-96. ISBN:978-963-269-774-1.

9. ACKNOWLEDGEMENT

I would like to express my sincere gratitude for my supervisor Dr Péter Korzenszky for his guidance and support throughout my PhD journey which started long time ago with my MSc back in 2017. His invaluable insights and expertise have been instrumental in shaping my research and pushing me to strive for excellence.

This work has been supported financially by the Stipendium Hungaricum Scholarship Programme and accomplished under the direction of the Mechanical Engineering Doctoral School at MATE (Szent István University formerly), Gödöllő, Hungary.

I want to express my gratitude and appreciation for Prof. István Farkas, the former head of the Mechanical Engineering Doctoral School, whose recommendations, suggestions, and support throughout my study have facilitated the fulfilment of all requirements for obtaining this PhD. In addition, I would like to extend my sincere gratitude to Prof. Gábor Kalácska, the current head of the Mechanical Engineering Doctoral School.

I would also like to thank the faculty and staff at The Hungarian University of Agriculture and Life Sciences for providing me with the resources and facilities necessary to carry out my research. Their support and encouragement have been a constant source of motivation.

I am deeply grateful to my family, wife, and friends for their unwavering support and encouragement during this challenging journey. Their love and understanding have kept me going even in the most difficult times.

I am also thankful for Mr MD Sazzad Hossain, Amer Yaqub, and Louai Haikal, who were under my supervision throughout their MSc studies between 2019 and 2022. Thanks for being part of my project and working hard in the lab to help achieve our aims, represented successfully by publishing many scientific articles from our research work in reputed journals.

I would like to express my sincere appreciation to Ms. Zsuzsanna Tassy, the International PhD Coordinator at the University's Doctoral and Habilitation Center, who deserves special recognition for her invaluable support and assistance throughout my MSc and PhD studies. It's difficult to put into words just how grateful I am for the guidance and help that she has provided me with.

I would like to express my heartfelt appreciation to the participants who generously gave their time and shared their experiences for this research. Without their participation, this study would not have been possible.

Finally, I would like to express my enormous appreciation to my wife, Mrs. Roxána Diána Szőcs, for being my most supportive partner ever. This superhero lady has been fantastic; she supported me enormously during these years and took care of me, despite also working all the time. Thanks to Roxána, my most patient sounding board, for being there whenever required. Additionally, my most enormous thanks to my family (father, mother, and siblings) for all the support they have shown me throughout this research.

Thank you once again for your support and guidance. I will always be grateful for your contribution to my academic and personal growth.

Sincerely,

Gödöllő, 19. 02. 2024

Rajab Ghabour